USAAMRDL-TR-77-45A

AERODYNAMIC DESIGN AND ANALYSIS OF PROPELLERS FOR MINI-REMOTELY PILOTED AIR VEHICLES

Volume I - Open Propellers

Henry V. Borst & Associates
203 W. Lancaster Avenue
Wayne, Penn 19087

January 1978

Final Report for Period June 1976 - August 1977

Approved for public release;
distribution unlimited.

Prepared for

U. S. ARMY AVIATION RESEARCH AND DEVELOPMENT COMMAND
P.O. Box 209
St. Louis, Mo. 63166

APPLIED TECHNOLOGY LABORATORY
U. S. ARMY RESEARCH AND TECHNOLOGY LABORATORIES (AVRADCOM)
Fort Eustis, Va. 23604

APPLIED TECHNOLOGY LABORATORY POSITION STATEMENT

This report provides a reasonable insight into the complexity involved with the design of small diameter (approximately 24 to 30 inches) free propellers for mini-remotely piloted vehicles (mini-RPV). Modifications to airfoil data used in the propeller blade design were generated to enable the program to be used for both conventional and low Reynolds number RPV propeller designs.

Mr. James Gomez of the Propulsion Technical Area, Technology Applications Division, served as Project Engineer for this effort.

Unclassified
SECURITY CLASSIFICATION OF THIS PAGE (When Data Entered)

REPORT DOCUMENTATION PAGE

READ INSTRUCTIONS BEFORE COMPLETING FORM

1. REPORT NUMBER: USAAMRDL-TR-77-45A
2. GOVT ACCESSION NO.
3. RECIPIENT'S CATALOG NUMBER
4. TITLE (and Subtitle): AERODYNAMIC DESIGN AND ANALYSIS OF PROPELLERS FOR MINI-REMOTELY PILOTED AIR VEHICLES, Volume I, Open Propellers.
5. TYPE OF REPORT & PERIOD COVERED: Final Report, Jun 76 - Aug 77
6. PERFORMING ORG. REPORT NUMBER
7. AUTHOR(s): Henry V. Borst
8. CONTRACT OR GRANT NUMBER(s): DAAJ02-76-C-0031
9. PERFORMING ORGANIZATION NAME AND ADDRESS: Henry V. Borst & Associates, 203 W. Lancaster Avenue, Wayne, Pa. 19087
10. PROGRAM ELEMENT, PROJECT, TASK AREA & WORK UNIT NUMBERS: 62209A 1F262209AH76 00 150 EK
11. CONTROLLING OFFICE NAME AND ADDRESS: U.S. Army Aviation R&D Command, P.O. Box 209, St. Louis, Missouri 63166
12. REPORT DATE: Jan 78
13. NUMBER OF PAGES: ~~130~~ 132 p.
14. MONITORING AGENCY NAME & ADDRESS (if different from Controlling Office): Applied Technology Laboratory, U.S. Army Research & Technology Laboratories (AVRADCOM), Fort Eustis, Virginia 23604
15. SECURITY CLASS. (of this report): Unclassified
15a. DECLASSIFICATION/DOWNGRADING SCHEDULE

16. DISTRIBUTION STATEMENT (of this Report)

Approved for public release; distribution unlimited.

17. DISTRIBUTION STATEMENT (of the abstract entered in Block 20, if different from Report)

DDC RECEIVED MAR 1 1978 F

18. SUPPLEMENTARY NOTES

Volume I of a two-volume report.

19. KEY WORDS (Continue on reverse side if necessary and identify by block number)

Propellers, Propulsion, Remotely Piloted Vehicles, Aerodynamics, Reynolds Number

20. ABSTRACT (Continue on reverse side if necessary and identify by block number)

This report presents the design and analysis of propellers applied to mini-remotely piloted vehicles. Modifications to the airfoil data used for predicting the profile drag losses were necessary to account for operation at the low Reynolds number encountered by mini-RPV propellers. Due to the lack of two-dimensional airfoil data, the correction to the drag coefficient is only a function of the design lift coefficient and Reynolds number.

DD FORM 1 JAN 73 1473 EDITION OF 1 NOV 65 IS OBSOLETE

Unclassified
SECURITY CLASSIFICATION OF THIS PAGE (When Data Entered)

390295

20. Abstract, Continued

This correction was determined from the available airfoil data and low Reynolds number propeller test data. Using the new correction, the existing computer program for calculating performance was modified so as to apply over the full range conditions of both conventional and RPV propellers. The short single-point method was also modified so as to apply at the low Reynolds number conditions encountered with RPV propellers.

The use of advanced type airfoils was considered for application to RPV propellers. It appears that these airfoils will offer both structural and performance advantages over conventional airfoil types. Additional airfoil data are needed before a propeller of this type can be designed and analyzed for this application.

Using the revised methods of propeller analysis, six optimum propellers were designed and analyzed for two different RPV's. The analysis showed that improved performance can be obtained with the new designs. A ducted propeller with sufficiently low blade tip clearances was also analyzed. This configuration appears to have superior performance to the open type propellers considered, as well as a potential for reduced noise. Propellers with variable blade angles also appear to offer advantages from both the noise and performance standpoints.

Volume II presents the ducted-propeller design for the Mini-RPV.

TABLE OF CONTENTS

TABLE OF CONTENTS (Continued)

LIST OF ILLUSTRATIONS

LIST OF ILLUSTRATIONS (Continued)

LIST OF ILLUSTRATIONS (Continued)

LIST OF ILLUSTRATIONS (Continued)

LIST OF TABLES

INTRODUCTION

Remotely piloted vehicles (RPV) are currently being developed for many applications. The smaller sizes, mini-RPV's, are powered with two-cycle reciprocating engines, usually driving two-bladed fixed-pitch propellers. The propellers used are less than three feet in diameter and operate in the subsonic speed range. As a result of the small blade chord and the low forward speed, the propeller sections operate at a Reynolds number of less than 300,000. At these low values of Reynolds number, little is known about the performance characteristics of propellers or how to design them for peak efficiency. Because of the need to maximize the performance of the mini-RPV's, a program was initiated to investigate the characteristics of small propellers and to develop the necessary procedures and data for determining their design and performance.

The study was to review the existing propeller theory and corresponding data to find the necessary corrections and modifications needed for the design and analysis of RPV propellers. All the available test data on small propellers was to be reviewed and analyzed.

CONVENTIONAL PROPELLER TECHNOLOGY

The technology of propellers used on conventional aircraft ranging in size from those used in general aviation to the largest transport has been developed over the years and is generally well understood. For propellers operating in the subsonic speed range, methods and data have been developed [1] so that it is possible to design for peak performance and to accurately determine the efficiency over the entire speed range.

Three general methods are available for determining the characteristics of propellers:

1. A strip analysis procedure for calculating performance from known conditions, given the propeller geometry.

2. A single-point analysis for calculating performance, also from known operating conditions and propeller geometry.

3. A strip analysis procedure for finding the optimum propeller geometry and performance for any set of given operating conditions.

Both strip analysis procedures determine the lift and drag characteristics at each blade station, and these are then resolved into the differential thrust and torque components. Integration of these components over the blade span results in values of total thrust and torque. The efficiency may then be found from the formula

$$\eta = TV_o/550\ HP \qquad (1)$$

where T = the total thrust, lbs
V_o = free-stream velocity, ft/sec
HP = propeller shaft horsepower.

With the strip analysis procedure, forces are usually determined at ten blade stations. To find these forces, the local velocity conditions, as determined by rotation and the free-stream components, must be known. When the propeller is operating in a flow field where these velocity components are influenced by external bodies, this change is taken into account.

---

[1] Borst, H.V., et al, SUMMARY OF PROPELLER DESIGN PROCEDURES AND DATA, Vols. I, II and III, USAAMRDL Technical Report 73-34A,B,& C, H.V. Borst & Associates, Eustis Directorate, U.S. Army Air Mobility Research & Development Laboratory, Fort Eustis, Virginia, Nov. 1973, AD 774831, AD 774836, and AD 776998.

To reduce calculation time, the strip analysis procedure for analyzing a propeller has been programmed for a high-speed computer. To run the strip analysis computer program it is necessary to know the local axial velocity at each blade station, the rotational speed, all the physical characteristics of the propeller, the power input, and the atmospheric conditions. The propeller physical characteristics needed include number of blades and diameter, as well as the distributions of thickness ratio, blade angle, camber, and blade chord.

Although the actual computer time required to analyze a propeller is small, time is required to set up the input. Further, the propeller characteristics needed for good performance may not be known. For these reasons, simplified methods of propeller analysis have been developed that can be used to find the efficiency in a minimum of time. These methods, known as single-point procedures, use the integrated characteristics of activity factor and integrated design lift coefficient for describing the blade properties. The single-point methods can be used to determine the performance of a large number of propellers in a very short period of time, using a desk calculator, and are useful for establishing the general properties of the propellers needed. By analyzing a number of propellers using the single-point method at the important operating conditions of the airplane, the general size required can be determined.

When the best propeller and blade characteristics must be established for a critical operating condition, the optimum strip analysis procedure is used. With this procedure,[1] the blade characteristics are found that will give the peak efficiency for any operating condition. Usually, the results of the single-point method establish the general range of parameters for high performance; then, the optimum method is used to establish the blade details that will give the peak efficiency. The blade number, propeller, diameter, and thickness distribution, as well as the design operating condition, must be specified for determining the optimum propeller and its performance. The thickness ratio distribution of the blade is established by structural and fabrication considerations. From the results of this calculation the detailed geometry of the blade is established, including the distributions of chord, blade angle, and section camber (design C_L).

In calculating the detailed characteristics of the optimum blade, the planform becomes very wide inboard, resulting in an impractical blade configuration. For this reason the blade

[1] Borst, et al.

chord and its distribution is also specified prior to the calculation. This is generally done on the basis of single-point analysis. Then, with the chord and thickness distribution plus the diameter and blade number, the optimum distributions of camber and blade angle are determined for any given operating condition. The efficiency determined is the peak for that condition within the restrictions of blade number, diameter, and chord for the airfoil section type chosen. This design procedure, using the theory of Calculations of Variations,[1] determines the best distribution of the blade angle and section camber for peak efficiency. This is done by finding the optimum distribution which minimizes the combination of the profile and induced losses.

RANGE OF OPERATION

The two-strip analysis procedures described above and given in Reference 1 apply to propellers with

- fixed blade angle
- variable blade angles
- 2, 3, 4, 5 and 6 blades
- activity factors 10 to 300.

To use the strip analysis procedures, airfoil data corresponding to the operating condition and airfoil sections are used. The airfoil data used in the computer program corresponds to

- NACA 16 and 65 series airfoils
- Thickness ratios 1.0 to .02
- Design lift coefficients 0 to .7, only at thickness ratios of .06 to .18. At other thickness ratios, a reduced design C_L range applies.
- Reynolds numbers $.5 \times 10^6$ to 6.0×10^6
- Mach numbers .3 to 1.6.

The strip analysis program can be used with any set of two-dimensional airfoil data with suitable modifications.

The single-point method [1] applies to propellers with

- variable blade angles
- 2, 3 and 4 blades
- activity factors 10 to 300
- integrated design C_L blades of 0 to .5
- Reynolds number $.5 \times 10^6$ to 6.0×10^6
- Mach numbers below the critical.

---

[1] Borst, et al.

As indicated previously, the airfoil data used in the strip analysis is not valid at the low operating Reynolds numbers of RPV propellers. It is, therefore, necessary to analyze the existing design procedures and data and modify where necessary so that they can be used for the design and analysis of mini-RPV propellers.

METHOD OF ANALYSIS AND THEORY

The strip analysis procedure used to calculate the performance and design of the propeller depends on the Theodorsen [2] vortex theory of propellers. This theory is used to find the three-dimensional flow effects induced by the propeller so that two-dimensional airfoil data can be applied for finding the correct lift and profile drag at each blade station. The change between the apparent relative velocity and that induced by the entire propeller represents the induced losses. This loss is similar to the induced drag loss on a wing. Once the lift and drag of each blade section are found they can be resolved into the thrust and torque planes and integrated to find the thrust, power, and efficiency developed by the propeller. This resolution is illustrated in Figure 1, where the velocity components and forces of a typical blade section are given.

The induced velocity w' at each blade station is directly proportional to the blade loading represented by the term C_L, the blade solidity times the section operating lift coefficient. When finding the induced velocity by the vortex theory, it is assumed that a rigid wake is shed by the propeller. This is the same as assuming that the loading on the blades is an optimum. Similar assumptions are made in wing theory for determining the induced drag. When calculating the induced velocity at each blade station, independence of blade sections is assumed. Knowing the blade angle and velocity triangle at each station, Figure 1, the true wind angle can be found using the procedure given in Reference 1. For the blade section being considered, the following equation must be satisfied:

$$\beta = \phi + \alpha \qquad (2)$$

The lift coefficient corresponding to the two-dimensional angle of attack must be the same as that which determines the true wind angle ϕ based on

$$\tan \phi = (1 + \bar{w}) \tan \phi_o \qquad (3)$$

---

[1] Borst, et al.

[2] Theodorsen, T., THEORY OF PROPELLERS, McGraw Hill, 1948.

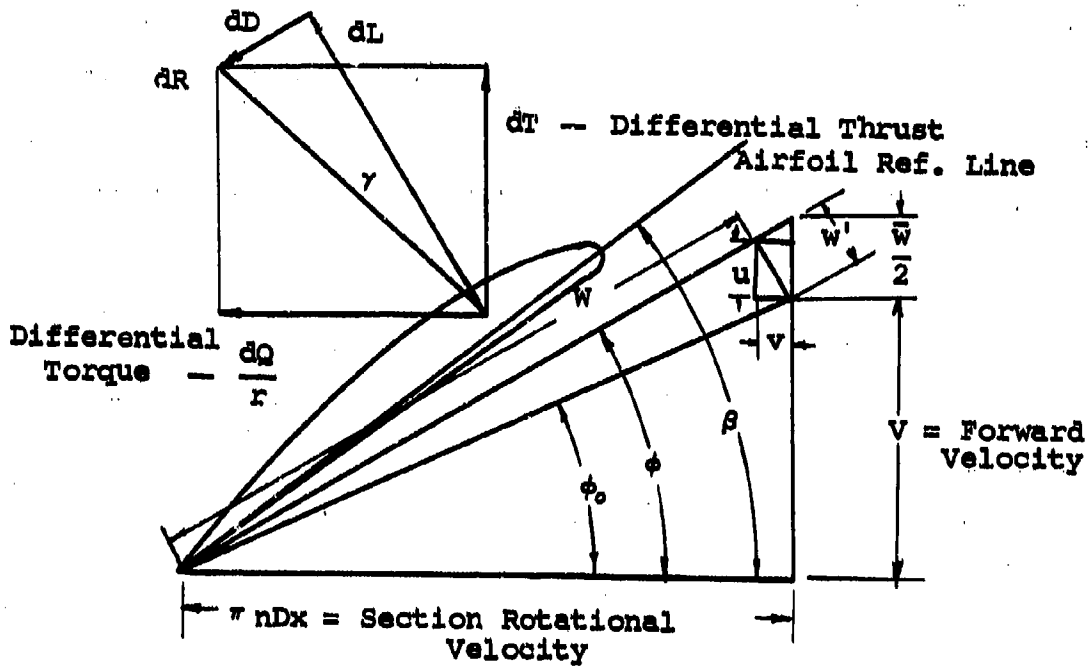

dQ/r	=	Section Torque
dL	=	Section Lift
dD	=	Section Drag
β	=	Blade Angle
ϕ	=	True Wind Angle
ϕ_o	=	Apparent Wind Angle
$\bar{W}/2$	=	Displacement Velocity
W	=	Apparent Velocity
w'	=	Induced Velocity
u	=	Induced Axial Velocity
v	=	Induced Radial Velocity
γ	=	Drag Lift Angle = $\tan^{-1} CD/C_L$

Figure 1. Propeller Velocity and Force Diagram — Single Rotation Propellers.

After the lift coefficient at each blade station is found that satisfies the above criteria, the drag coefficient is determined from two-dimensional airfoil data. The induced drag is already accounted for by the difference between the apparent and the true wind angles ϕ_o and ϕ, Figure 1. The two-dimensional airfoil data used to find the drag coefficient has been obtained at Reynolds numbers above 800,000, which is generally in excess of the critical. Since the blade sections of conventional full-scale propellers generally operate at Reynolds numbers above the critical, the two-dimensional airfoil drag data is not corrected for these effects. When the thickness ratio is above 25%, as in the case of the inboard blade sections, Reynolds number effects on both the lift and drag coefficients are encountered. These effects are accounted for in the conventional propeller strip analysis procedures.[1] Because the effect of the blade shank is small from overall performance considerations, these Reynolds number corrections have little influence on the efficiency.

The equations for the thrust and torque coefficients, derived from Reference 1, are

$$C_Q = \int_0^{1.0} \sigma C_L \frac{\pi x^2}{8} J^2 \left[\frac{1 + \frac{\bar{w}}{2}(1-\sin^2\phi)}{\sin\phi}\right]^2 (\sin\phi + \tan\gamma \cos\phi)dX \qquad (4)$$

$$C_T = \int_0^{1.0} \sigma C_L \frac{\pi x}{4} J^2 \left[\frac{1 + \frac{\bar{w}}{2}(1-\sin^2\phi)}{\sin\phi}\right]^2 (\cos\phi - \tan\gamma \sin\phi)dX \qquad (5)$$

Since $C_p = 2\pi C_Q$ (6)

the efficiency may be found from the equation

$$\eta = \frac{TV}{P} = \frac{C_T J}{C_p} \qquad (7)$$

---

[1] Borst, et al.

Another useful equation in determining propeller efficiency is

$$\eta = \frac{\tan \phi_o}{\tan(\phi+\gamma)} \qquad (8)$$

ACCURACY OF STRIP ANALYSIS PROGRAM

The procedures [1] and data for calculating the propeller performance have been programmed to run on high-speed computers. A comparison of the calculated efficiency, using the B-87 Propeller Strip Analysis Program, with the test results of References 3 through 5 is shown in Figures 2 through 4. The propellers analyzed had a diameter of at least four feet and operated at blade section Reynolds number above 400,000. Figures 2 and 3 illustrate typical comparisons of the variation in the thrust, torque, and efficiency as a function of advance ratio for propellers operating at a constant blade angle. Because power is a major parameter influencing the induced efficiency of the propeller, all comparisons of the efficiency and the thrust coefficient are made for the case where the calculated and test power coefficients are within ± 3%. To accomplish this the blade angle is adjusted from the measured value until agreement is reached. For a controllable blade angle propeller such an adjustment automatically takes place, so that such a procedure is considered valid. This comparison, shown in Figures 2 and 3, shows reasonable agreement between calculated and test values of the thrust coefficient and efficiency. The nominal operating Reynolds number at the 0.7 radius blade station is between $.4 \times 10^6$ and 1.06×10^6. Generally at the higher loadings, i.e., high C_p, the agreement between the measured and test is excellent. The error in the calculated efficiency increases with decreased loadings, which indicates that the drag used in the calculation is low.

---

[1] Borst, et al.

[3] Delano, J.B., & Carmel, M.M., TESTS OF TWO-BLADE PROPELLERS IN THE LANGLEY 8-FOOT HIGH-SPEED TUNNEL TO DETERMINE THE EFFECT ON PROPELLER PERFORMANCE OF A MODIFICATION OF INBOARD PITCH DISTRIBUTION, NACA TN 2268, Langley Aeronautical Lab., Langley Field, Va., Feb. 1951, Washington.

[4] Pendley, R.E., EFFECT OF PROPELLER-AXIS ANGLE OF ATTACK ON THRUST DISTRIBUTION OVER THE PROPELLER DISK IN RELATION TO WAKE-SURVEY MEASUREMENT OF THRUST, ARR No. L5J02b, NACA, Washington, Wartime Report.

[5] Maynard, J.D., & Steinberg, S., EFFECT OF BLADE SECTION THICKNESS RATIOS ON AERO. CHARACTERISTICS OF RELATED FULL-SCALE PROPELLERS AT MACH NOS. UP TO 0.65, NACA Rpt. 1126, 1953.

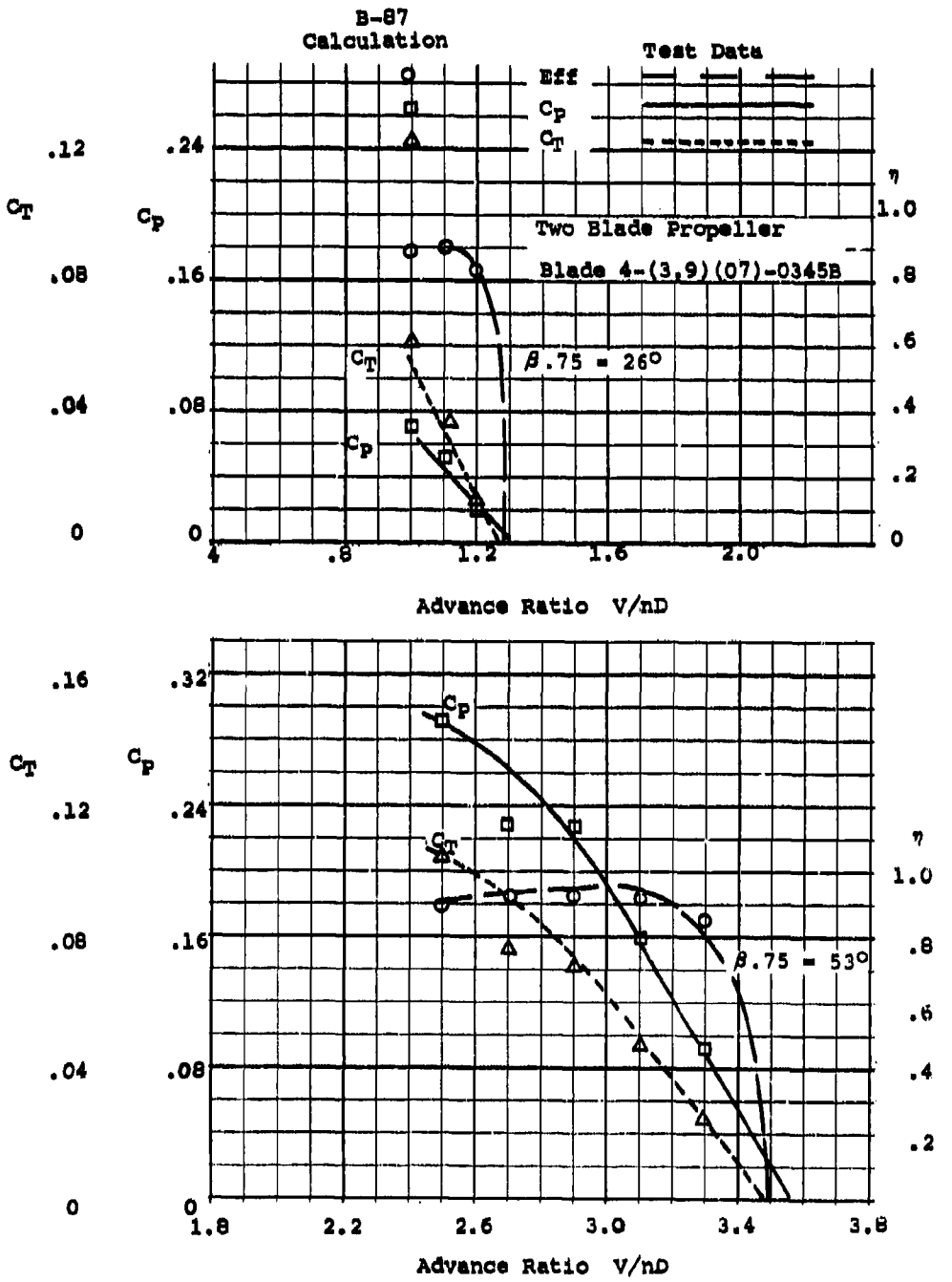

Figure 2. Comparison of Calculated Propeller Performance With Wind Tunnel Test Results.

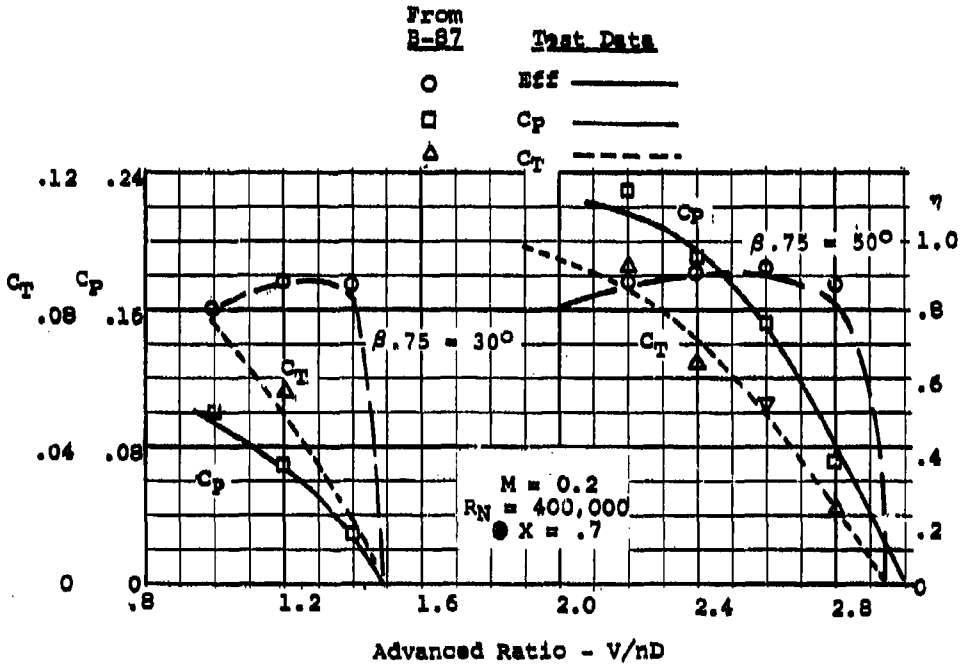

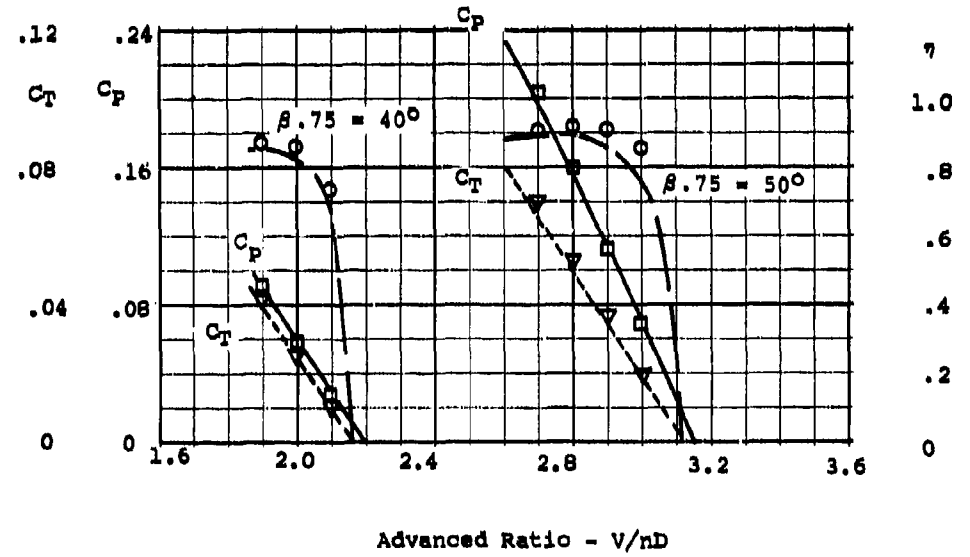

Figure 3. Comparison of Calculated Propeller Performance With Wind Tunnel Test Results.

A more extensive comparison of the efficiency difference between that calculated and determined by test is given in Figure 4. Based on this comparison, the calculated efficiency is generally within ± 5%. Because of the random type of error indicated, the changes necessary to improve the computer program accuracy are not apparent. Thus it is believed that the method and data for calculating the performance of full-scale propellers is accurate and within the same range of reliability as test data. Until more accurate test data becomes available, further attempts to improve the full-scale propeller performance calculation methods are not considered to be warranted. Full-scale propellers are considered to operate at Reynolds numbers above 500,000.

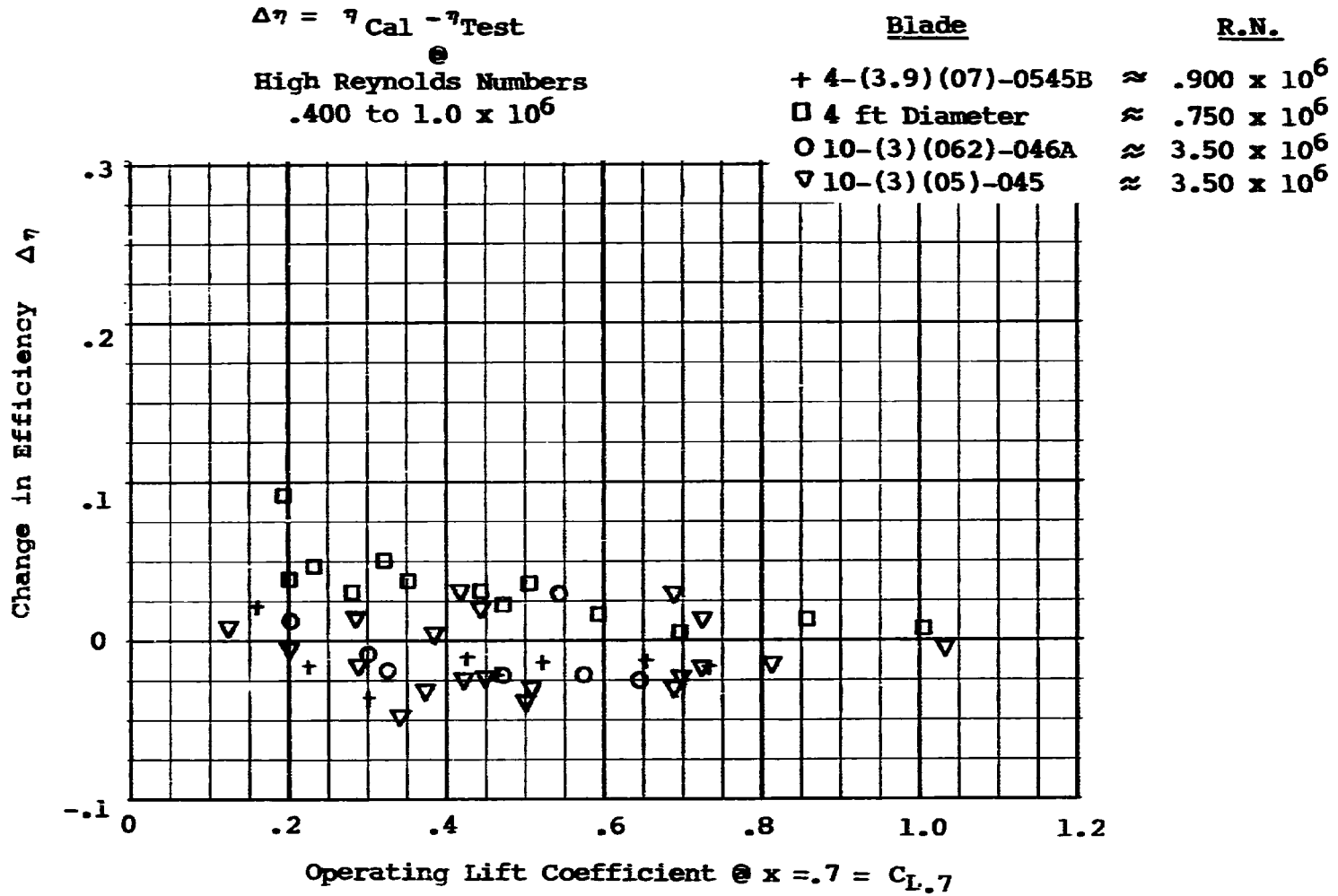

Figure 4. Difference Between Test and Calculated Propeller Efficiency at High Reynolds Numbers.

PROPELLERS FOR MINI-RPV VEHICLES

Propellers used on mini-RPV's are generally less than three feet in diameter. With blades of normal solidity in the range of 80 to 200 activity factor and operating at the speeds of less than 200 knots, the operating Reynolds number will be below 500,000. Since present methods of calculating the performance of propellers has only been proven to be suitable when operating at Reynolds numbers above 500,000, it is necessary to investigate the effects of the low Reynolds number on the characteristics of propellers designed for mini-RPV's. To do this it is necessary to examine the effects of low Reynolds number on both airfoil and propeller performance.

LOW REYNOLDS NUMBER CONDITIONS

In the Reynolds number range below 500,000, the lift and drag characteristics of the airfoils depend on the type of boundary encountered. The Reynolds number where the flow transforms from the laminar to the turbulent condition is defined as the critical Reynolds number, and is 500,000 on a flat plate. When the boundary layer is laminar the airfoil is operating in the subcritical Reynolds number range, and it is very thin. Under these conditions, the laminar boundary layer does not have the ability to take energy from the outer flow. As a result in the case of any divergent flow, it adheres poorly to the surface and separates as in the case of the upper surface of the airfoil. This causes a large increase in drag and a loss of lift.

In the supercritical operating range the boundary layer becomes turbulent. When this occurs, the flow remains attached to the airfoil for a much greater distance with a corresponding increase of lift and a decrease of drag. The Reynolds number at which this transition takes place depends on the amount of divergence in the flow or curvature in the upper airfoil surface. The critical Reynolds number thus increases with angle of attack and airfoil thickness ratio. Because of the large increase in drag and decrease in lift when operating below the critical Reynolds number, it is important that this range of operation be avoided. This can be done by selecting the proper airfoil sections and operating conditions.

To determine the performance of RPV propellers, airfoil data are needed that cover the entire Reynolds number range. Ideally, the critical Reynolds number should also be identified as a function of airfoil type and angle of attack.

AVAILABLE LOW REYNOLDS NUMBER DATA

To determine the effects of Reynolds number on the characteristics of small propellers, the available airfoil and propeller data was reviewed. This was done for the cases where the operating conditions are less than the critical, i.e., Reynolds number less than 500,000.

Airfoil Data

The airfoil data used for the design and analysis of conventional propeller blades was combined from a great many tests that were run at Reynolds numbers in excess of one million. The airfoil data was compared and analyzed until a systematic set of data was developed for a large range of airfoil parameters, including thickness ratios of .04 to 1.0 and design C_L's of 0 to 0.7. The data was developed to apply over a range of angles of attack to the stall angle and Mach numbers up to 1.6. These airfoil data are given in Reference 1.

The low Reynolds number airfoil data available is sparce compared with that for airfoils operating above the critical. Usually, airfoil data is run at Reynolds numbers in excess of 1.0×10^6, whereas data is needed for the mini-RPV propeller analysis in the Reynolds number range of 5×10^4 to 5×10^5. The available data span a large number of years and represent tests that were run in a number of different wind tunnels with different levels of turbulence. Because of this, direct comparisons of the results is questionable as some of the tunnels used had a very high turbulence factor, whereas others had very low levels of turbulence. Since the Reynolds number for flow separation is extremely important, the turbulence level in the tunnel has a large influence on the test results.

---

[1] Borst, et al.

References 6 through 14 give the only available data in the 5×10^4 to 5×10^5 Reynolds number range required for mini-RPV propeller analyses.

In Reference 6 the results of tests of NACA four-digit airfoils with and without high lift devices are presented for Reynolds numbers from 40,000 to 3×10^6. These tests were conducted in the NACA variable-density tunnel. This tunnel has a very high turbulence factor, which influences the drag and maximum lift

---

6 Jacobs, E.N., & Sherman, A., AIRFOIL SECTION CHARACTERISTICS AS AFFECTED BY VARIATIONS OF THE REYNOLDS NUMBER, NACA TR 586, 1937.

7 Relf, E.F., Jones, R., & Bell, A.H., TESTS OF SIX AIRFOIL SECTIONS AT VARIOUS REYNOLDS NUMBERS IN THE COMPRESSED AIR TUNNEL, Rpts. & Memoranda No. 1706, April 1936.

8 Jones, R., & Williams, D.H., THE EFFECT OF SURFACE ROUGHNESS ON THE CHARACTERISTICS OF THE AIRFOILS NACA 0012 AND RAF 34, Rpts. & Memoranda 1708.

9 Lnenicka, Jareslay, UNPUBLISHED TEST OF A NACA 4412 AIRFOIL AT REYNOLDS NUMBER 20,000 to 250,000, Letter to L.K. Loftin of NASA, 19 March 1974.

10 Althaus, D., EXPERIMENTAL RESULTS FROM THE LAMINAR WIND TUNNEL OF THE INSTITUT FÜR AERO AND GASDYNAMIK DER UNIVERSITAT STUTTGART, Stuttgarter Profilkatalog I, 1972.

11 Schmitz, F.W., AERODYNAMICS OF THE MODEL AIRPLANE, PART 1, Translated by Translation Branch Redstone Scientific Information Center Research & Development, Directorate, U.S. Army Missile Command, Redstone Arsenal, Ala., N70-39001.

12 Deslauriers, E.J., BLADE PERFORMANCE AT LOW REYNOLDS NUMBERS, General Electric, Rpt. No. R54AGT605, dated 1-14-55.

13 Lippisch, A., UNSTETIGKECTEN IM VERLSUF DES PROFILWIDERSTANDES, Messerschmitt, A.G. Augsburg, March 1941.

14 Lippisch, A.M., WING SECTIONS FOR MODEL PLANES, Air Trails Pictorial, April 1950.

characteristics measured as discussed in Reference 15. In a tunnel with a high turbulence factor it is, at best, difficult to find the effective Reynolds number and so interpret the test data. For example, the effective Reynolds number of 792,000 was estimated in Reference 15 for a test value of 300,000. This very large difference between the test and effective Reynolds number is questioned, [15] so only the trends observed in this report are considered to be valid. These trend comparisons are made at the measured or test value of Reynolds number only.

The variation of the drag coefficient with lift for three NACA four-digit airfoils with cambers corresponding to design lift coefficients of 0, 0.33, and 0.63 from Reference 6 is given in Figures 5 through 7 for a series of Reynolds numbers. The corresponding variation of the lift coefficient is also given in Figures 5 through 7. These data indicate that at test Reynolds numbers above about 170,000 the drag is nearly constant when the airfoil is operating near the minimum drag. Thus, for the symmetrical airfoil operating at lift coefficients $\pm$ .6 the drag is nearly independent of Reynolds number. For the cambered sections the same trend is observed but at higher lift coefficients. Below Reynolds numbers of 170,000 and at lift coefficients above and below those for minimum drag, the data in Figures 5 through 7 show a large drag increase with Reynolds number. It would appear that where the drag increases rapidly the airfoil is operating in the subcritical Reynolds number range.

The data of Reference 6 shows that the slope of the lift curve is generally unaffected by the Reynolds number; however, the maximum lift coefficient and variation of C_L about the stall is greatly affected. Because of the question of tunnel turbulence effects, these data are not directly used for RPV propeller analysis.

The data of Reference 12 was taken in a tunnel with nearly the same turbulence factor as that of the NACA Variable Density Tunnel; [6] and the same trends noted were also observed, but for airfoils with much higher levels of camber. In Reference 9, however, the angle for zero lift and the corresponding lift

---

[6] Jacobs and Sherman.

[9] Lnenicka.

[12] Deslauriers.

[15] Hoerner, S.F., & Borst, H.V., FLUID DYNAMIC LIFT, published by Hoerner Fluid Dynamics, Brick Town, N.J. 08723, 1975.

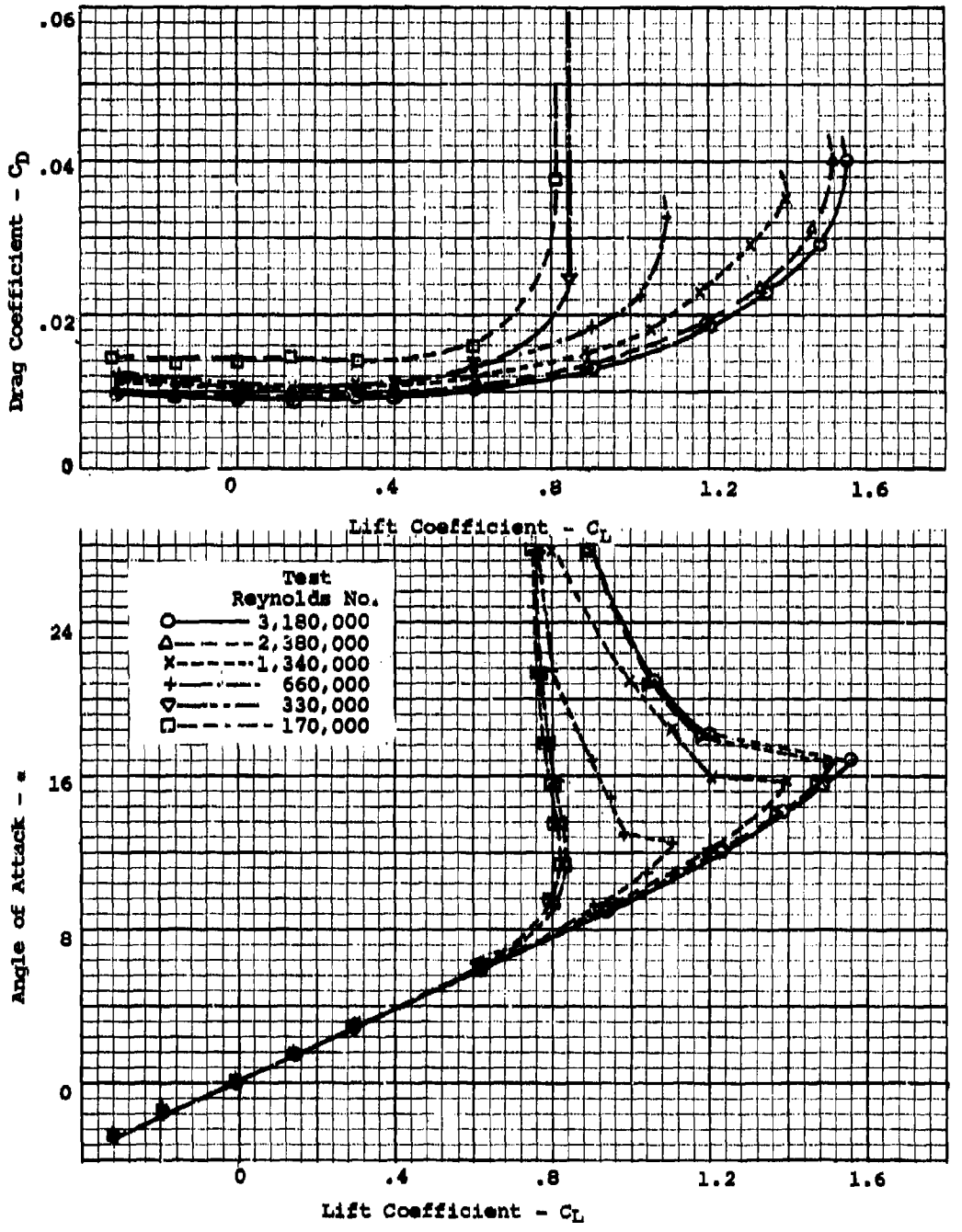

Figure 5. Two-dimensional Airfoil Data Run in the NACA Variable Density Wind Tunnel as a Function of Reynolds Number — NACA 0012 Airfoil.

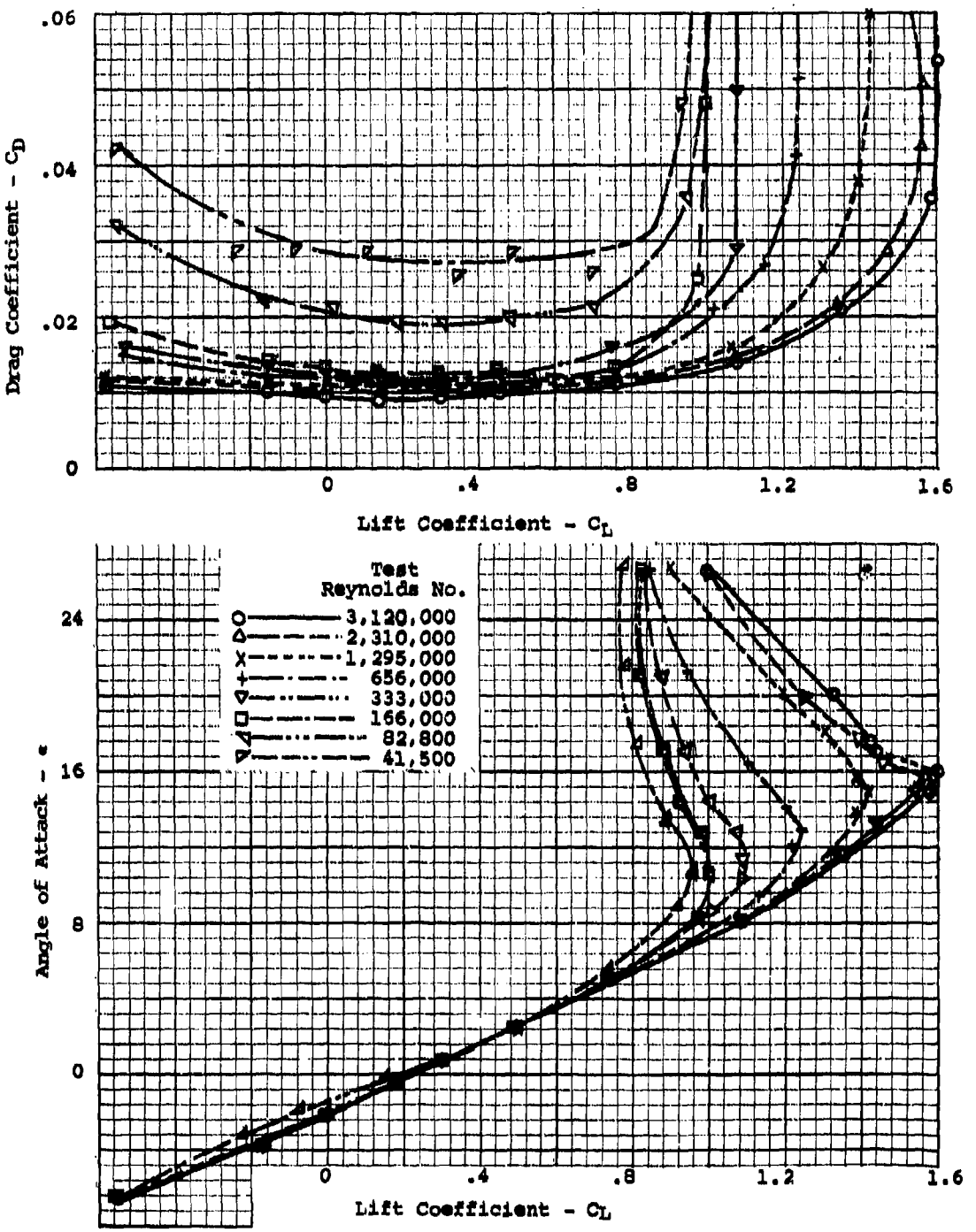

Figure 6. Two-dimensional Airfoil Data Run in the NACA Variable Density Wind Tunnel as a Function of Reynolds Number — NACA 2412 Airfoil.

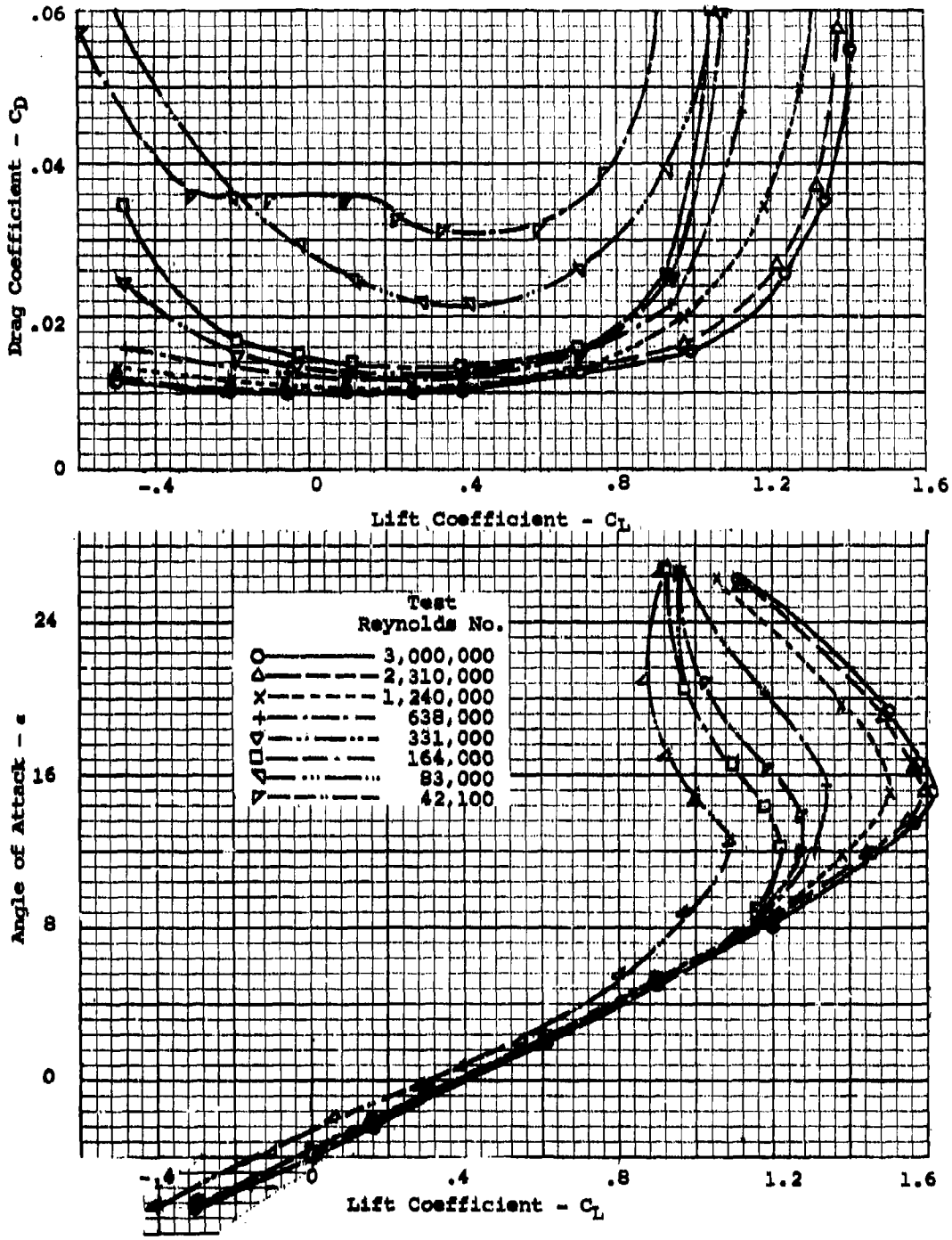

Figure 7. Two-dimensional Airfoil Data Run in the NACA Variable Density Wind Tunnel as a Function of Reynolds Number — NACA 4412 Airfoil.

curve were also influenced by Reynolds number. The meager data of Reference 9, Figure 8, shows an increase in drag with Reynolds number with the same type of trend as observed in Figures 5 through 7. Since nothing is known about the tunnel or test conditions, these data also can only be used as supportive information.

To achieve good reliability for application of the airfoil data it should be based on data taken in a low turbulence tunnel. These test operating conditions are the best representations of the expected operating conditions. For these reasons, the test results given in References 10 and 11 are considered to be the most reliable low Reynolds number airfoil data available. Unfortunately, the low Reynolds number data obtained in low turbulence tunnels is very sparce. The results shown in Figure 9 for the high camber FX 63-137 airfoil from Reference 10 are considered to be reliable. These data show a much larger change in drag with Reynolds number than would be expected due to the change in drag for an airfoil with turbulent flow conditions. Although the drag change with Reynolds number is of the same order of magnitude as measured in the Variable Density Tunnel,[6] the actual level is less.

The most complete study available on the performance of airfoils operating at low Reynolds number is that given in Reference 11. This was an award-winning effort that covered tests of several different airfoil types run in a low turbulence wind tunnel. These data show the lift, drag and moment characteristics of airfoils operating in the sub- and super-critical flow ranges. For the standard types of airfoils tested the critical Reynolds number is in the range of 40 to 160 thousand, depending on the camber and angle of attack. This is significantly below the critical Reynolds number of a flat plate and below the operating Reynolds number expected for mini-RPV propellers. The variation of the drag with Reynolds number through the critical range is illustrated in Figure 10 for the N-60 airfoil. The N-60 airfoil is similar to airfoils normally used on propellers. It has a camber of 4% with a corresponding design C_L of 0.55 and a thickness ratio of 12.4%.

---

6 Jacobs and Sherman.

9 Lnenicka.

10 Althaus.

11 Schmitz.

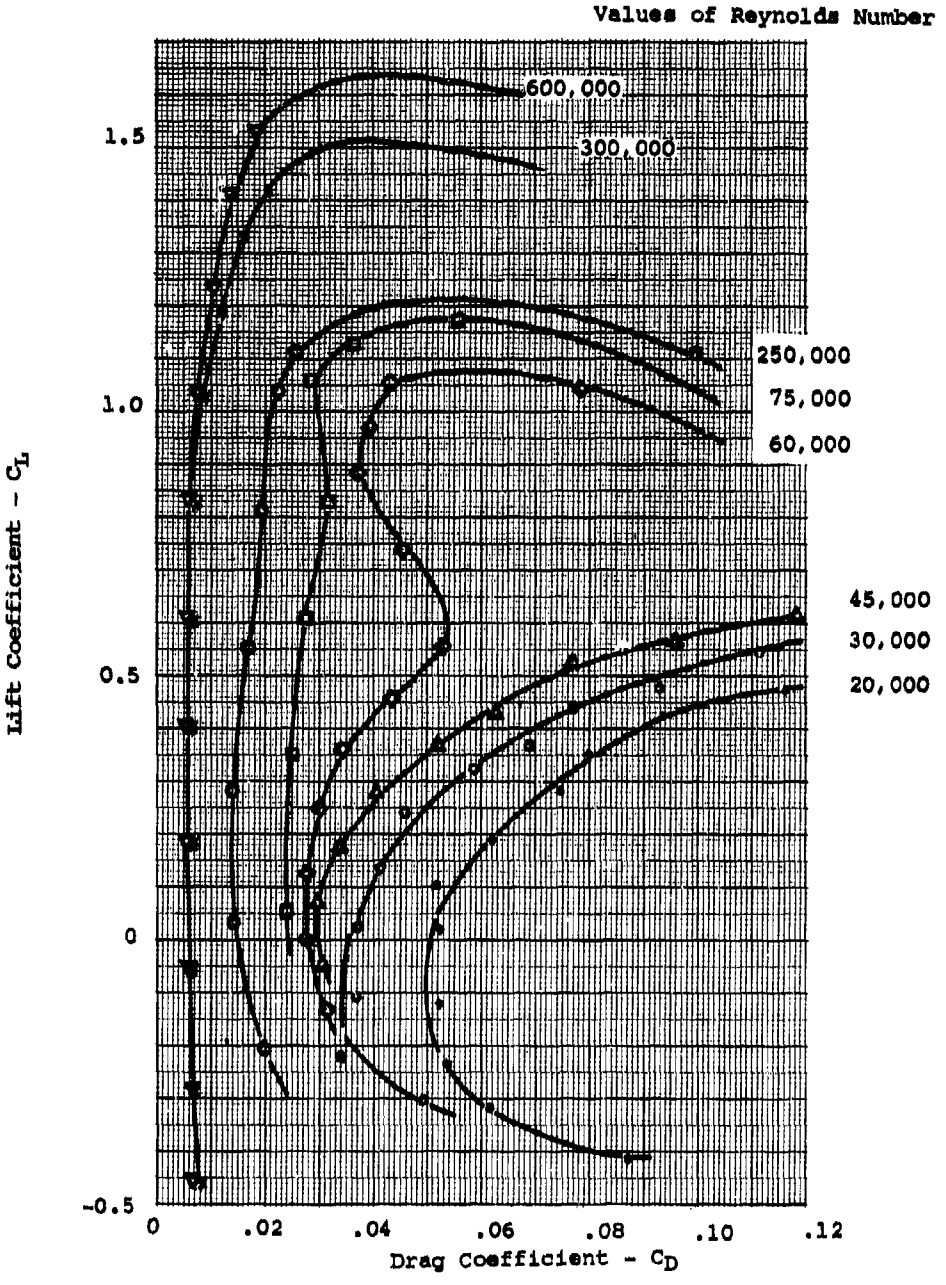

Figure 8. Two-dimensional Airfoil Data for NACA 4412 Airfoil as a Function of Reynolds Number.

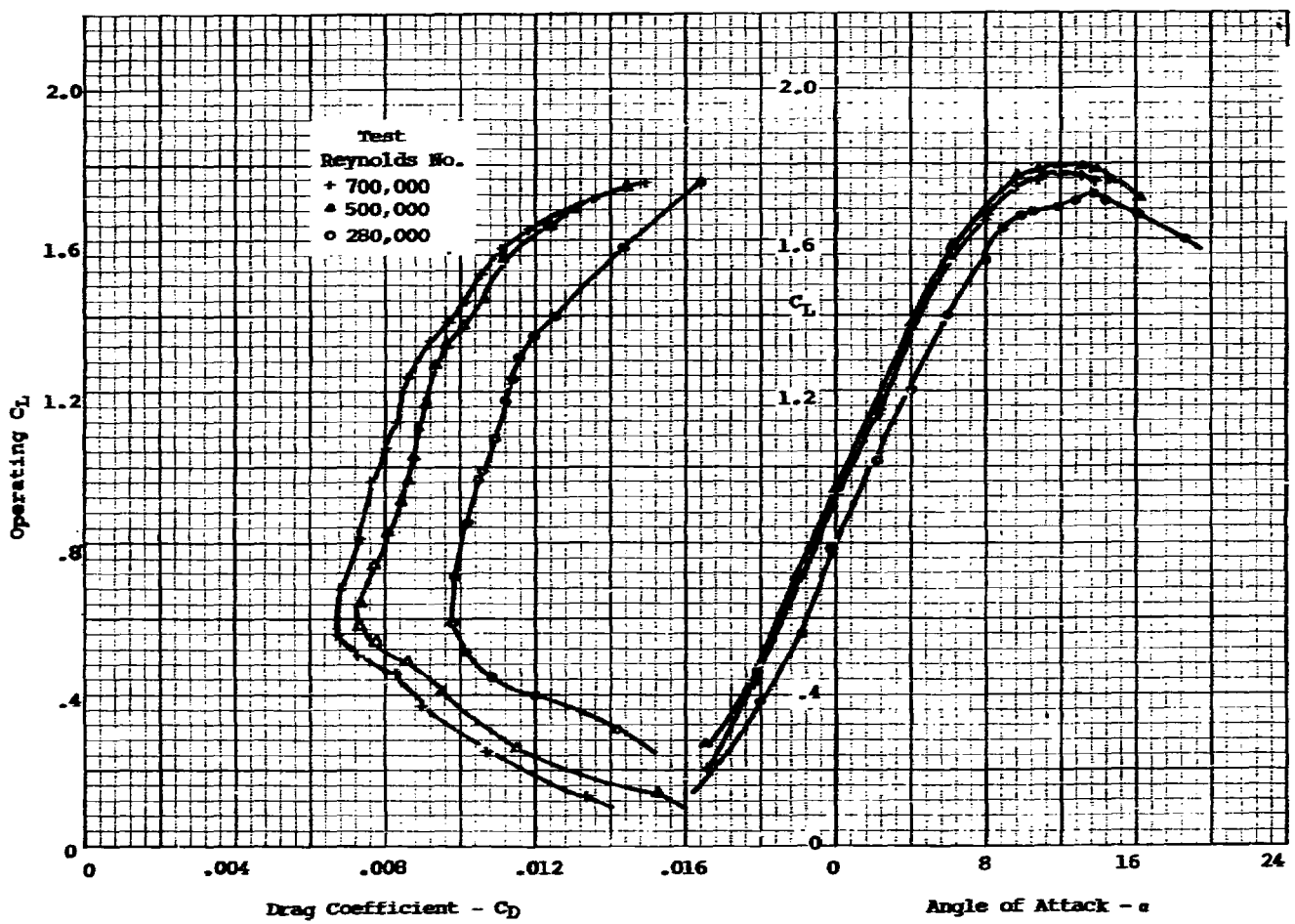

Figure 9. Two-dimensional Airfoil Data Run in a Low Turbulence Wind Tunnel FX 63-137.

The trends illustrated for the N-60 airfoils were also obtained for the other airfoils tested. In the transition range the drag decreases, going from subcritical to supercritical. This change occurs for a given angle of attack at a higher Reynolds number when measured with an increase of velocity than it does with a decrease of velocity. Tests made at higher levels of turbulence showed a decrease in the critical Reynolds number. It should be noted that the critical Reynolds number increases with increasing angle of attack.

The variation of the drag and lift coefficients for the N-60 airfoil at a series of Reynolds numbers is illustrated in Figure 11. When the airfoil is operating at speeds above the critical Reynolds number the drag remains relatively low, and the minimum value decreases with increased Reynolds number. When the laminar separation takes place the lift drops sharply and a large drag increase is encountered until it approaches the level measured at the lower Reynolds numbers.

From this review of the available low Reynolds number airfoil data it was found that sufficient systematic changes of C_L and C_D were not available to allow the performance of mini-RPV propellers to be calculated by the vortex theory of strip analysis. To do such calculations it is necessary to have tests covering the complete range of variables of thickness ratio and design C_L for the range of Reynolds number, such as those given in Reference 1.

Since such data is not available, it becomes necessary to develop corrections to the high Reynolds number airfoil data used in the strip analysis program. The application of these corrections should make it possible to find the performance of propellers for mini-RPV's at any operating condition, and to determine the losses due to Reynolds number as well as due to the other design and performance variables.

LOW REYNOLDS NUMBER PROPELLER TEST DATA

Because of the concern with regard to the effects of Reynolds number on the performance of propellers, most of the modern test data was run at conditions above the critical. For instance, the large number of two-bladed propellers tested by NACA in the 8- and 16-foot high-speed tunnels[3,5] are unsuitable for use in evaluating propellers for mini-RPV's because of the relatively high operating Reynolds numbers.

[1] Borst, et al.

[3] Delano and Carmel.

[5] Maynard and Steinberg.

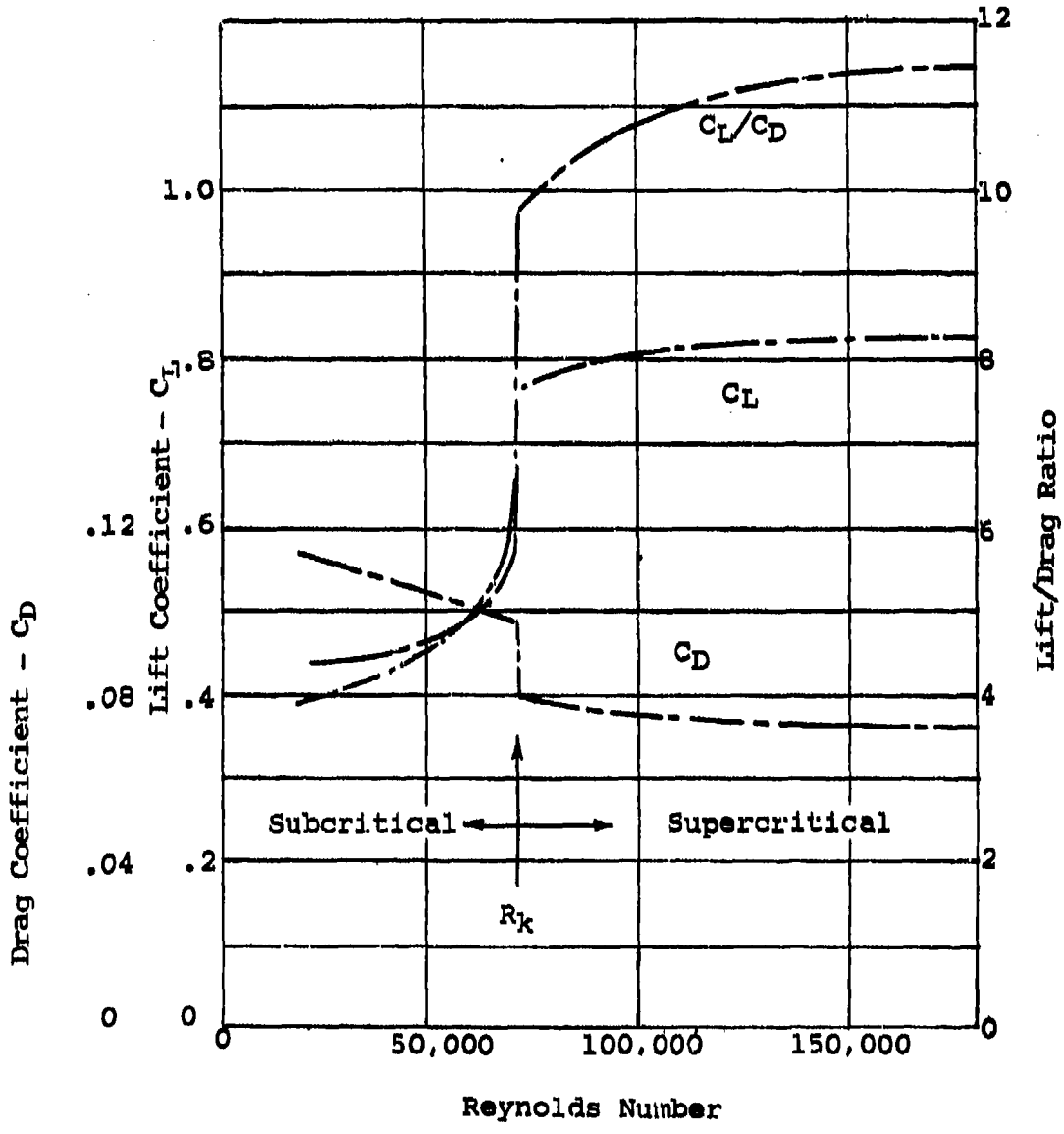

Figure 10. Variation of L/D and the Lift and Drag Coefficients With Reynolds Number for N-60 Airfoil at a Constant Angle of Attack of 6°.

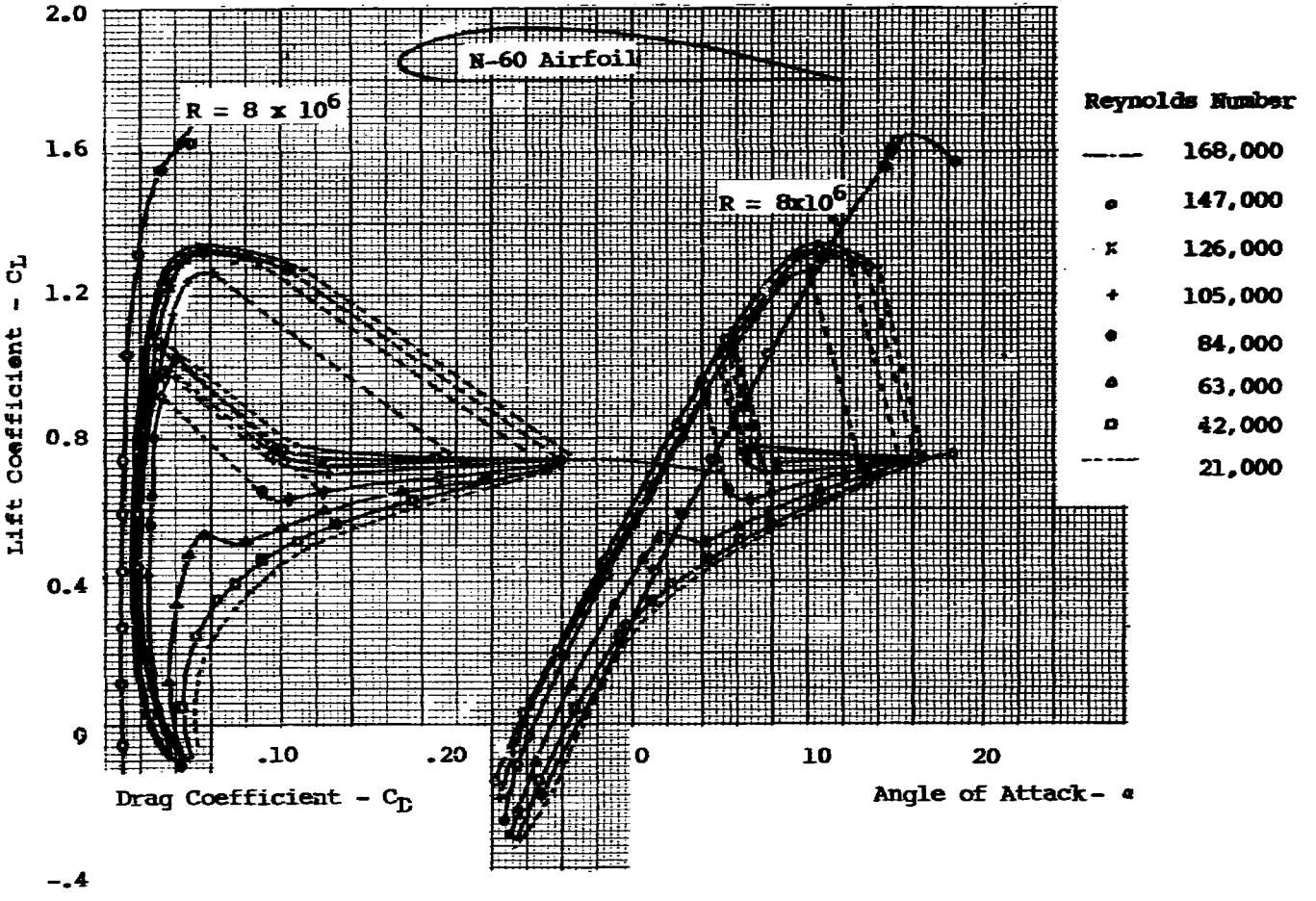

Figure 11. Lift and Drag Coefficient as a Function of Reynolds Number for N-60 Airfoil Tested in a Low Turbulence Wind Tunnel.

A literature search was conducted to find propeller test data that would be suitable to evaluate the effects of low operating Reynolds numbers on performance. The data given in References 16 through 20 appear to be the best available for this purpose. The data that appears to be the most useful and extensive are the series of propellers run at Stanford University by E. Reid for NACA. [16-18] These tests were run with three-bladed propellers with a diameter of 2.8 feet in the Stanford 7.5-foot wind tunnel. The Reynolds numbers of these tests cover a large portion of the operating range expected with mini-RPV propellers. In fact, the tests that were run are very close to those that would have been specified for the study of mini-RPV propellers if new tests were to be run. In addition to providing thrust and torque data for the entire propeller, detailed wake survey measurements were also made. These measurements of both torque and thrust are unique and are the only such known data available on propellers. Wake survey data of this type is now available for axial flow compressors and is very useful for investigating the details of the flow for each blade station of the compressor or propeller.

---

[16] Reid, E.G., THE INFLUENCE OF BLADE-WIDTH DISTRIBUTION ON PROPELLER CHARACTERISTICS, NACA TN No. 1834, March 1949.

[17] Reid, E.G., WAKE STUDIES OF EIGHT MODEL PROPELLERS, NACA TN No. 1040, July 1946.

[18] Reid, E.G., STUDIES OF BLADE SHANK FORM AND PITCH DISTRIBUTION FOR CONSTANT-SPEED PROPELLERS, NACA TN No. 947, January 1945.

[19] Grose, R.M., & Taylor, H.D., WIND TUNNEL STUDIES OF THE EFFECTS OF BLADE THICKNESS RATIO, CAMBER AND PITCH DISTRIBUTION ON THE PERFORMANCE OF MODEL HIGH-SPEED PROPELLERS, Hamilton Standard Rpt. No. HS-1352, June 1955.

[20] Grose, R.M., & Brindley, D.L., A WIND TUNNEL INVESTIGATION OF THE EFFECT OF BLADE ACTIVITY FACTOR ON THE AERODYNAMIC PERFORMANCE OF MODEL PROPELLERS AT FLIGHT MACH NUMBERS FROM 0.3 TO 0.9, Hamilton Standard Rpt. No. HS-1125, March 1954.

ANALYSIS OF LOW REYNOLDS NUMBER PROPELLER TEST DATA

To determine the effects of Reynolds number on propeller performance, the test data of References 16 through 18 were compared to that calculated using the strip analysis method and data of Reference 1. Since the accuracy of the strip analysis calculation procedure was demonstrated to be good for conditions corresponding to high Reynolds number, the difference between the efficiency measured by test and that calculated can be considered to be due to operation at a Reynolds number below 500,000.

As in the case of the analysis of the accuracy of the calculated propeller performance at high Reynolds number, the difference between the test and calculated results was found for a range of operating C_L at $x = .7$ and is given in Figure 12. The Reynolds numbers of the test were in the range of 1.3 to 2×10^5 for the working portion of the blade. Thus, the difference in performance shown is that due to changes caused by operation at low Reynolds number. The efficiency change given in Figure 12 applies for propellers with blades using NACA 16 and Clark Y sections and with an integrated design C_L of 0.7 for a range of planforms and, therefore, loadings.

The difference between the test and calculated efficiency shown in Figure 12 shows the importance of the operating lift coefficient in comparison to the design value. When the operating C_L is near design, the change in efficiency due to Reynolds number is small. However, when C_L is several points below the design C_L, large differences in efficiency are obtained. These changes in efficiency reflect a large drag change due to Reynolds number in much the same way as were measured for two-dimensional airfoils (Figure 11). The drag change between high and low Reynolds numbers also showed little change at C_L near the design value, but large drag changes at other conditions.

Detailed comparisons of the test and calculated efficiency for Model 4 of Reference 17 are shown in Figures 13 and 14. These were done for Reynolds number of about 1.5×10^5. The results

---

[1] Borst, et al.

[16] Reid.

[17] Reid.

[18] Reid.

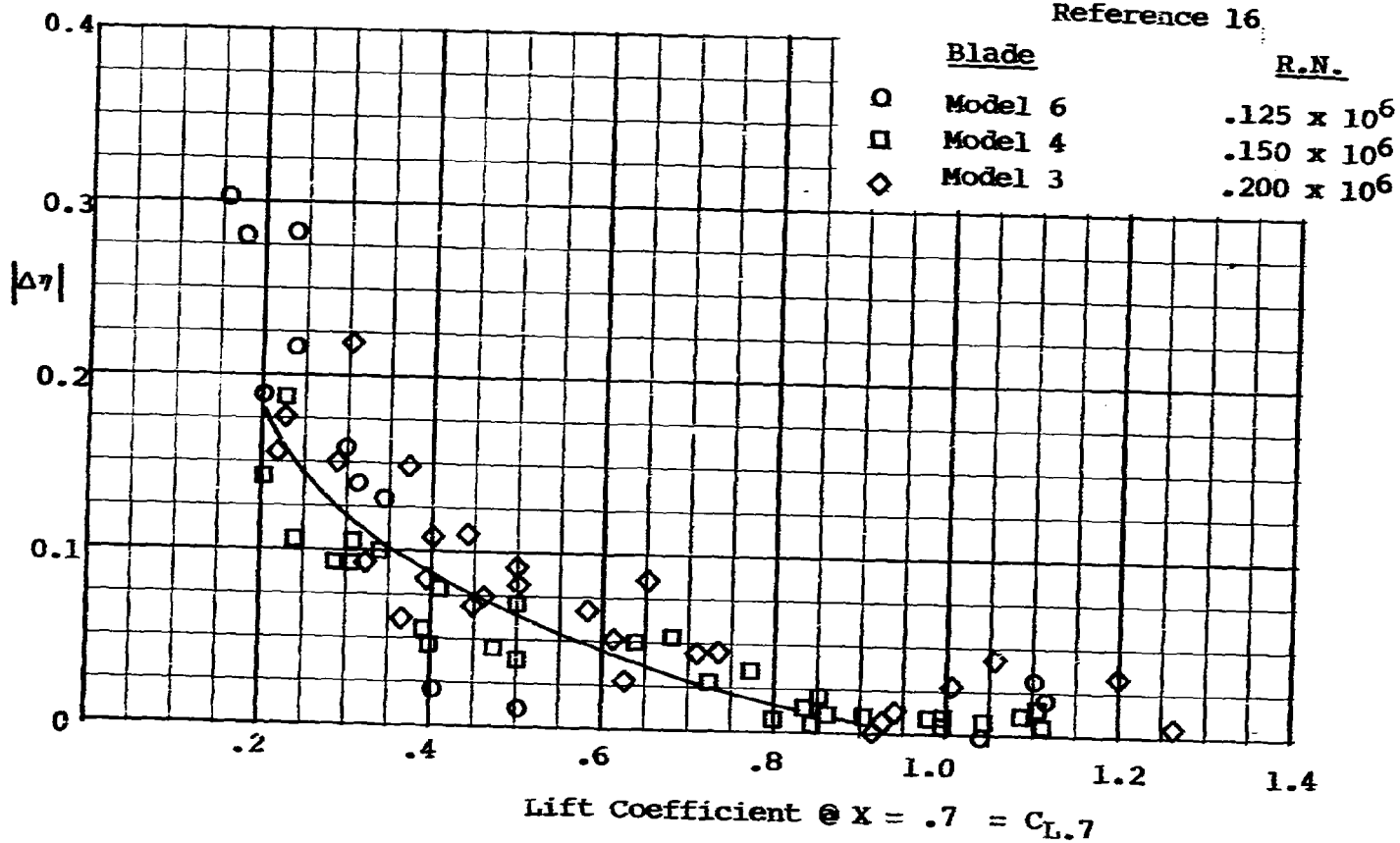

Figure 12. Difference Between Calculated and Test Efficiency as a Function of Operating Lift Coefficient — Airfoil Data Uncorrected for Reynolds Number.

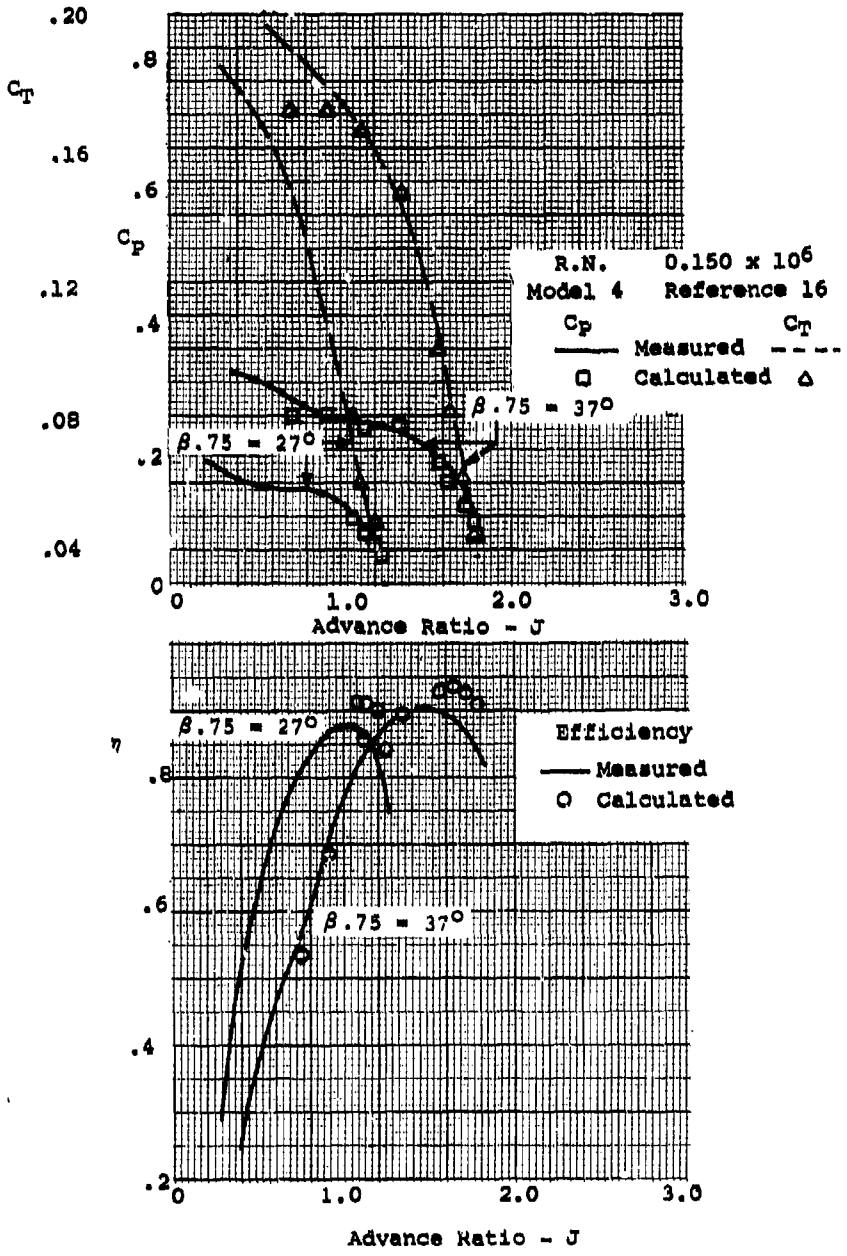

Figure 13. Comparison of Calculated Propeller Performance Data With Test Data at Low Reynolds Number — Airfoil Data Uncorrected for Reynolds Number.

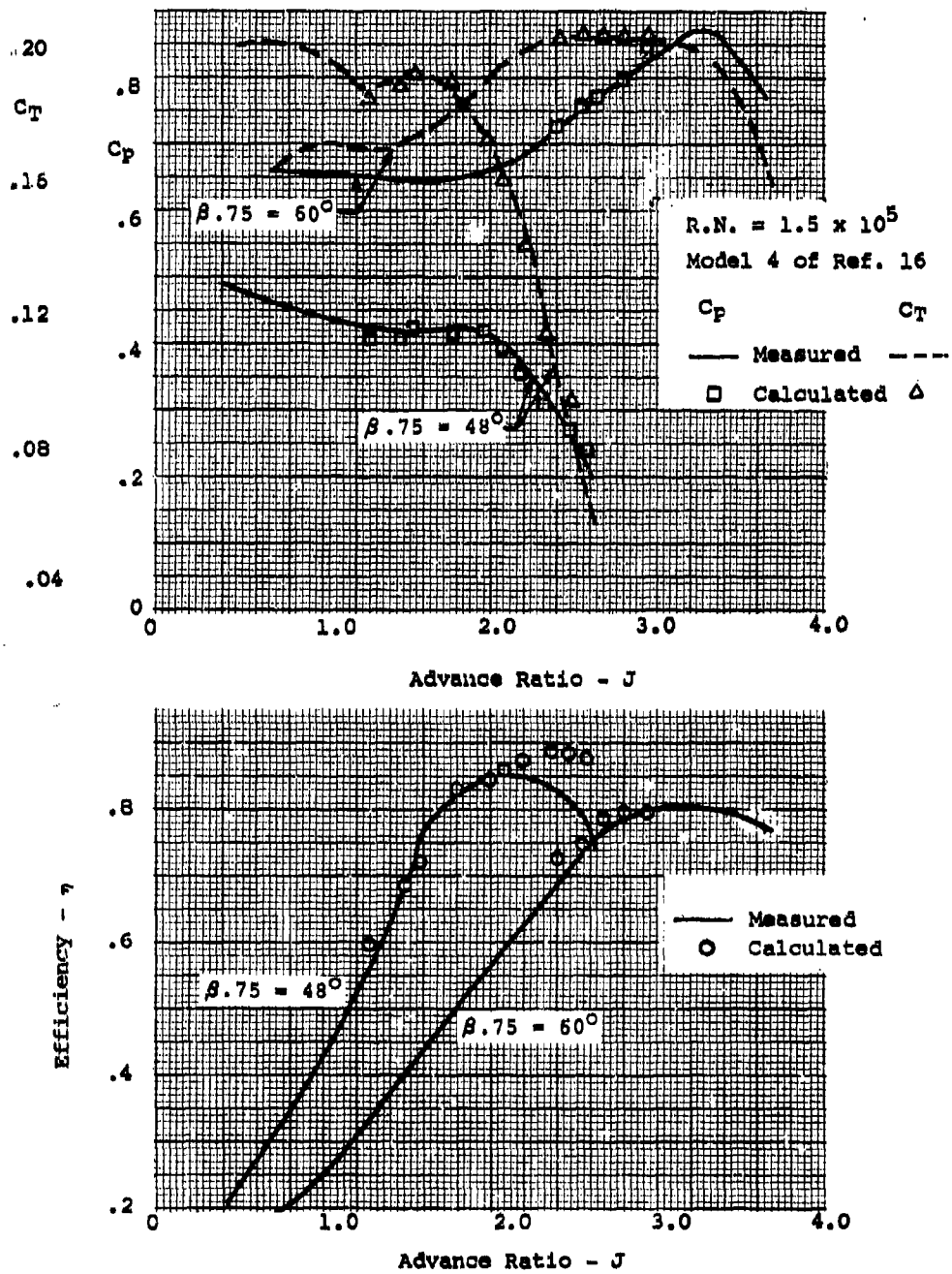

Figure 14. Comparison of Calculated Propeller Performance Data With Test Data at Low Reynolds Number — Airfoil Data Uncorrected for Reynolds Number.

again show good agreement in propeller efficiency and thrust coefficients for the higher power levels or at conditions where C_L operates near the design C_L. As the power coefficient and, therefore, the operating C_L decrease, the test efficiency becomes much lower than the calculated value for all four blade angles investigated.

Detailed comparisons of the variation of test vs calculated values of the thrust and torque distributions for the Model 4 propeller were also made (Figures 15 and 16). As indicated, these comparisons of thrust and torque are unique for propellers and were very useful in determining the necessary changes in the airfoil data due to operation at low Reynolds numbers.

PROPELLER TEST DATA REDUCTION

With the measurements of the thrust and torque coefficients aft of the propeller, the operating lift and drag coefficients can be found if the theory used to calculate the equivalent two-dimensional flow conditions is valid. Since, as shown previously, the calculations using theory to find the induced angle of attack are accurate, the results of the propeller data reduction to section lift and drag coefficients should be reasonably good. This assumes that the measured values of thrust and torque at each blade station in the wake truly represent the conditions on the blade at that station.

To calculate the lift and drag coefficients from the measured thrust and torque coefficients, the following equations are used:

$$C_L = \frac{4}{B}\left(\frac{nD}{W}\right)^2 \frac{1}{(b/D)} \left(\frac{dC_T}{dx}\cos\phi + \frac{dC_Q}{dx}\frac{2}{x}\sin\phi\right) \qquad (9)$$

$$C_D = \frac{4}{B}\left(\frac{nD}{W}\right)^2 \frac{1}{(b/D)} \left(\frac{dC_Q}{dx}\frac{2}{x}\cos\phi - \frac{dC_T}{dx}\sin\phi\right) \qquad (10)$$

where

$$W/nD = J\left(\frac{1 + \bar{w}/2(1-\sin\phi}{\sin\phi}\right) \qquad (11)$$

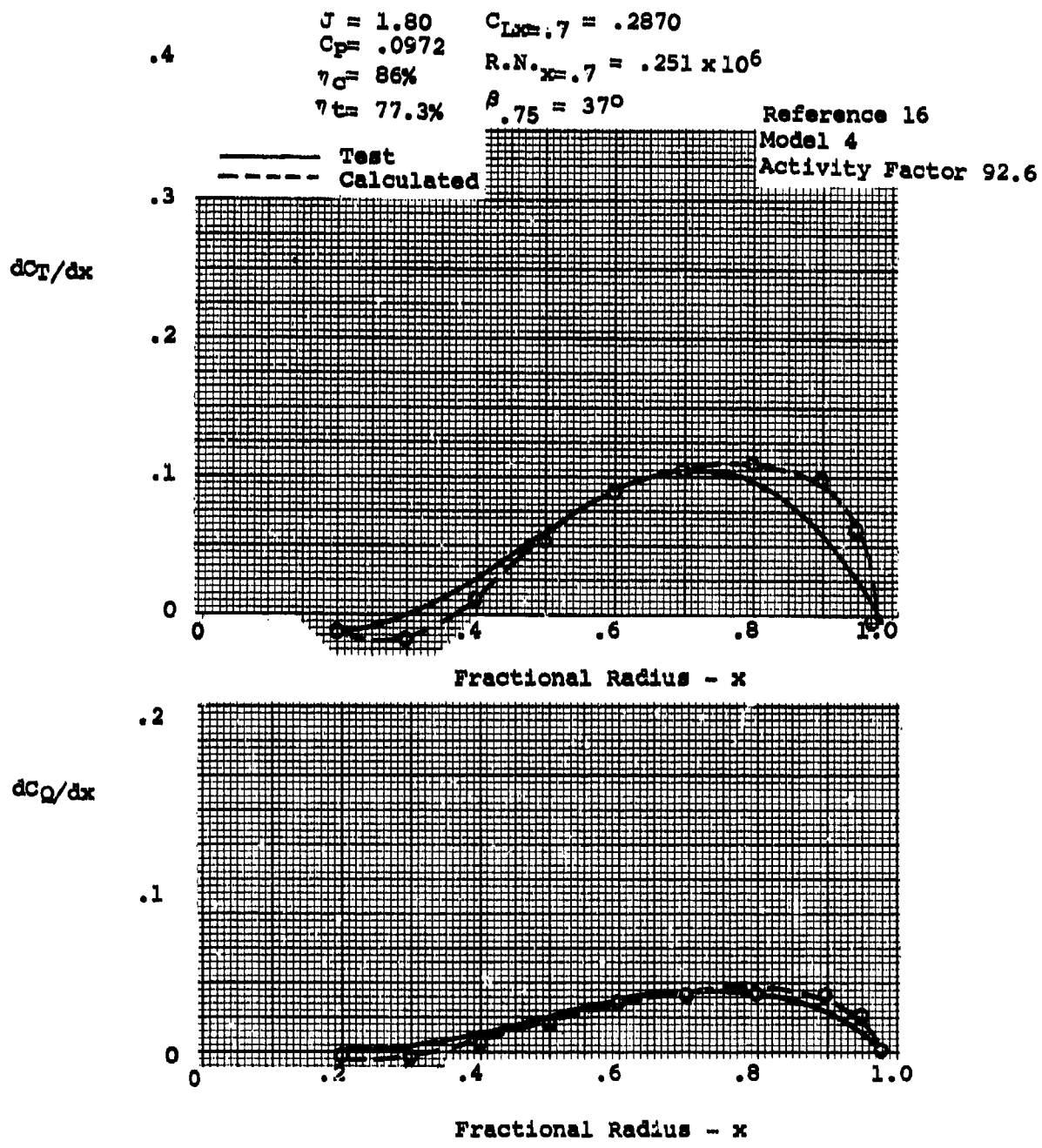

Figure 15. Comparison of Measured and Calculated Load Distribution — Airfoil Data Uncorrected for Reynolds Number.

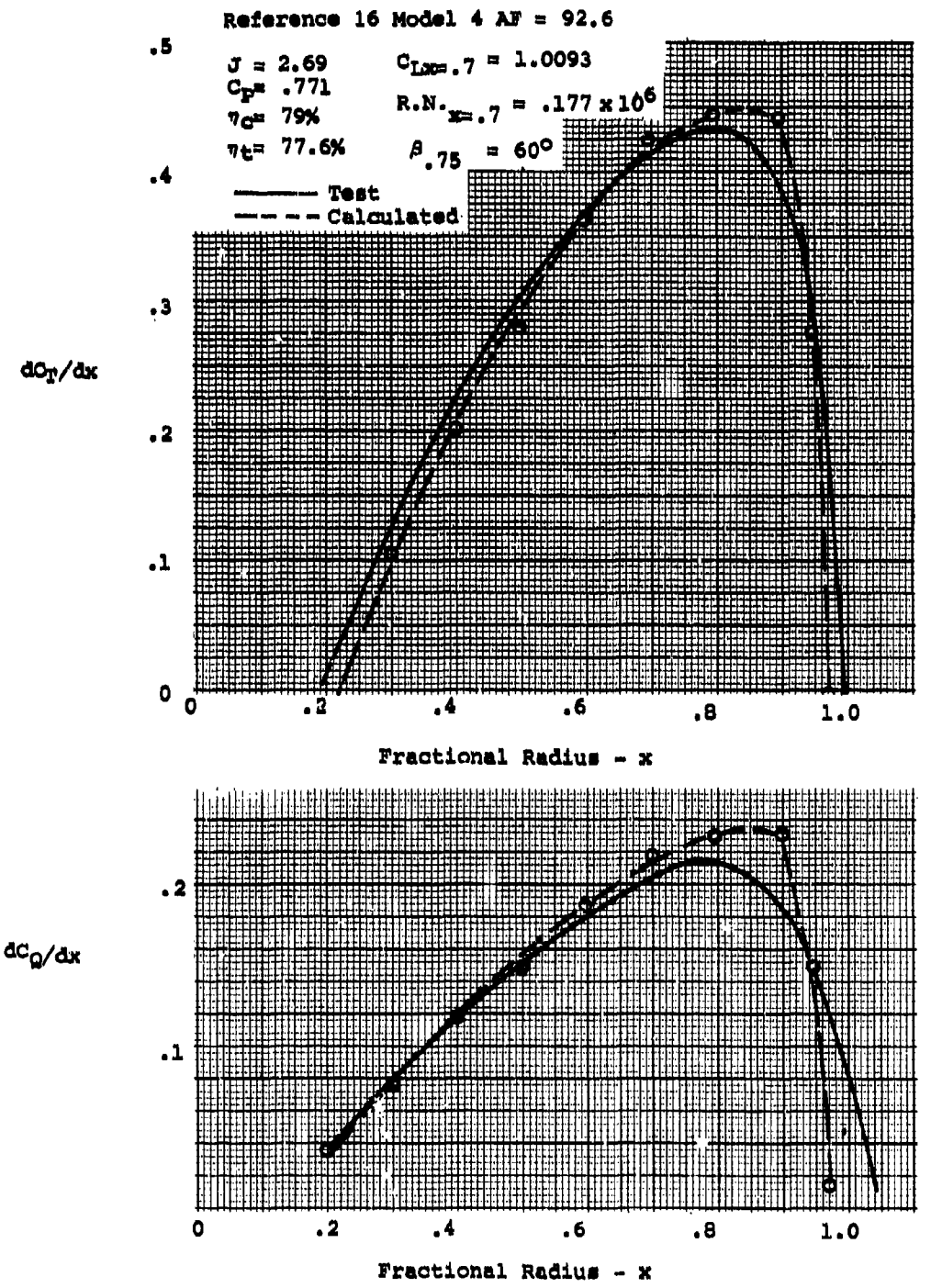

Figure 16. Comparison of Measured and Calculated Load Distribution — Airfoil Data Uncorrected for Reynolds Number.

These equations are easily derived from the dC_Q/dx and dC_T/dx equations of Reference 1 and Equations (4) and (5).

The wind angle ϕ is a function of the lift coefficient and must be determined to find the operating C_L and C_D from test data. Because there was no direct measurement of the swirl angle, it is necessary to use theory [1] for finding ϕ. Thus, knowing test values of dC_Q/dx and dC_T/dx the lift and drag coefficients can be calculated using the theoretical variation of the wind angle as determined.

Lift Data from Propeller Wake Survey

Using the wake survey data of Reference 17 and Equation (9), lift coefficients were calculated from the test data of several different blade models, one of which is shown in Figure 17. Comparison of the lift coefficients determined from the wake survey and the two-dimensional airfoil data used in the standard strip calculation B-87 showed reasonably good agreement. At the lower lift coefficients there appears to be an error of angle of attack of about 1 to 2 degrees. However, the agreement over the angle of attack range between the two sets of data, including conditions approaching the maximum lift coefficient C_{Lx}, is quite good.

The B-87 two-dimensional airfoil data was obtained mainly from References 21 and 22. Although these data were run at Reynolds numbers above the critical, the maximum lift appears to be questionable. A comparison of the maximum lift obtained from that of Reference 15 with the values estimated from Reference 22 shows that C_{Lx} used in the B-87 program propeller calculations is too low. For normal propeller performance estimates, this generally does not present a problem; however, where the blade operating C_L does approach the maximum as at the low-speed takeoff condition, it is necessary to modify the basic

---

[1] Borst, et al.

[15] Hoerner and Borst.

[17] Reid.

[21] Abbott, Ira H., & Von Doenhoff, A.E., THEORY OF WING SECTIONS, Dover Publications, Inc.

[22] Lindsey, W.F., Stevenson, D.B., & Daley, Bernard N., AERODYNAMIC CHARACTERISTICS OF 24 NACA SERIES AIRFOILS AT MACH NUMBER BETWEEN 0.3 and 0.8, NACA TN 1546.

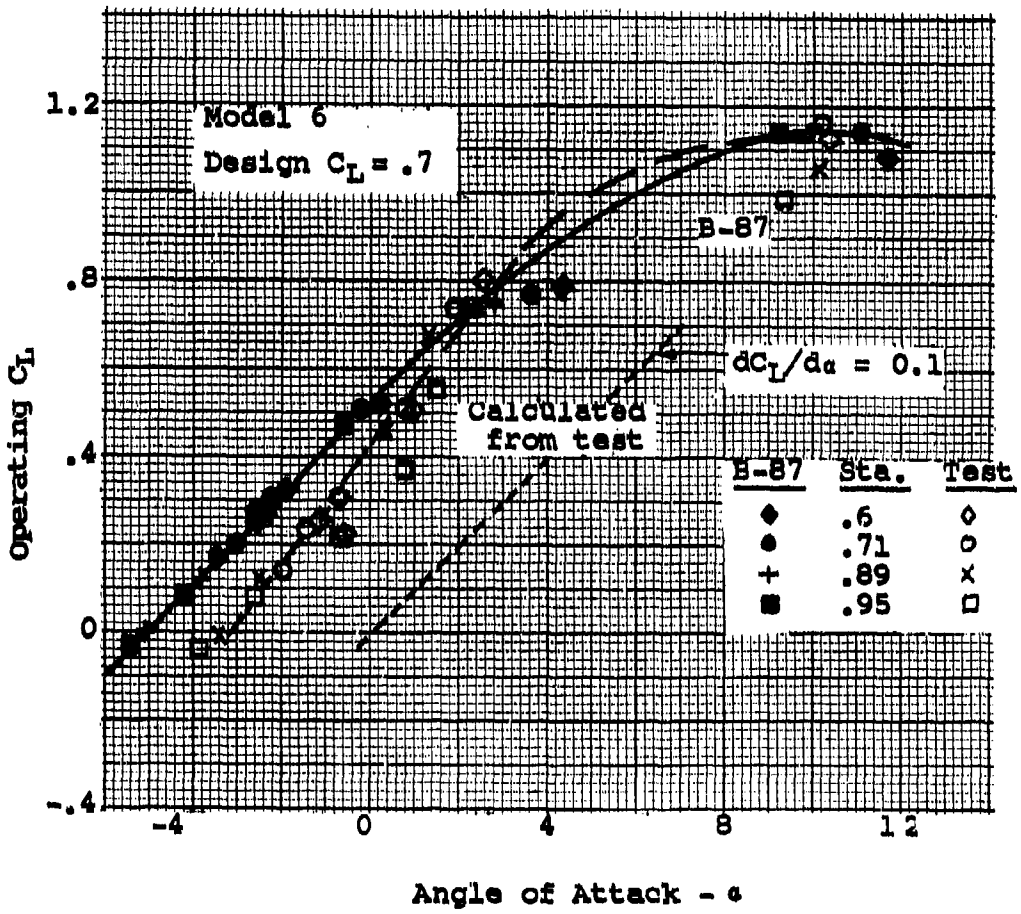

Figure 17. Comparison of Lift Coefficient Calculated From Propeller Test Data With C_L From Two-dimensional Airfoil Data, B-87 Propeller Strip Analysis Program — Reynolds Number = 1.24×10^5.

airfoil data as described in Reference 1 to account for a more realistic C_{Lx}. Because of this low value of C_{Lx} and the variation of C_L with the angle of attack used for performance calculations in the B-87 program, it appears to be suitable for the analysis of mini-RPV propellers. This is apparent when one compares the C_L reduced from the model test data of Reid with that of B-87. Based on the C_L of the reduced propeller test data for low Reynolds numbers and the available low Reynolds number airfoil data, such as shown in Figure 17, it appears that no corrections are required for modifying the B-87 airfoil lift data for application to the design and analysis of RPV propellers. This is especially true as the main problem with Reynolds numbers in the case of lift is that of C_{Lx}. Since the mini-RPV propellers are generally designed for the condition for highest expected loading such as climb, the airfoils will be operating at lift coefficients well below their maximum. High efficiency will then be obtained at the peak loading conditions.

Drag from Propeller Test Data

Two-dimensional drag coefficient data was also found from the propeller wake survey data of Reid, using Equations (9) and (10); the results of one model are given in Figure 18. The drag data obtained from the propeller wake survey measurements agree with the two-dimensional data of B-87 when the operating C_L is well below the design value. At higher values of operating C_L, near the design value, the data obtained from the wake survey data results in negative drag coefficients. Since clearly negative values of drag are not real, the procedure for reducing the propeller wake survey was examined to determine the cause.

A composite curve derived from the several models tested is shown in Figure 19. In examining the results of the reduction of the wake survey data, it is noted that the shape of the drag curve, Figure 18, as a function of C_L appears to be reasonable. Based on the physical quantities used in determining C_D, the most likely sources of error are the measurements of dC_Q/dx, dC_T/dx, x and the calculation of ϕ. Integrations of wake survey thrust and torque data are in good agreement with the force measurements and, therefore, are not considered the cause of error. Analysis of the calculation of the wind angle ϕ indicated that the differences required to account for the values of negative drag obtained could not exist and still achieve the accuracy observed in checking propeller-induced efficiency. Therefore, the assumption that the measured values of x in the wake corresponded to x on the blade appeared to be the source of error that caused the negative drag coefficients.

[1] Borst, et al.

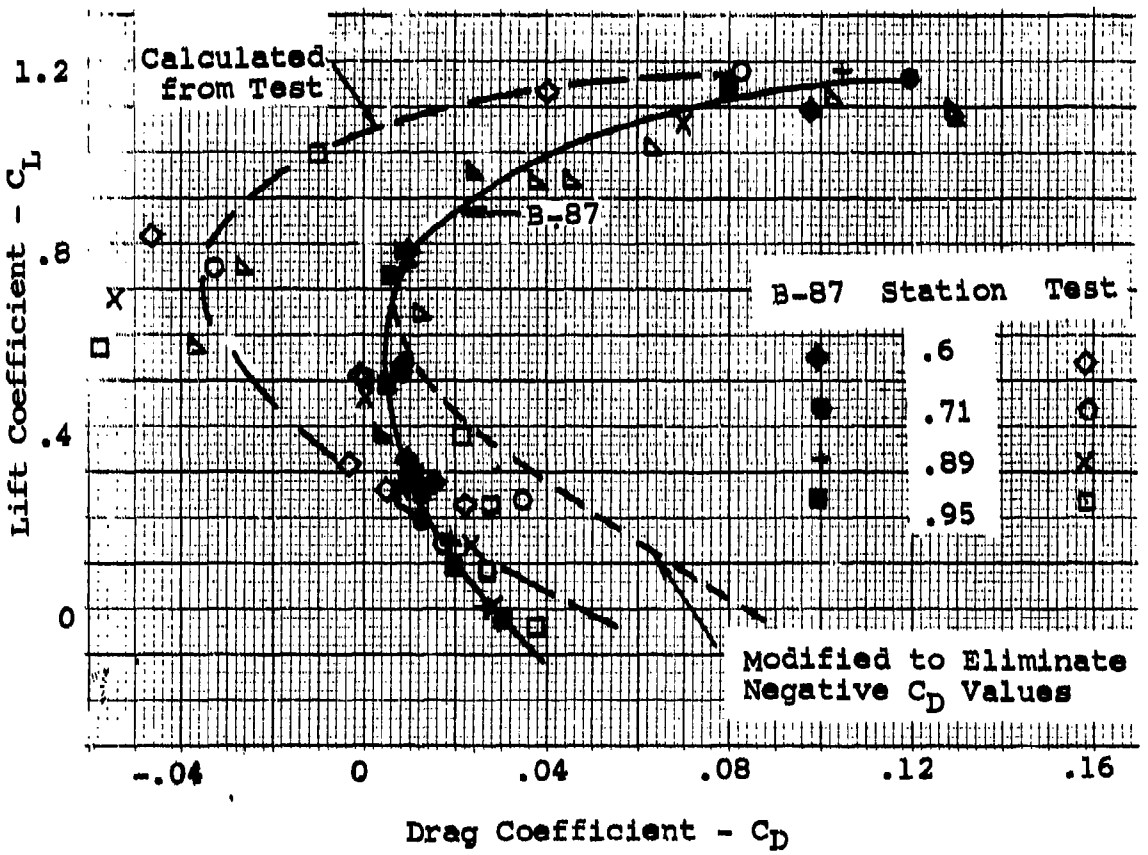

Figure 18. Comparison of Lift and Drag Coefficients Calculated From Propeller Test Data With Two-dimensional Airfoil Data, B-87 Propeller Strip Analysis Program — Reynolds Number = 1.24×10^5.

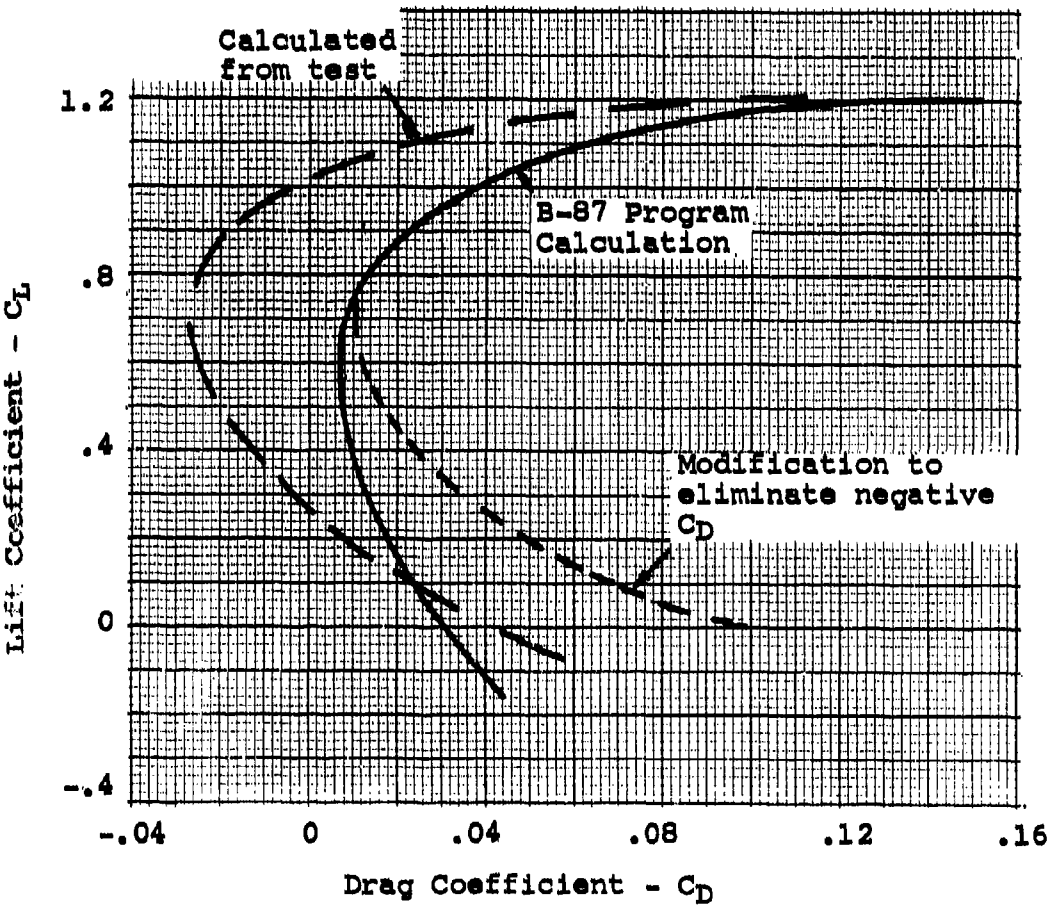

Figure 19. Composite Airfoil Characteristics With Modification. Reynolds Number = 120,000 $C_{L_1} = .7$

Based on the low Reynolds number test data it was observed that when the airfoil is operating above the critical, the drag, when the operating C_L is near the design C_L of the airfoil, will be equal to that at the high Reynolds number (Figure 18). Thus, the drag coefficient in the rangeof $C_L = .7$ from the Reid wake survey data should correspond closely to that in the B-87 program, rather than be negative as shown in Figure 18. It was found that using the dC_T and dC_Q values for wake station $x = .71$ would result in correct C_D calculation for blade stations $x = .65$, and wake station $x = .89$ corresponded to blade station $x = .82$, etc. Furthermore, since finite values of thrust and torque were measured at wake station 1.05 it could be concluded that the errors resulting in negative drag coefficients were caused by the expansion of the slipstream.

Based on the above analysis the drag curve calculated from the wake survey data should be shifted so that the data agrees with the B-87 data at a C_L equal to the design C_L. The curve shift corresponding to this change is shown in Figure 19. After this adjustment, the change in C_D due to operating at the lower Reynolds numbers can now be estimated.

LOW REYNOLDS NUMBER CORRECTION

Since sufficient systematic low Reynolds number two-dimensional airfoil data was not available for calculating the performance of mini-RPV propellers, it is necessary to find a Reynolds number correction for the B-87 airfoil data. In developing this correction, the available low Reynolds number data from both two-dimensional airfoil data and the propeller wake survey data was used. The use of the propeller wake survey data for finding the correction to the airfoil is an important advantage, as the data then applies directly.

It was necessary to find only a correction to the drag coefficient data for the Reynolds number, as the lift data already used in the B-87 computer data applies (as previously shown). In determining the correction to the drag data of the B-87 for the Reynolds number, it was necessary to assume that it would apply to the data for all types of airfoil and would be independent of Mach number. From the available data it appears that the drag change will be constant over a range of operating lift corresponding to the design lift coefficient plus 0.2. Thus, the drag correction for the Reynolds number is a function of the quantity

$$f_d = f\left|C_{Li} + .2 - C_{Lo}\right| \qquad (12)$$

where f_d = C_D low Reynolds number/ C_D high Reynolds number

C_{Li} = Design C_L

C_{Lo} = Operating C_L

The drag coefficient correction for the Reynolds number f_d then becomes a multiplying factor to the B-87 airfoil data and is a function of design C_L and Reynolds number. Basically, the correction shown in Figure 20 is considered to apply at Reynolds numbers above and below the critical. Although the location of the critical Reynolds number is difficult to identify for all the airfoils, the f_d variation shown does account for operation above the critical. The variation of f_d with $|C_{Li} + 0.2 - C_{Lo}|$ shown for the various Reynolds numbers in Figure 20, is based mainly on the reduction of the wake survey test data.

Ducted Fans

When calculating the performance of ducted propellers, procedures have been developed to correct the flow field in the duct so that two-dimensional airfoil data can be used to find the forces on the rotor. The theory for finding the induced

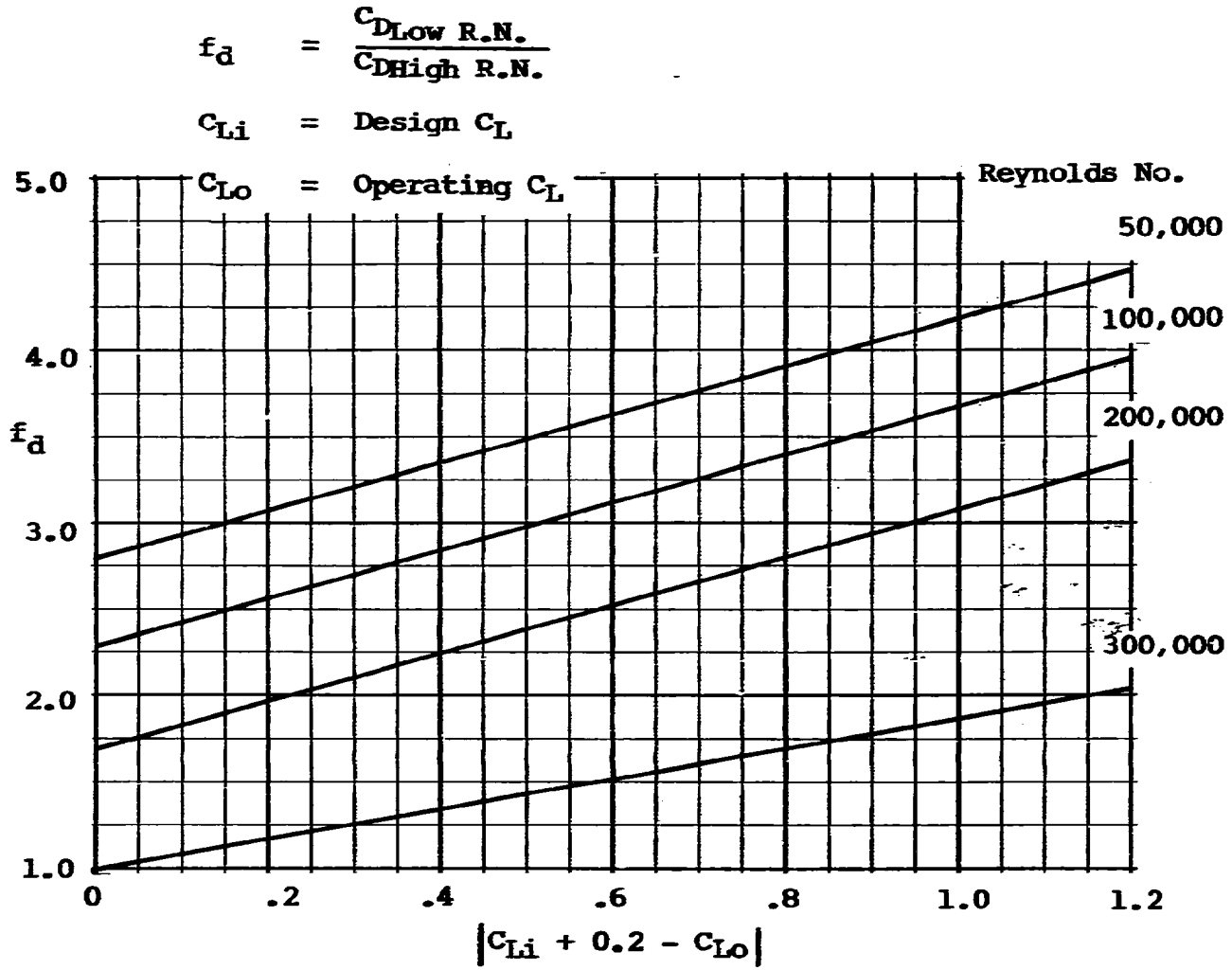

Figure 20. Correction to Drag Coefficient for Reynolds Number.

flow conditions at the rotor, and thus the induced efficiency, is similar to that used for an open propeller. The only differences are those made necessary by the application of the duct. Since two-dimensional airfoil data are used for the analysis of ducted fans, the f_d correction to the corrected B-87 data can be applied for the analysis of ducted fans operating at low Reynolds numbers.

CHECK OF THE REYNOLDS NUMBER f_d CORRECTION

Using the Reynolds number correction to the drag coefficient shown in Figure 20, the low Reynolds number propeller test data by Reid was analyzed. Comparison of the test efficiency with that calculated with the modified B-87 strip analysis computer program indicates that the drag correction has improved the accuracy of the calculated results. As shown in Figure 21, the calculated efficiency agrees with the test values at low Reynolds number within plus or minus 5%. This is nearly the same accuracy as that achieved for full-scale propellers and is believed to be within the accuracy of the basic test data.

RANGE OF OPERATION

With the new correction to drag, Figure 20, to account for Reynolds number above and below the critical, the performance and characteristics of propellers can now be determined over the complete range of operation. This can be done using the strip analysis procedures described in the B-87 computer program and the equivalent hand calculation described in Reference 1. The methods and data now apply for the range of operation of the original strip analysis program plus Reynolds number down to 50,000. This includes all the operating range encountered by mini-RPV propellers.

---

[1] Borst, et al.

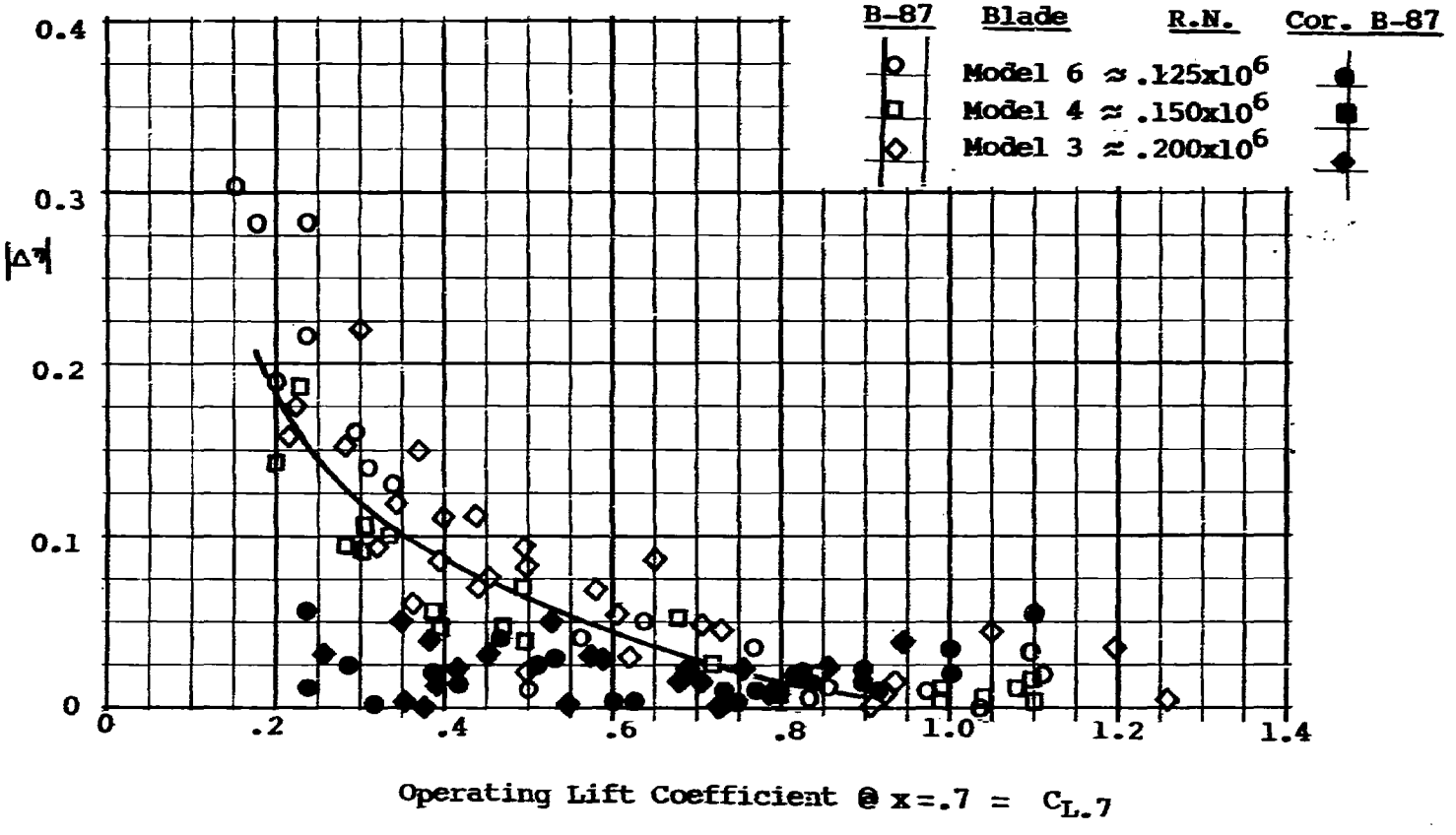

Figure 21. Comparison of Test and Calculated Propeller Efficiency With and Without the Reynolds Number Drag Correction.

SINGLE-POINT METHOD

For preliminary design studies the single-point method of determining propeller performance has been developed.[1] Such methods have been found to be useful as the performance can be quickly estimated using only charts and desk calculators for a large variety of configurations. Based on these performance estimates, the most promising configurations can then be further studied and optimized. The single-point method applies only for variable pitch constant speed propellers operating at high Reynolds numbers. To be useful for the analysis of RPV propellers the single-point method must be modified to apply at low Reynolds numbers and for propellers with a fixed blade angle.

THEORY

The theory of the single-point method is based on the assumption that the operating conditions of the blade can be specified by those occurring at one blade station. Thus, if the propeller is operating at a given blade loading, the lift coefficient at the .75 radius will describe the lift/drag ratio of the blade. The blade lift/drag ratio depends on the camber and blade angle distribution. Also, at a given advance ratio the profile performance of the propeller is a function of only the operating lift coefficient. The lift/drag ratio for the given camber level operating lift coefficient is thus independent of the blade number and activity factor.

In addition to the blade profile losses determined by the lift/drag ratio, there are the induced drag losses which are dependent on the total loading, blade number and advance ratio. The induced losses are considered to be independent of the lift/drag ratio and are determined based on the assumption that the blades are operating at the optimum load distribution. Since the desired propeller will be one that develops peak performance, this assumption is valid.

The basic development of the single-point method and the necessary charts for its application are given in Reference [1]. The charts can be used to calculate the performance of 2-, 3-, and 4-bladed propellers using blades with integrated design lift coefficients of 0 to .5 and activity factors 50 to 250. The charts for determining the lift/drag ratio of the blade apply in the Reynolds number range above 500,000. Since mini-RPV propellers operate at Reynolds numbers below the 500,000 and it is necessary to be able to find the blade angle for each power input, the single-point method must be modified.

[1] Borst, et al.

SINGLE-POINT METHOD FOR RPV PROPELLERS

The single-point method for calculating performance of RPV propellers is based on that given in Reference 1, modified to account for operation at low Reynolds numbers and fixed blade angles typical of RPV propellers. In addition, the procedure is set up so that the change due to interference losses of the installation can be estimated. The basic calculation procedure for the single-point method is given in Table 1, with the charts for finding the profile and induced losses given in Figures 22 through 28. The drag/lift ratio, representing the profile losses, shown in Figures 22 through 28 are corrected for the effects of Reynolds number using Figure 20, which was previously developed for the strip analysis calculations.

The single-point method of calculation for RPV propellers is based on the previously described concept that the performance at the three-quarters blade station will represent that of the entire propeller. Thus, to calculate the performance, it is necessary to find equivalent loading conditions for determining the operating lift/drag ratio and the conditions that determine the induced loading and, therefore, the induced efficiency. These quantities are basically a function of C_P and J_L, which are calculated in steps 10 and 11 from the given input as indicated in Table 1. J_L is based on the average local velocity due to body interference as determined in a later section of this report. At this given advance ratio J_L, the operating lift coefficient is a function of the loading parameter LO_1, which determines the drag/lift angle for a blade with a given integrated design C_L, IC_{Li} and J_L. Thus, LO_1 is calculated in step 12 and the drag/lift angle is found from Figures 22 through 24 knowing LO_1 and J_L, step 13.

The drag/lift angle γ, given on Figures 22 through 24, applies only for propellers operating at Reynolds numbers above 500,000. When the Reynolds number is below 500,000, γ must be corrected. To determine if this correction is needed and its value, the operating Reynolds number is found using the equation shown in step 14, Table 1. When the Reynolds number is less than 500,000, steps 15 through 22 are completed to find the true or corrected value of γ. This is done by finding the operating C_L at the .75x blade station, which can be shown to be a function of a new loading parameter LO_2 defined by the equation 13 and also step 18

$$LO_2 = \frac{4000 C_P \sin\phi_{.75}}{B(AF)J^2} \qquad (13)$$

[1] Borst, et al.

This loading parameter is used, instead of LO_1, as it normalizes the effect of the parameter J. From Equations (3) and (5)

$$\frac{dC_P}{dx} = \sigma C_L \frac{(\pi x)^2}{4} J^2 \left[\frac{1+\frac{\bar{w}}{2}(1-\sin^2\phi)}{\sin\phi}\right] \sin\phi(1+\tan\gamma\tan\phi) \quad (14)$$

Since $\sigma = bB/\pi xD$ and $AF = 1562(b/D)$ for rectangular blades

$$C_{L_{.75}} = f\left[\frac{C_P \sin\phi}{B(AF)J^2}\right] = f\left[\frac{LO_1 \sin\phi}{J^2}\right] = f(LO_2) \quad (15)$$

The variation of C_L @ $x=.75$ with LO_2 is shown on Figure 25. In determining LO_2 for finding the operating lift coefficient, it is necessary to know the true wind angle $\phi_{.75}$. This angle can be determined knowing the apparent wind angle $\phi_{o_{.75}}$ and the induced efficiency. The induced efficiency η_i is a function of C_P, J_L and B. The induced efficiency is efficiency of the propeller when the profile drag is zero, $\gamma = 0$, and is read from Figures 26 through 28.

To find the correction for Reynolds number to the drag/lift angle γ, f_d is read from Figure 20 knowing the quantity

$$|(IC_{Li} + 0.2 - C_{Lo})| = |(C_{Li} + 0.2 - C_{Lo})| \quad (16)$$

With the corrected value of γ_{corr}, step 22, the true efficiency can be calculated, step 23. The shaft efficiency is then found, step 24, along with the operating blade angle, step 25. This is the value normally quoted as it is the quantity from which the thrust is calculated, knowing the free stream velocity.

Since the foregoing calculation used the local velocity for determining the true efficiency, the loss of efficiency due to body interference is found by repeating steps 11 through 24, using V_o instead of V_L. This loss $\Delta\eta$ is then

$$\Delta\eta = \eta T_{@V_o} - \eta T_{@V_L} \quad (17)$$

TABLE 1. SINGLE-POINT METHOD FOR CALCULATING EFFICIENCY

Steps	Item	Symbol		Example
1.	Propeller Shaft Horsepower	HP	Input	4
2.	Propeller RPM	N	Input	5000
3.	Air Density Ratio $\rho/\rho_o = \sigma$		Input	.81
4.	Forward Velocity	V_o	Input	126.7 fps
5.	Average Local Velocity	V_L	Input	124.1 fps
6.	Propeller Diameter	D	Input	2.5 ft
7.	Propeller Blade Number	B	Input	2
8.	Blade Activity Factor	AF	Input	81
9.	Blade Integrated Design C_L	IC_{Li}	Input	.493
	Procedure			
10.	$C_p = (.0005HP)/\sigma\left(\frac{N}{1000}\right)^3\left(\frac{D}{10}\right)^5$		Calculate	.020
11.	$J_L = 60V_L/(ND)$		Calculate	.596
12.	$LO_1 = 400\ C_p/B(AF)$		Calculate	.049
13.	$\gamma = \tan^{-1} D/L$		Read Figures 22-24	2^o
14.	$RN = (\nu_{SL}/\nu)4AF\ D\sqrt{V_L^2 + (.75\pi ND/60)^2}$		Calculate	$.307 \times 10^6$
15.	η_i knowing B, C_p & J		Read Figures 26-28	.95
16.	$\phi_{o.75} = \tan^{-1}\ 0.4244J$		Calculate	14.2
17.	$\phi_{.75} = \tan^{-1}(\tan\phi_o/\eta_i)$		Calculate	14.9
18.	$LO_2 = 4000\ C_p \sin\phi_{.75}/B(AF)J^2$		Calculate	.355
19.	C_{Lo} = operating C_L		Read Figure 25	.360
20.	$\lvert IC_{Li} + 0.2 - C_{Lo} \rvert$		Calculate	.333
21.	fd = ($C_{D\text{corr. for RN}}$)/C_D		Read Figure 20	1.30
22.	$\gamma_{cor} = fd\gamma$		Calculate	2.60
23.	$\eta_T = \frac{\tan\phi_{o.75}}{\tan(\phi_{.75}+\gamma)}$		Calculate	.80
24.	$\eta_S = \eta_T\ V_o/V_L$ (See Eqs. 18 & 19)		Calculate	.82
25.	$\beta_{.75} = 10C_{Lo} - 6.34\ IC_{Li} + \phi_{.75}$		Calculate	15.4^o

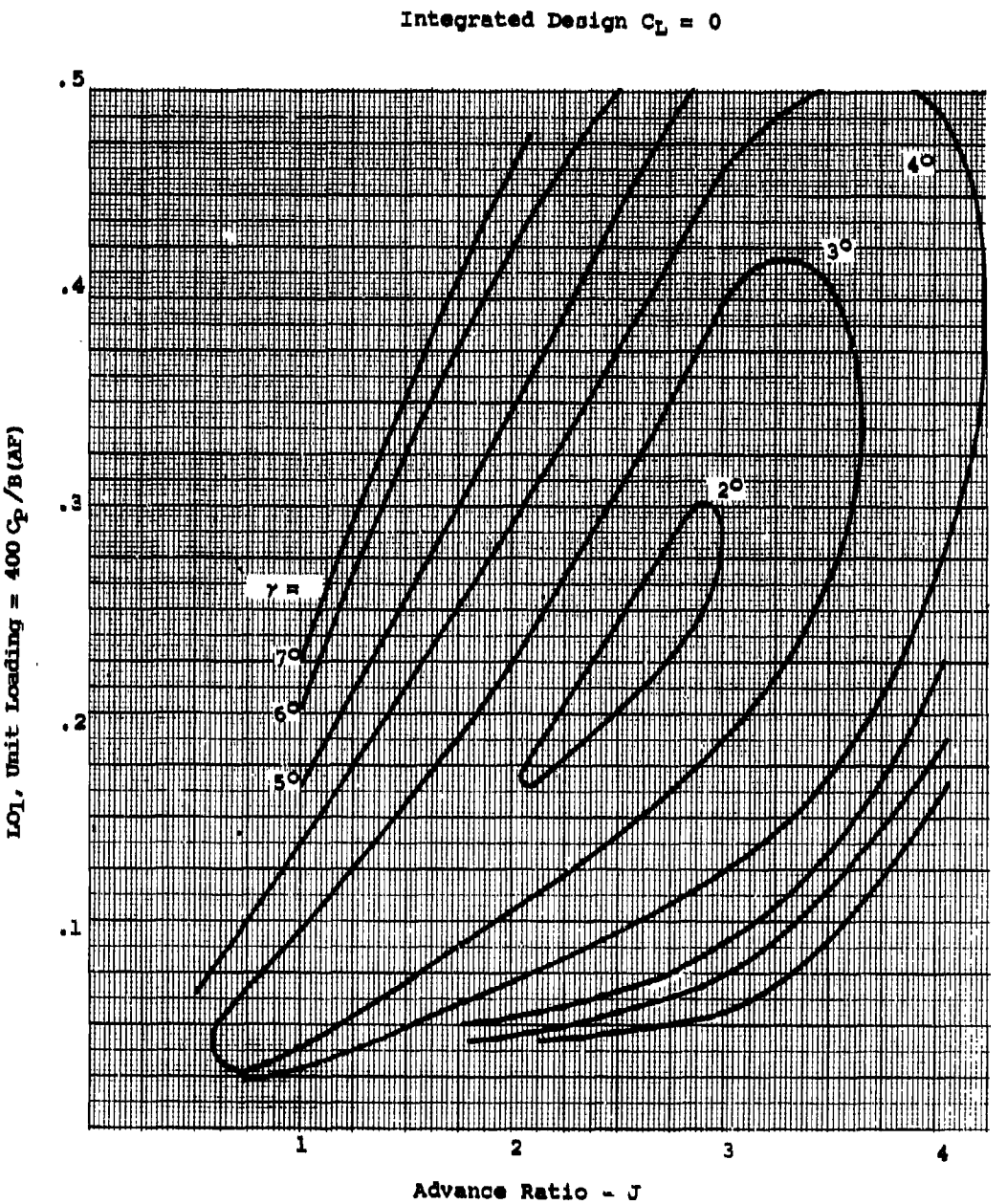

Figure 22. Propeller Profile Drag/Lift Characteristics - IC_{Li} = 0.

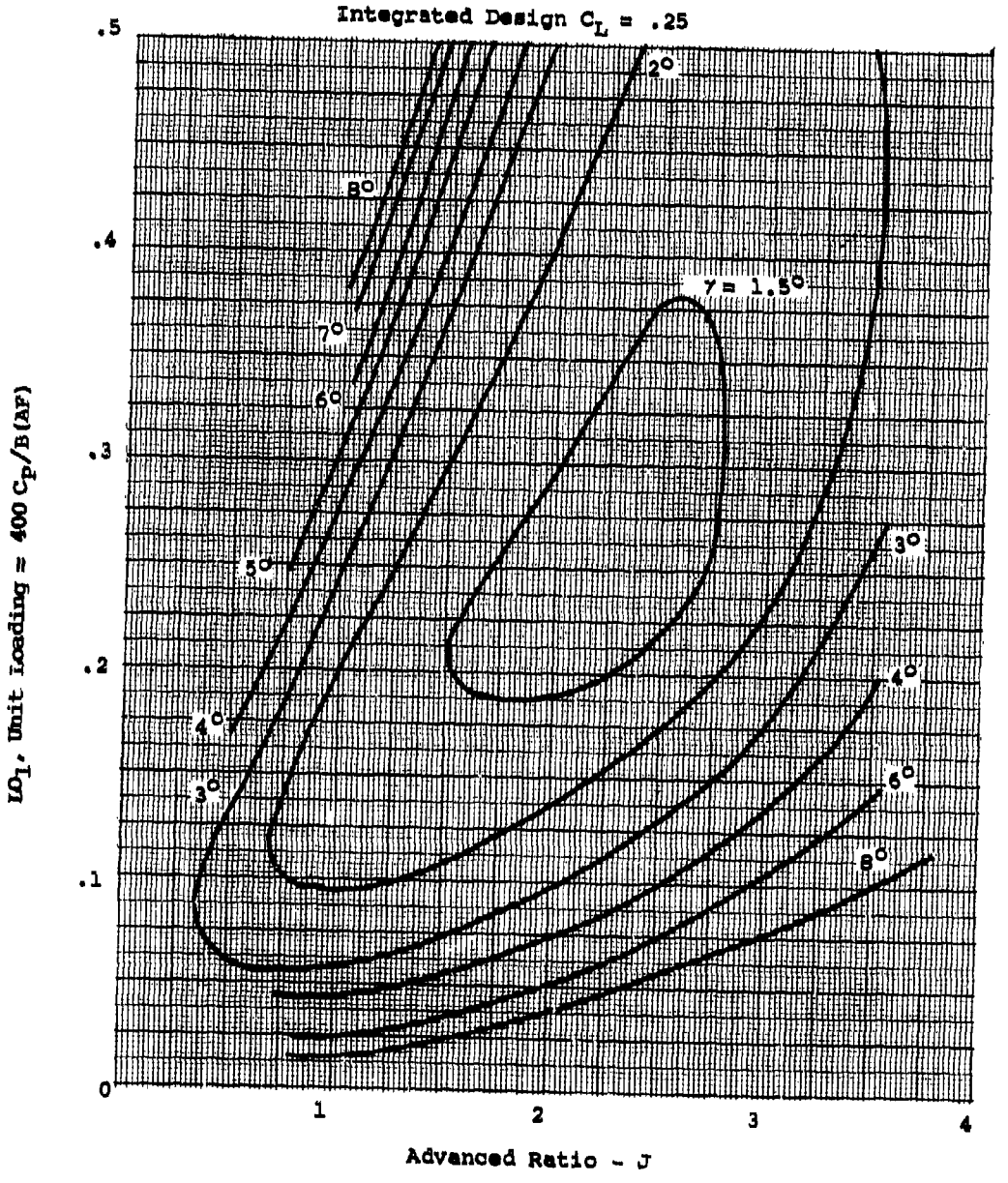

Figure 23. Propeller Profile Drag/Lift Characteristics — IC_{Li} = .25.

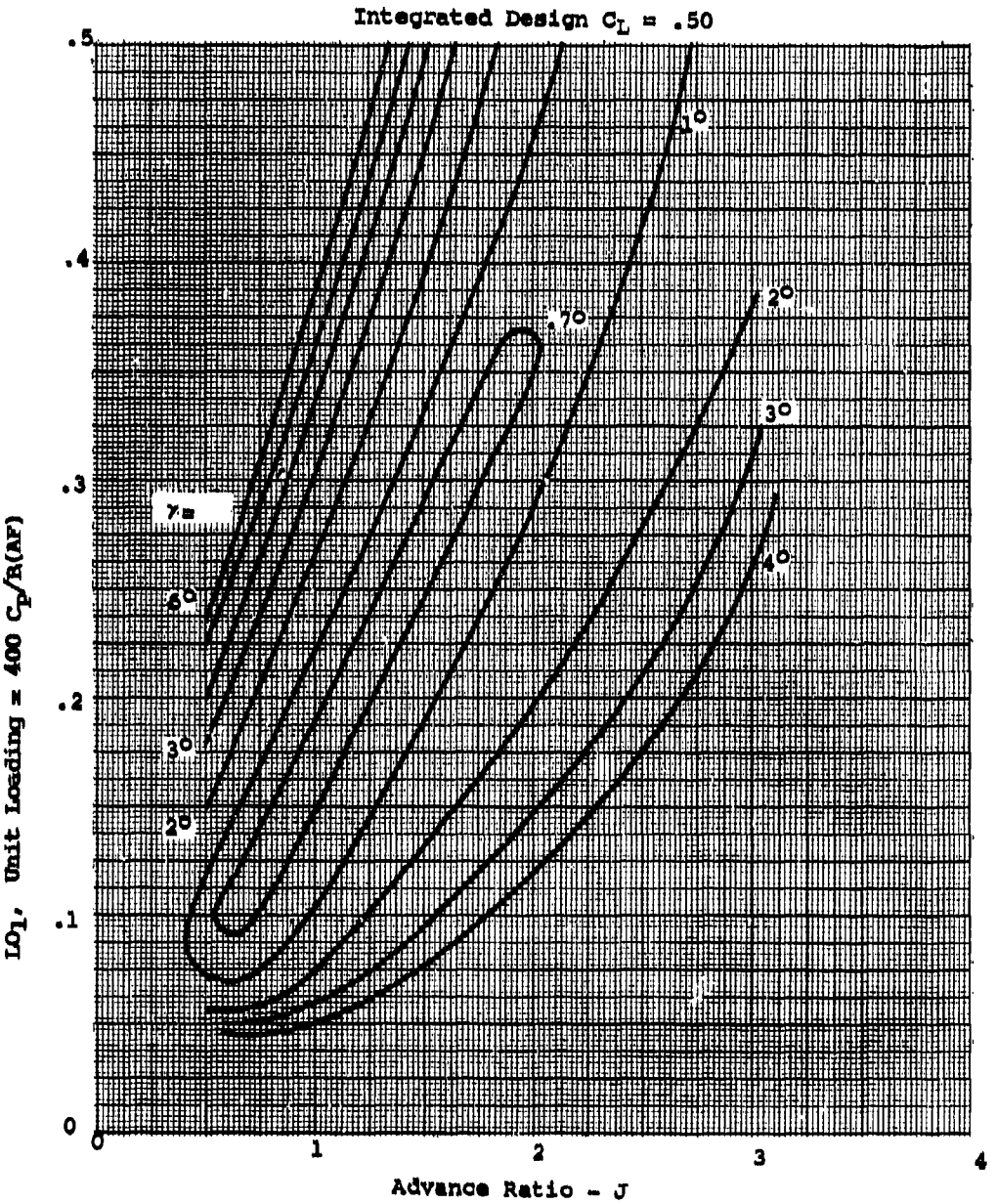

Figure 24. Propeller Profile Drag/Lift Characteristics — IC_{Li} = .5.

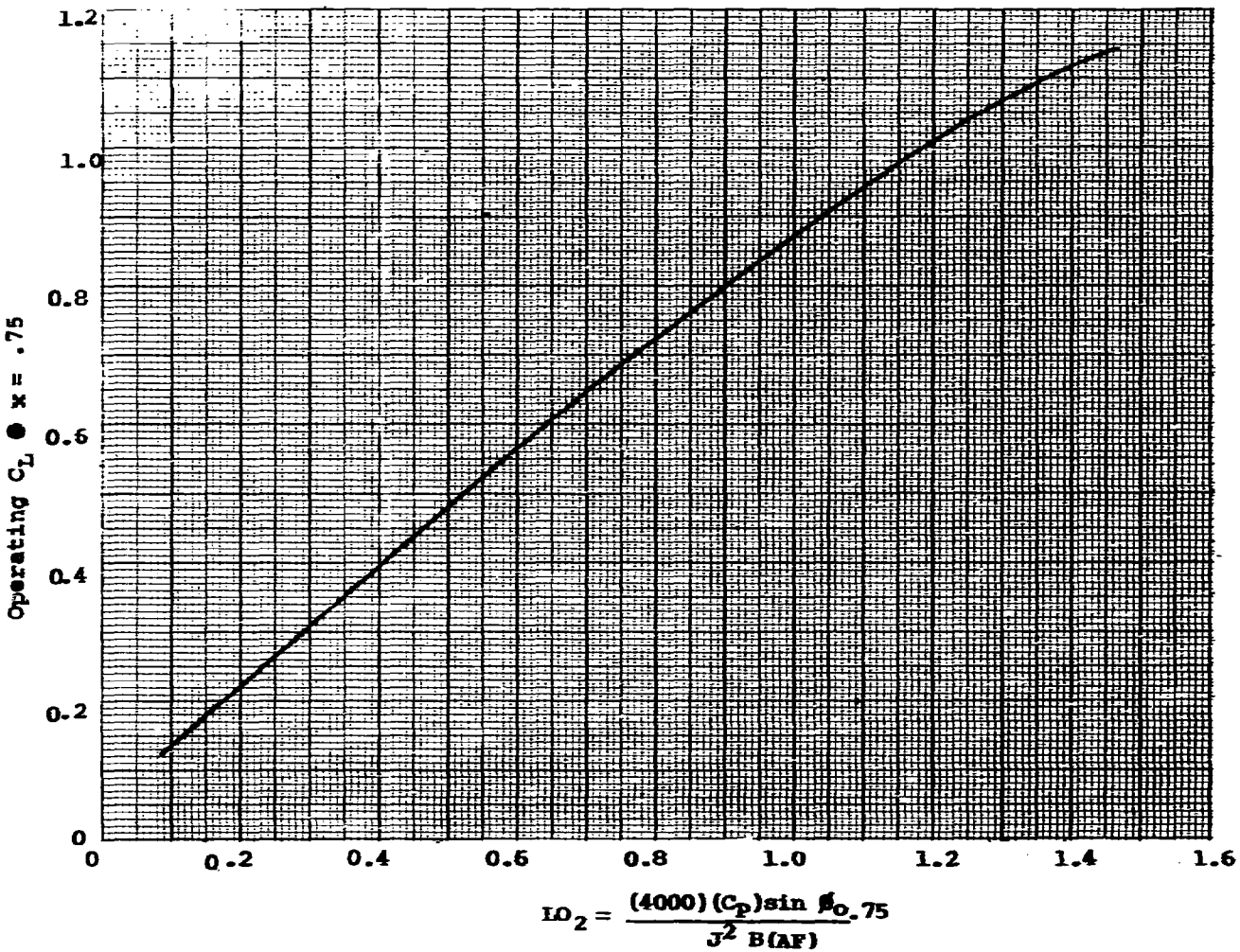

Figure 25. Integrated Loading Parameter as a Function of Operating Lift Coefficient.

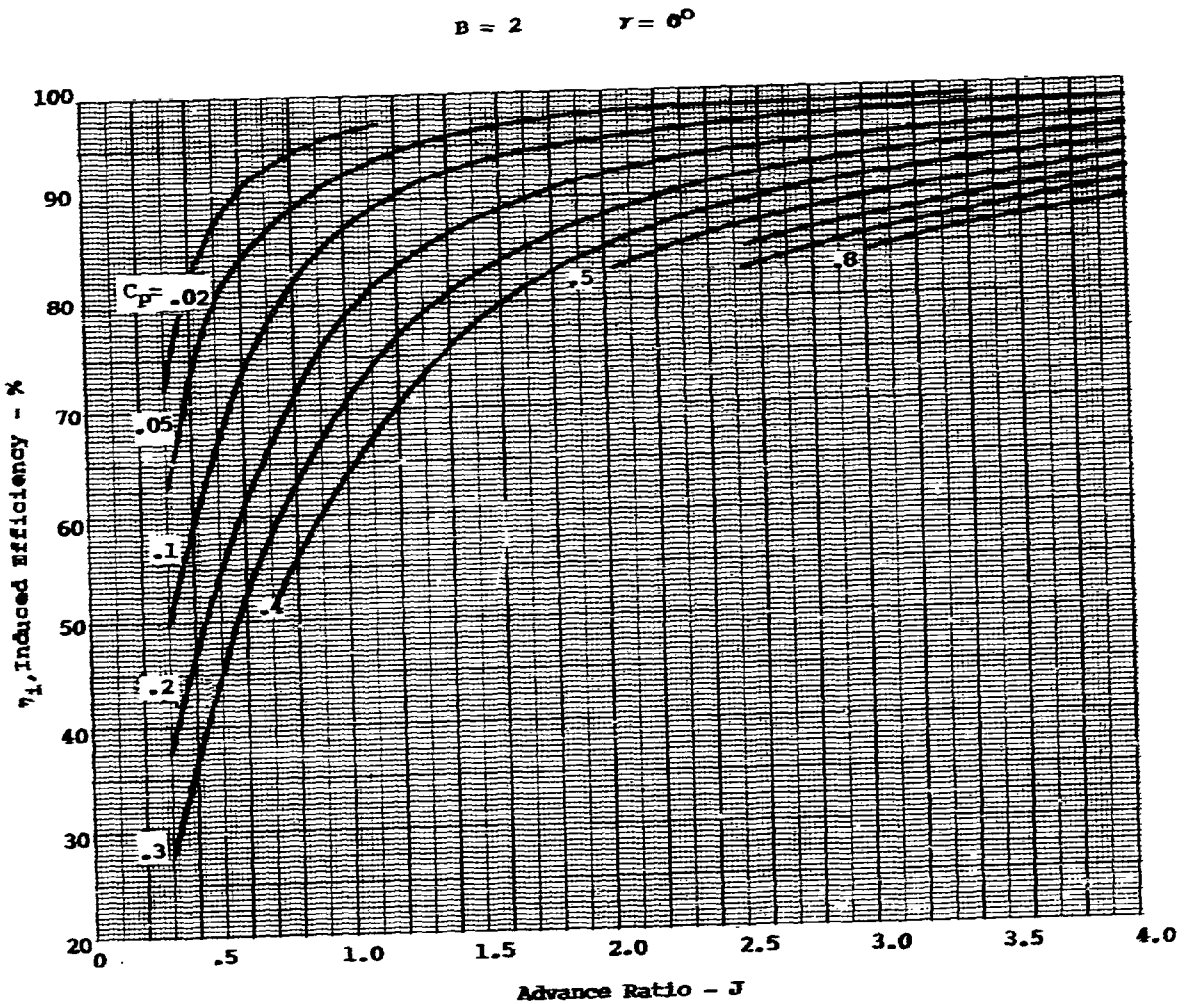

Figure 26. Efficiency at Drag/Lift Ratio of Zero as a Function of Advance Ratio — Two-bladed Propeller.

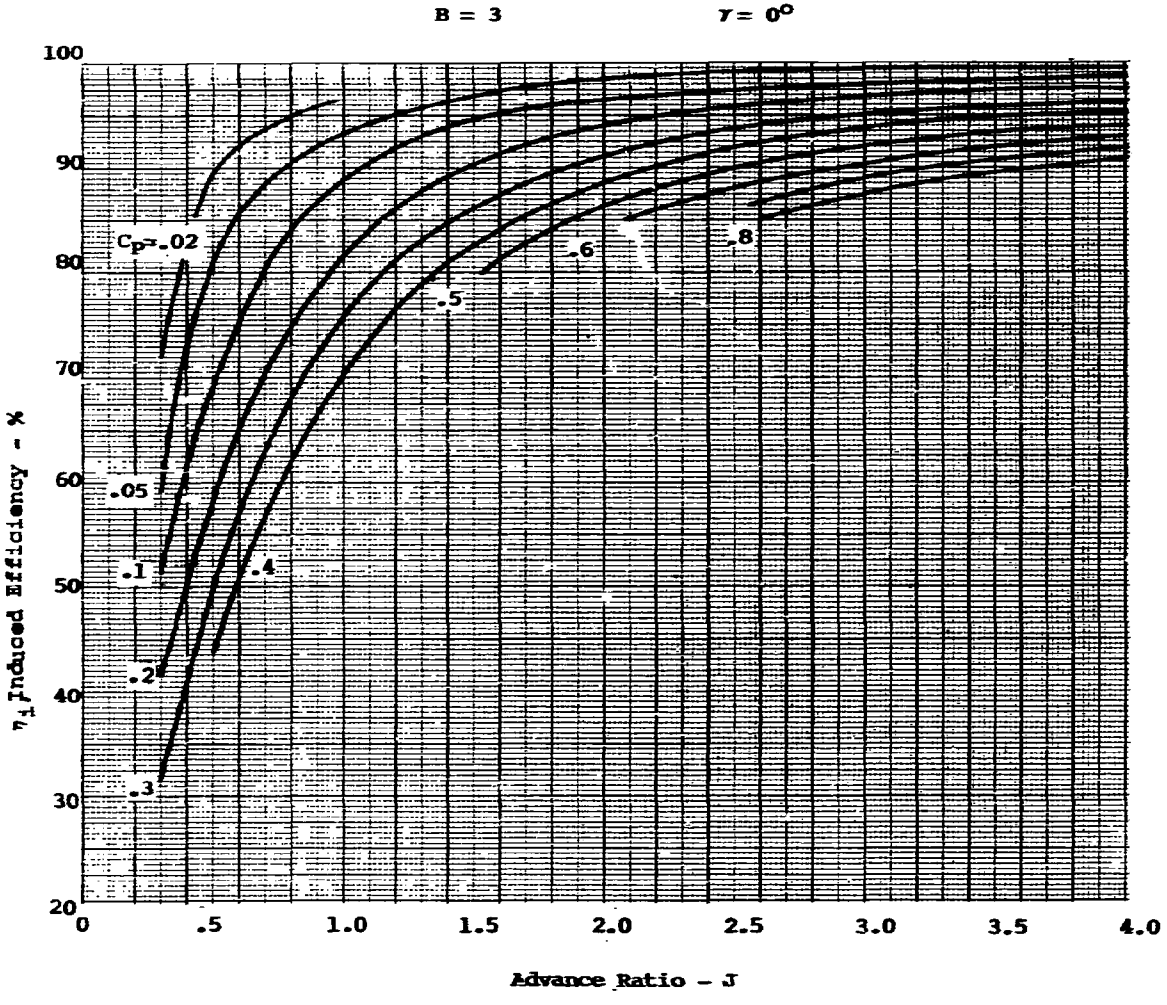

Figure 27. Efficiency at Drag/Lift Ratio of Zero as a Function of Advance Ratio — Three-bladed Propeller.

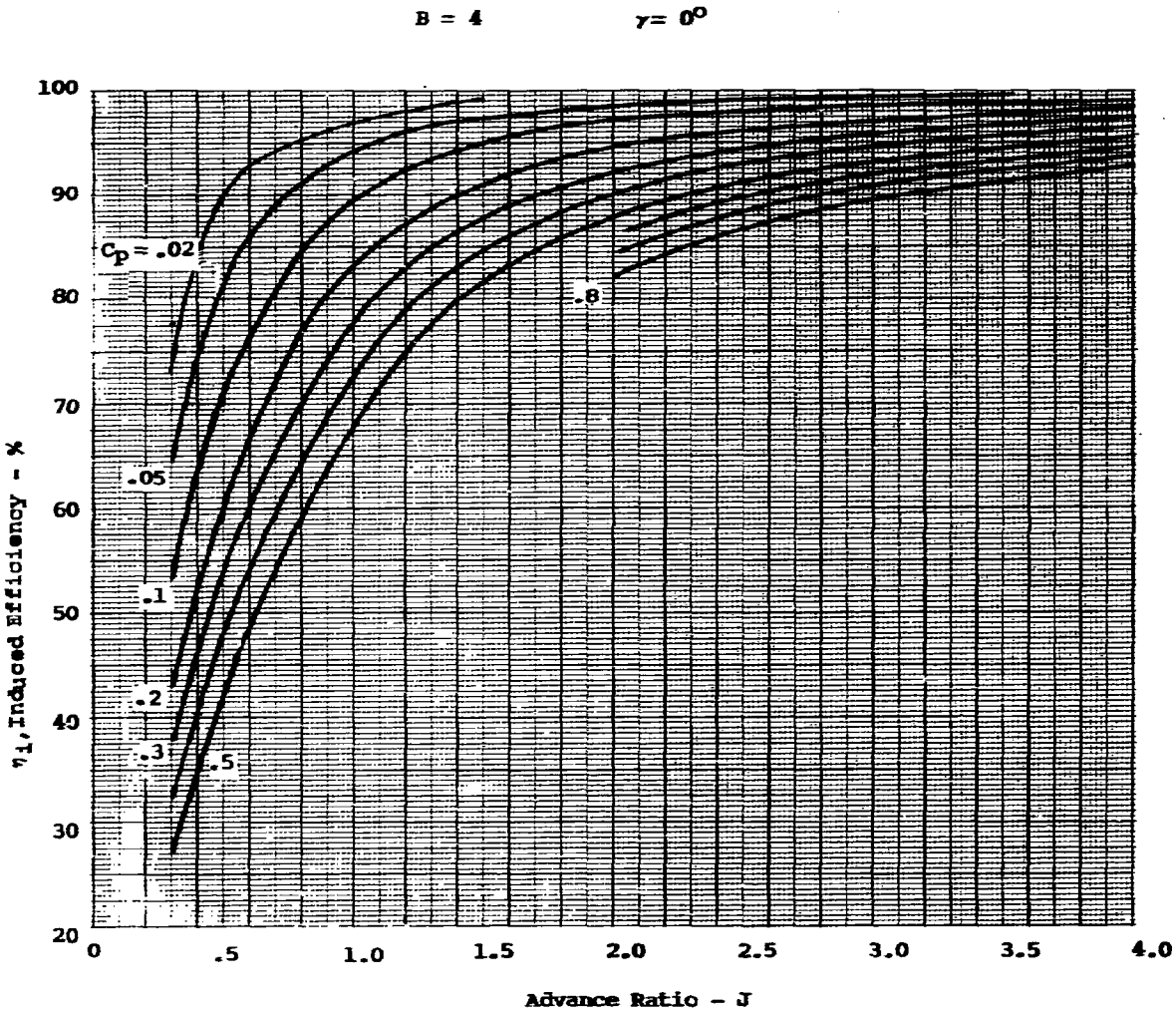

Figure 28. Efficiency at Drag/Lift Ratio of Zero as a Function of Advance Ratio - Four-bladed Propeller.

AIRFOIL SELECTION FOR MINI-RPV PROPELLERS

The selection of the best airfoil type for application to RPV propellers is hampered by the lack of low Reynolds number test data. The only available two-dimensional airfoil data for the normal operating Reynolds number of RPV propellers is that given in References 6 through 14. With the exception of one test these data do not cover the modern airfoils of NASA and others. Further, much of these data are considered to be unreliable due to testing in wind tunnels with a high turbulence factor. For these reasons the selection of the best airfoil type must be made based on their operating characteristics at Reynolds numbers above the critical.

In addition to the more conventional NACA airfoils, the 16 and 65 series sections and the older propeller airfoil types including the RAF 6, Clark Y and the double cambered Clark Y, there are new computer-generated airfoils that have been developed by NASA and others. Considerable design and test work on these airfoils has been done by Whitcomb [23], [24], Wartmann [25] and

---

6 Jacobs and Sherman.

7 Relf, Jones and Bell.

8 Jones and Williams.

9 Lnenicka.

10 Althaus.

11 Schmitz.

12 Deslauriers.

13 Lippisch.

14 Lippisch.

23 Whitcomb, R.T., & Clark, L.R., AN AIRFOIL SHAPE FOR EFFICIENT FLIGHT AT SUPERCRITICAL MACH NOS., NASA TM X-1109, 1965.

24 Whitcomb, R.T., REVIEW OF NASA SUPERCRITICAL AIRFOILS, ICAS Paper No. 74-10, Haifa, Israel, August 1974.

25 Wortmann, F.X., A CRITICAL REVIEW OF THE PHYSICAL ASPECTS OF AIRFOIL DESIGN AT LOW MACH NUMBERS, Institut für Aerodynamik u. Gasdynamik, der Universitat Stuttgart, Published at the MIT Symposium "Technology & Science of Motorless Flight", Boston 1972.

Bocci.[26] The Bocci airfoil designs were developed especially for propellers. The test data of all the new airfoil types has indicated that improved performance can be obtained in terms of lift/drag ratio and maximum lift. The new airfoils also have better structural characteristics than the older types, due to increased thickness ratio and much higher lead and trailing-edge radii.

With RPV propellers the profile drag loss encountered is a higher proportion of the total than with conventional propellers. This is caused by the higher drag encountered at low Reynolds numbers. Thus, gains in efficiency can be expected for RPV propellers only if the performance advantages of the new airfoil sections extend to the lower Reynolds numbers. Due to the lack of this type of data, a quantitative evaluation of these gains is not possible.

An important advantage of the new airfoil sections as applied to propellers is the improved structural characteristics due to increased thickness ratios and greater leading-edge radii. These advantages are especially important when operating in a hostile environment and are considered to be a sufficient reason for their selection.

The two-dimensional airfoil data for the new NASA GAW series and the Bocci [26] airfoils is very limited so that the effects of changes in camber, Mach number and Reynolds number needed for the design of an optimum propeller cannot be determined. For this reason, it was necessary to design the optimum propellers using the standard propeller airfoil data and the correction for Reynolds number developed and presented in Figure 20. The propeller designs developed for such analysis can be expected to have the efficiency level determined from the calculation. The technical risk is low as the methods and data have been checked against many tests of propellers. For these reasons, the propellers for the RPV were designed using NACA 65 series section data.

Although there is a lack of both two-dimensional and propeller test data for the new airfoil sections, the structural and possible performance advantages warrant their application to RPV propeller blades. To do this, airfoils must be designed and tested in the range of thickness ratios from 21% to approximately 6%. With such data a blade can be designed to be competitive with those with conventional airfoil sections.

---

[26] Bocci, A.J., A NEW SERIES OF AIRFOIL SECTIONS SUITABLE FOR AIRCRAFT PROPELLERS, Aeronautical Quarterly, Feb. 1977.

DESIGN AND ANALYSIS OF PROPELLERS FOR MINI-RPV'S

The procedures for the design and analysis of small propellers for RPV's have been used to determine six optimum configurations and their performance. Three optimum propeller configurations were developed for the optimized RPV configuration, referred to as the advanced RPV, and three for the Model B Aquila RPV.

OPERATING CONDITIONS

The following operating conditions and engine characteristics for the advanced RPV were provided for the optimum propeller study:

MODE	CONDITION	POWER SETTING	CLIMB RATE	TRUE AIR-SPEED, KTS
Launch	4000 ft/95°F	Maximum	610 fpm needed	60
Recovery	"	Maximum	200 to 610 fpm	60
Cruise	"	11 Shp	0	75 min
Dash	"	Maximum	0	100 min

Aircraft Gross Weight = 220 lb; Maximum Propeller Diameter = 30 in.

At the minimum cruise speed of 75 knots, operation at peak efficiency will result in minimum power and maximum endurance. When operating at peak power and efficiency, the cruise speed will be a maximum.

Electrical Load

The Aquila data also indicated a required electrical power for operation of 0.55 hp in launch, landing and dash, and 0.85 hp in cruise. The advanced RPV specifications did not give this information; however, it was assumed that there would be an electrical load requirement, so the same values were used for the advanced RPV.

The drag characteristics in terms of thrust horsepower (TV/550) and the engine power as a function of rotational speed used for the analysis of the advanced RPV are given in Figures 29 and 30. Although not furnished, the engine power to the propeller was reduced to account for the electrical load as in the case of the Aquila. This resulted in the power to the

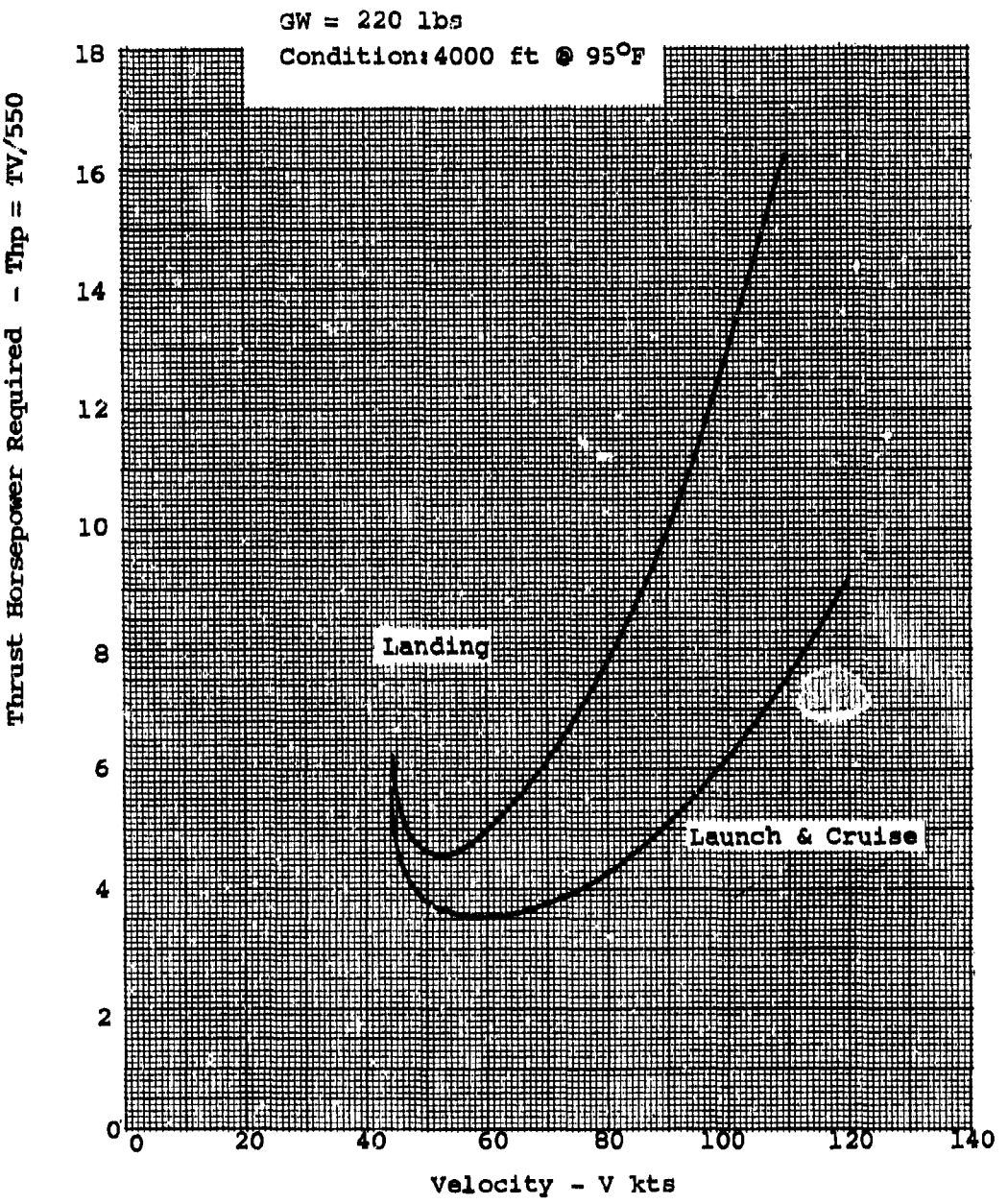

Figure 29. Thrust Horsepower Required vs Velocity for Advanced RPV.

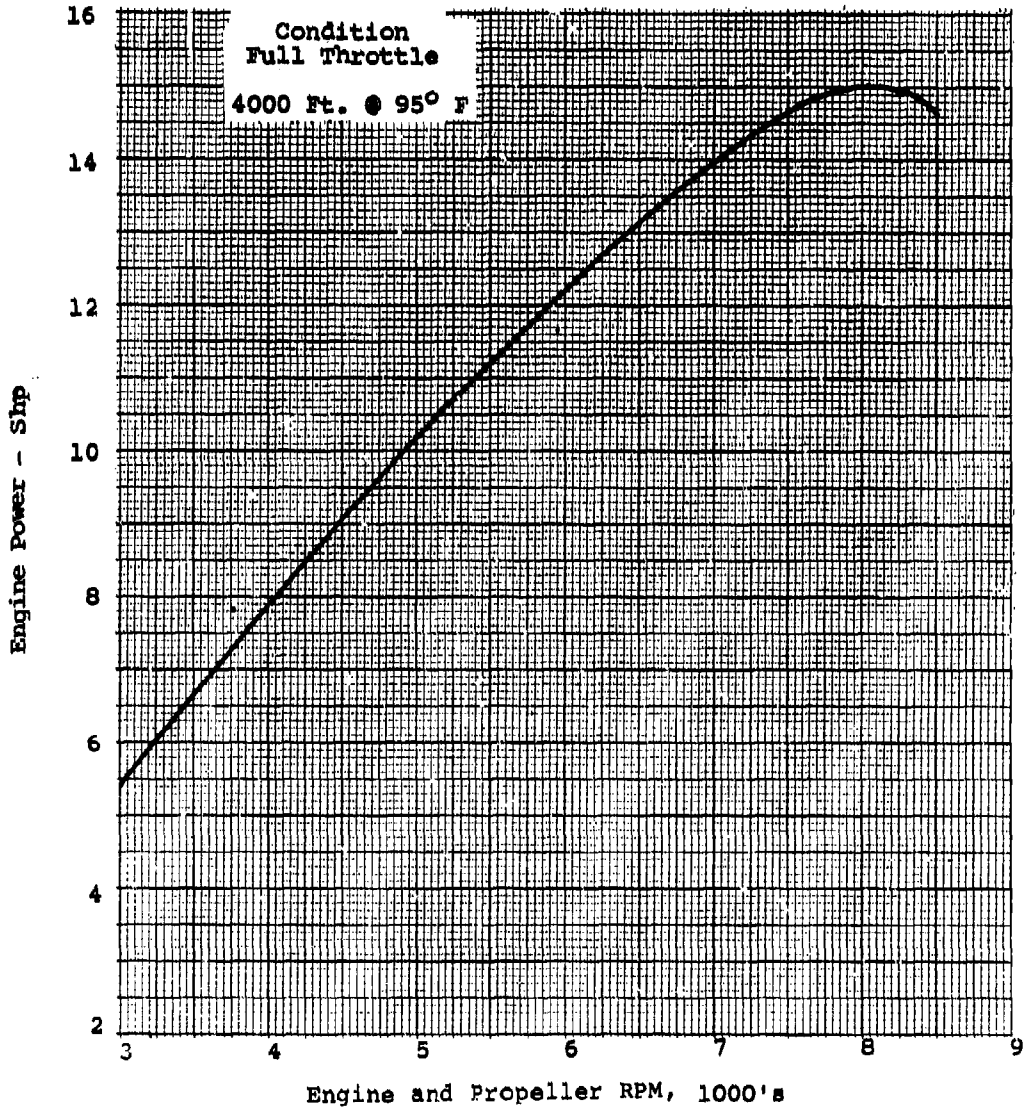

Figure 30. Shaft Horsepower Available for a Typical Advanced RPV. (Electrical Load Not Included)

propeller being

$$hp_{prop} = hp_{fig\ 30} - .55 \text{(launch, dash, landing)}$$

$$hp_{prop} = hp_{fig\ 30} - .85 \text{(cruise)}$$

The following operating conditions were provided for the Aquila RPV:

MODE	CONDITION	POWER SETTING	CLIMB RATE	TRUE AIR-SPEED, KTS
Launch	4000 ft/95°F	Maximum	667 fpm	60
Cruise	"			75 req'd
Dash	"	Maximum		peak
Landing	"	Maximum		60

Aircraft Gross Weight = 134 lbs

Maximum Propeller Diameter = 21 in.

The power characteristics for the engine installed in the Aquila are given in Figure 31. The electrical loads used for the design conditions are

$$hp_{prop} = hp_{fig\ 31} - .55 \text{ (launch, dash, landing)}$$

$$hp_{prop} = hp_{fig\ 31} - .85 \text{ (cruise)}$$

The Aquila aircraft drag characteristics are given in Figure 32. These were derived from drag polars.

RPV PROPELLER DESIGN CONSIDERATIONS

When considering propellers for mini-RPV, the characteristics of the fixed pitch propeller as installed on a two-cycle engine are of primary importance. Further, at each of the design conditions the propeller size requirements are different. Generally, large propellers are needed for the launch and landing conditions, whereas at cruise and dash smaller propellers will have superior performance. Unlike a variable pitch propeller, the fixed propeller will change rpm with changes in power and

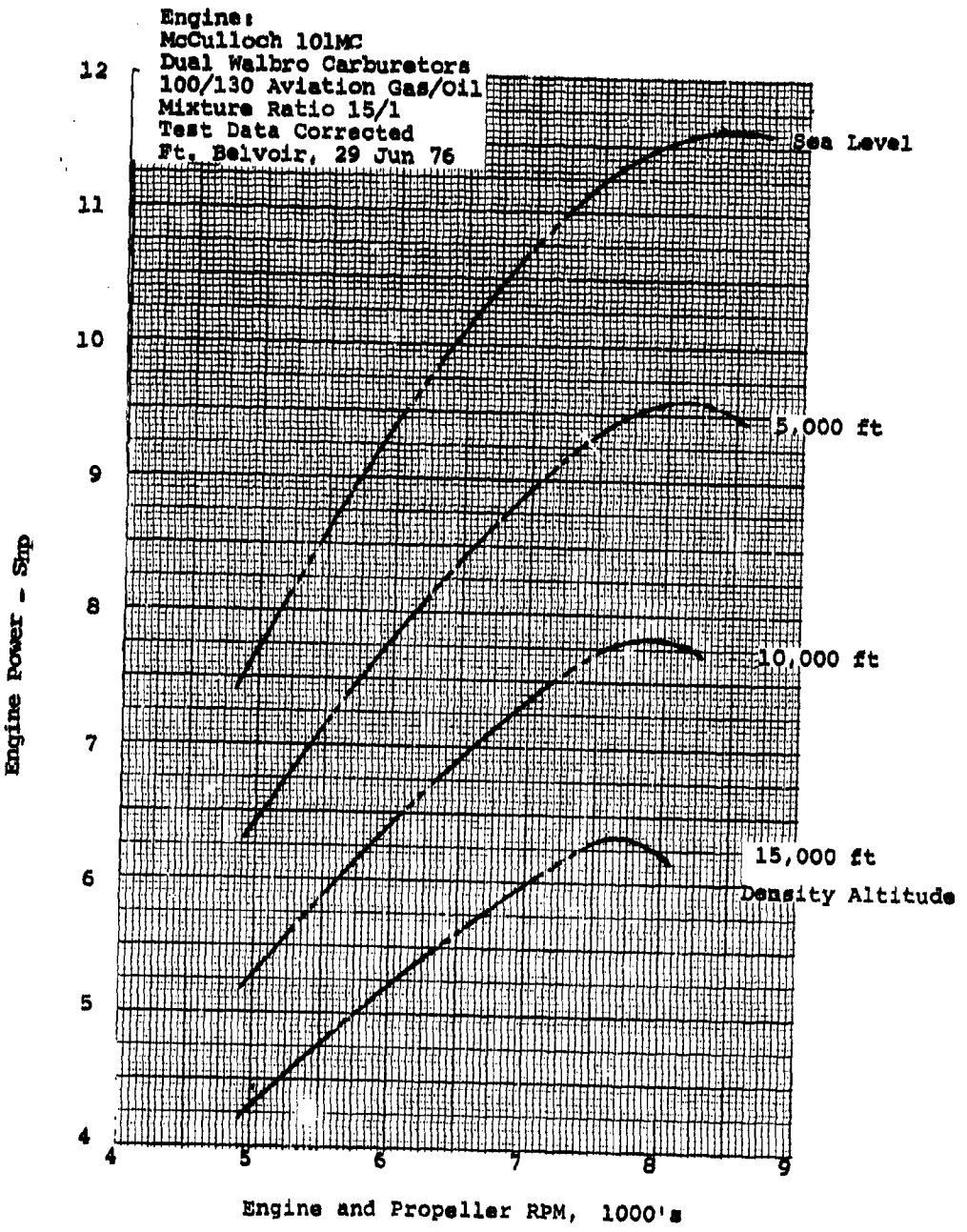

Figure 31. Shaft Horsepower Available for Model B Aquila RPV.

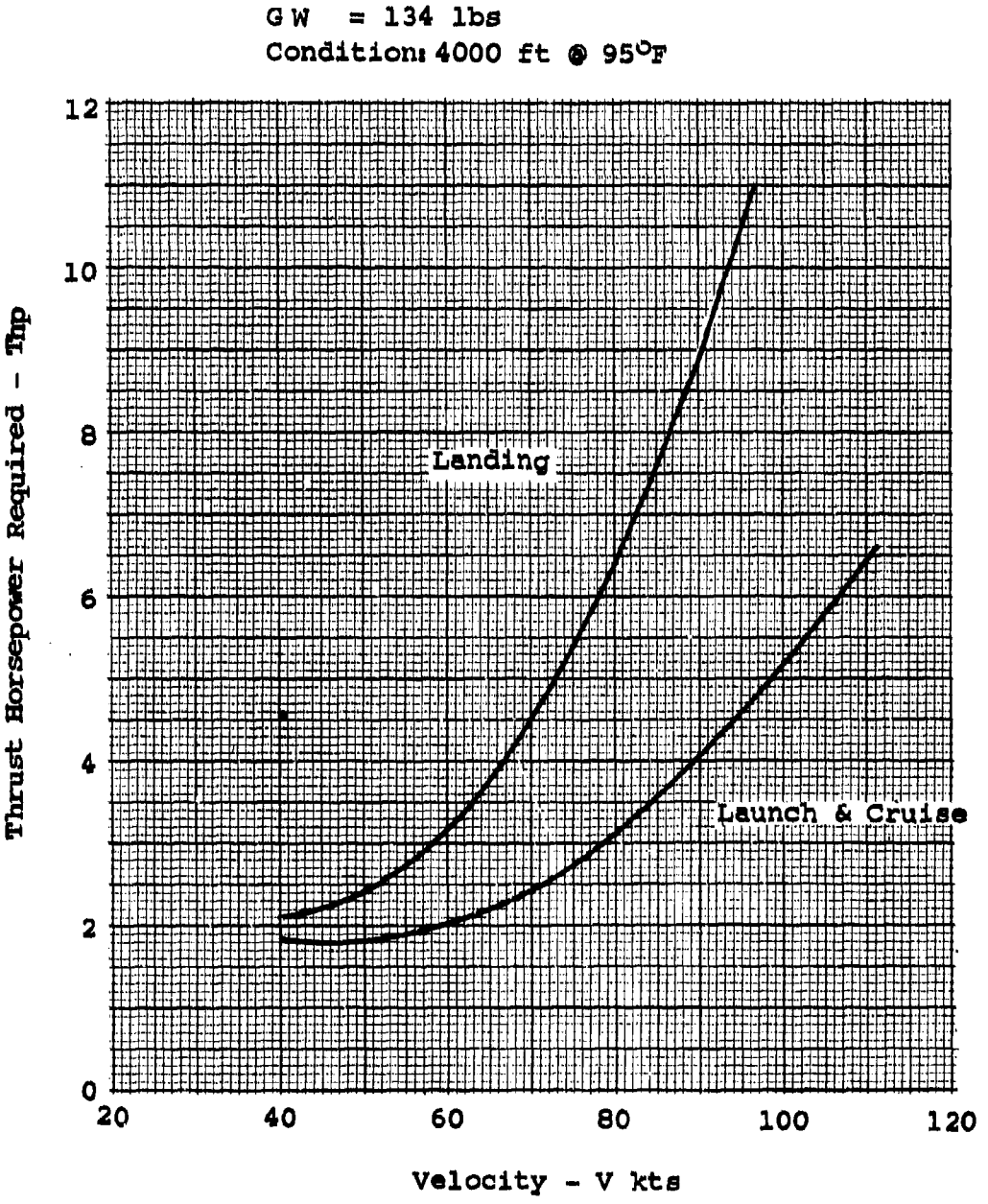

Figure 32. Thrust Horsepower Required vs Velocity for Model B Aquila.

forward speed. At a fixed-speed condition, the rotational speed will increase until the power absorbed by the propeller equals that of the engine. If the thrust produced equals that required by the airplane at this speed, the aircraft has reached equilibrium. If the engine RPM is maximum the aircraft has reached maximum speed. With a decrease of speed due to an increase in aircraft drag or rate of climb, the propeller is capable of absorbing increased power. When full throttle is reached, the engine becomes over-loaded and the rpm decreases.

Based on the above it is seen that if a fixed pitch propeller is designed to provide excess thrust for climb at a low-speed condition at full engine power, a speed increase of the aircraft will result in an increase of propeller rpm until the engine power limit is achieved. With the fixed requirement of a climb rate of 610 fpm at the 60-knot launch, the performance criteria for the selection of the best propeller will be the power, the rpm characteristics at the other flight conditions, and the efficiency. The operating rpm at full throttle determines the power level of the engine, so it is of importance, as well as the efficiency in the selection of RPV propellers.

PRELIMINARY RPV PROPELLER DESIGN SELECTION

The performance of several propellers was determined for the advanced RPV for the specified design conditions. The propellers were analyzed based on wind tunnel data. Using these data, the four basic designs were analyzed for the launch condition using 2- and 2.5-foot-diameter propellers operating at a series of rotational speeds and full power for the specified engine, Figure 30. For each propeller analyzed, the fixed blade angle for all flight conditions is established by the rpm at full power needed to meet the specified 610 fpm rate of climb at the launch condition. The results of the analysis for all eight propellers operating at the specified flight condition are given in Table 2.

The most important design conditions for the Aquila are launch and landing at a speed of 60 knots. Although the dash speed required is to be a peak, the differences in performance possible at this condition are relatively unimportant, so the design emphasis has been placed on the launch and landing conditions. Using the above test data, the performance of two different fixed pitch two-bladed propellers of 1.625 feet in diameter was determined for the Aquila operating conditions. The operating blade angle was established based on full power at 8000 rpm at launch velocity. At this fixed blade angle, the performance at the cruise and dash conditions was found based on the test data. For the cruise condition, an rpm

TABLE 2. PRELIMINARY RPV PROPELLER DESIGNS

				Launch (60 kts)					Cruise				Dash			
Blade	B	AF	Diam (ft)	RPM	SHP	R/C (ft/min)	η_T	β	RPM	SHP	V (kts)	η_T	RPM	SHP	V (kts)	η_T
1	2	128	2	6100	12.4	610	61	26	6450	10.8	114	77	7100	14.1	130	78
2	2	128	2.5	5600	11.3		67.5	15	6500	11.0	105	61	7000	14.0	112	59
3	2	79	2	7000	14.0		54	23	7750	11.0	120	84	8050	14.0	135	84
4	2	79	2.5	5300	10.8		70	17.5	6650	11.1	118	81	7300	14.1	132	80
5	4	90.3	2	5450	11.1		68	23.5	6800	10.9	118	82	7500	14.6	130	78
6	4	90.3	2.5	4700	9.5		81	17	6650	11.1	109	72	7400	14.7	123	65
7	2	132	2	6700	13.5		56	22	7500	10.9	115	78	8500	14.8	133	78
8	2	132	2.5	5500	11.2		67.5	17	6900	10.9	113	73	7400	14.7	130	72

of 7000 was assumed; this established the speed where the power available equals power required. An rpm of 8000 was assumed for the dash condition. The effects of a diameter increase to 1.75 feet were also determined. These results are given in Table 3 along with the estimated performance of the existing Aquila propeller.

Improved performance was obtained for all three propellers over that of the existing Aquila propeller. The advantage of increased diameter on performance at all the operating conditions is also noted. From these results, each of the three propellers was optimized for the launch and landing conditions.

OPTIMUM PROPELLER DESIGN STUDY -- ADVANCED RPV

Based on the results of the preliminary design studies three propellers for the advanced RPV were chosen for detailed blade optimization studies:

1. Two-blade, 81 AF, 2.5 ft diameter -- selected for best performance at launch and recovery.
2. Two-blade, 79 AF, 2 ft diameter -- best configuration at 11 horsepower cruise condition.
3. Two-blade, 79 AF, 2.5 ft diameter -- best maximum diameter propeller for cruise and dash.

Two-bladed propellers were selected in preference to three- or four-bladed configurations because of the low solidity requirement needed for operating at the lift coefficients for high lift/drag ratios. With three- or four-bladed propellers the solidity required would result in blades with activity factors in the range of 50 or less, which results in impractical blades.

The propellers studied were analyzed based on the assumption of the velocity in the disk being equal to the free-stream velocity. This was necessary as the vehicle design was not known. If the body of the vehicle is large relative to the propeller diameter, a velocity reduction could be encountered which could cause a loss of efficiency. This loss due to body interference can be determined as discussed on page 107. The three propellers chosen were optimized for the flight condition for which they were selected, in terms of blade angle and design lift coefficient for the specified blade number and diameter. The optimization procedure used is based on the theory of Calculus of Variations to find the distribution of the camber and blade angle for peak efficiency. In this study the profile and induced losses are minimized.

The blade characteristics of the optimized propellers for the advanced RPV are given in Tables 4 through 6. An efficiency

TABLE 3. PRELIMINARY AQUILA PROPELLER DESIGNS

Blade	B	AF	Diam (ft)	Launch (60 kts)					Cruise				Dash			
				RPM	SHP	R/C (ft/min)	η	β	RPM	SHP	V (kts)	η	RPM	SHP	V (kts)	η
1	2	128	1.625	8000	8.85	714	61	24°	7000	4.6	86	78	8000	6.7	101	78
2	2	132	1.75	8000	8.85	742	62	22°	7000	5.0	90	82	8000	7.0	105	82
3	2	132	1.625	8000	8.85	663	58	22°	7000	3.7	78	78	8000	5.3	92	79
4*	2	150	1.625	8050	8.85	561	53	20°	7000	4.5	78	64	8000	6.5	92	65

* Existing Aquila Blade

TABLE 4. BLADE DESIGN CHARACTERISTICS

Advanced RPV Propeller 2B81-2.5 No. of Blades 2
Propeller Optimized at 60 knot Launch & Recovery Conditions
Integrated Design Lift Coefficient .493
Activity Factor 81.1

Airfoil Section NACA 65-XXX

x	C_{Li}	h/b	b/D	β
.200	0.0	.300	.0719	34.1
.300	0.0	.210	.0789	30.4
.400	0.60	.180	.0825	26.6
.500	0.65	.154	.0829	23.0
.600	0.65	.130	.0787	20.3
.700	0.69	.110	.0709	18.1
.800	0.59	.098	.0595	16.3
.900	0.50	.089	.0448	14.5
.950	0.43	.085	.0365	13.9
.975	0.37	.084	.0320	13.5

Note: h = Thickness
x = r/R
C_{Li} = Section Design C_L
b = Chord
D = Diameter
β = Blade Angle

TABLE 5. BLADE DESIGN CHARACTERISTICS

Advanced RPV Propeller 2B79-2 No. of Blades 2
Propeller Optimized at the 11 hp Cruise Condition
Integrated Design Lift Coefficient .405
Activity Factor 78.8

Airfoil Section NACA 65-XXX

x	C_{Li}	h/b	b/D	β
.200	0.0	.300	.069	52.0
.300	0.350	.210	.069	40.0
.400	0.575	.180	.069	35.5
.500	0.600	.154	.069	31.5
.600	0.580	.130	.068	28.0
.700	0.550	.110	.065	24.5
.800	0.500	.098	.058	21.5
.900	0.390	.089	.047	19.0
.950	0.300	.085	.043	18.0
.975	0.100	.084	.040	15.4

Note: h = Thickness
x = r/R
C_{Li} = Section Design C_L
b = Chord
D = Diameter
β = Blade Angle

TABLE 6. BLADE DESIGN CHARACTERISTICS

Advanced RPV Propeller 2B79-2.5 No. of Blades 2
Propeller Optimized at Cruise and Dash Conditions
Integrated Design Lift Coefficient .247
Activity Factor 78.8

Airfoil Section NACA 65-XXX

x	C_{Li}	h/b	b/D	β
.200	0.0	.300	.069	39.0
.300	0.0	.210	.069	38.0
.400	.50	.180	.069	34.2
.500	.45	.154	.069	28.3
.600	.40	.130	.068	23.9
.700	.35	.110	.065	20.9
.800	.30	.098	.058	17.7
.900	.25	.089	.047	15.4
.950	.10	.085	.043	14.3
.975	0.0	.084	.040	13.6

Note: h = Thickness
x = r/R
C_{Li} = Section Design C_L
b = Chord
D = Diameter
β = Blade Angle

map was prepared for each of these propellers using the revised B-87 strip analysis computer program that applies at low Reynolds numbers. From these maps, Figures 33 through 35, the efficiency can be found at any operating condition of a fixed or variable blade angle propeller. Thus, each fixed pitch propeller could be analyzed at the other design conditions of the advanced RPV, and the effects of the use of variable pitch and two-position propellers could be determined.

PERFORMANCE OF OPTIMUM PROPELLERS -- ADVANCED RPV

For the important operating conditions of the advanced RPV the performance of the optimum propeller designed for the launch condition was determined and is given in Table 7. This 2.5-foot-diameter propeller using two 81-activity factor blades meets the launch requirements with an efficiency of 68% when operating at a blade angle of 16° and an rpm of 5800. The same level of performance is obtained at the landing condition. When operating at the fixed blade angle of 16° the efficiency at cruise and dash is 82%. Due to the increased speed and fixed blade angle, the rotational speed will increase to 7250 rpm at cruise and 8200 at dash. This is a typical operation for a fixed-pitch propeller and illustrates the need for designing the propeller to operate at low rotational speeds at the launch condition if a high cruise or dash speed is required. This requirement will not be encountered using variable pitch propellers.

The performance of the propeller optimized for the 11 hp cruise condition of the advanced RPV is given in Table 8. This optimum 2.5-foot-diameter fixed-blade angle propeller, using two 79-activity factor blades, has an efficiency at cruise and dash of 83%. The rpm for the cruise and dash conditions are 7200 and 8000, respectively. The efficiency of the optimum propeller at launch and landing is 65%.

A thrust horsepower of 4 is required at the 75-knot, 4000-foot 95°F cruise condition of the advanced RPV. At this condition the efficiency of the propellers designed for the launch is 81.5%. The efficiency of the propeller designed for the high speed cruise condition is also 81.5% at the 75 knot cruise condition. Since these propellers have about the same solidity it appears that the level of design C_L is nearly correct for peak efficiency. However, if the low-speed cruise condition becomes important, a 2.5 foot-diameter propeller should be designed for optimum performance to determine the possible improvement.

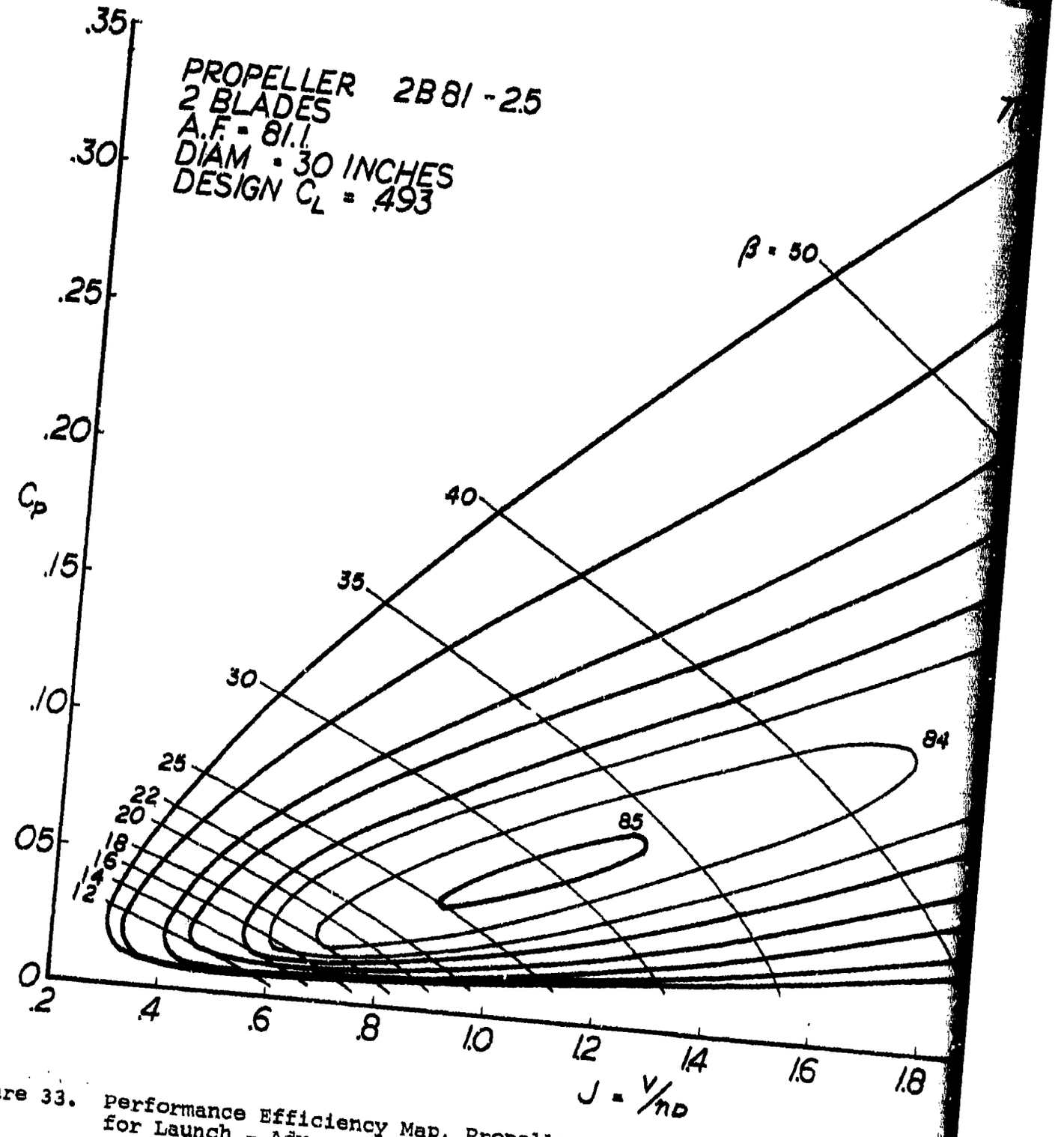

Figure 33. Performance Efficiency Map, Propeller Optimized for Launch - Advanced RPV Propeller 2B81-2.5.

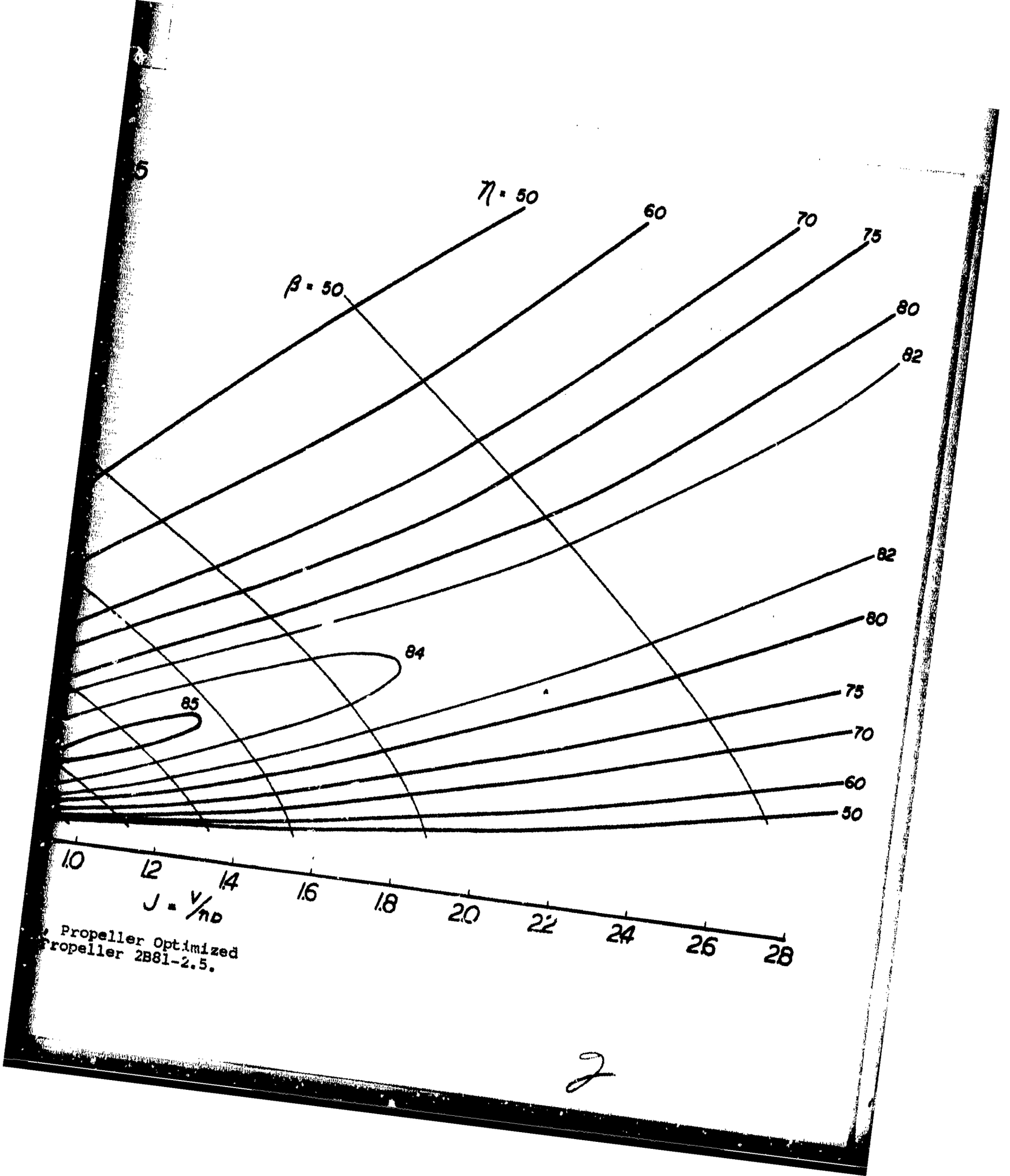

Propeller Optimized
Propeller 2B81-2.5.

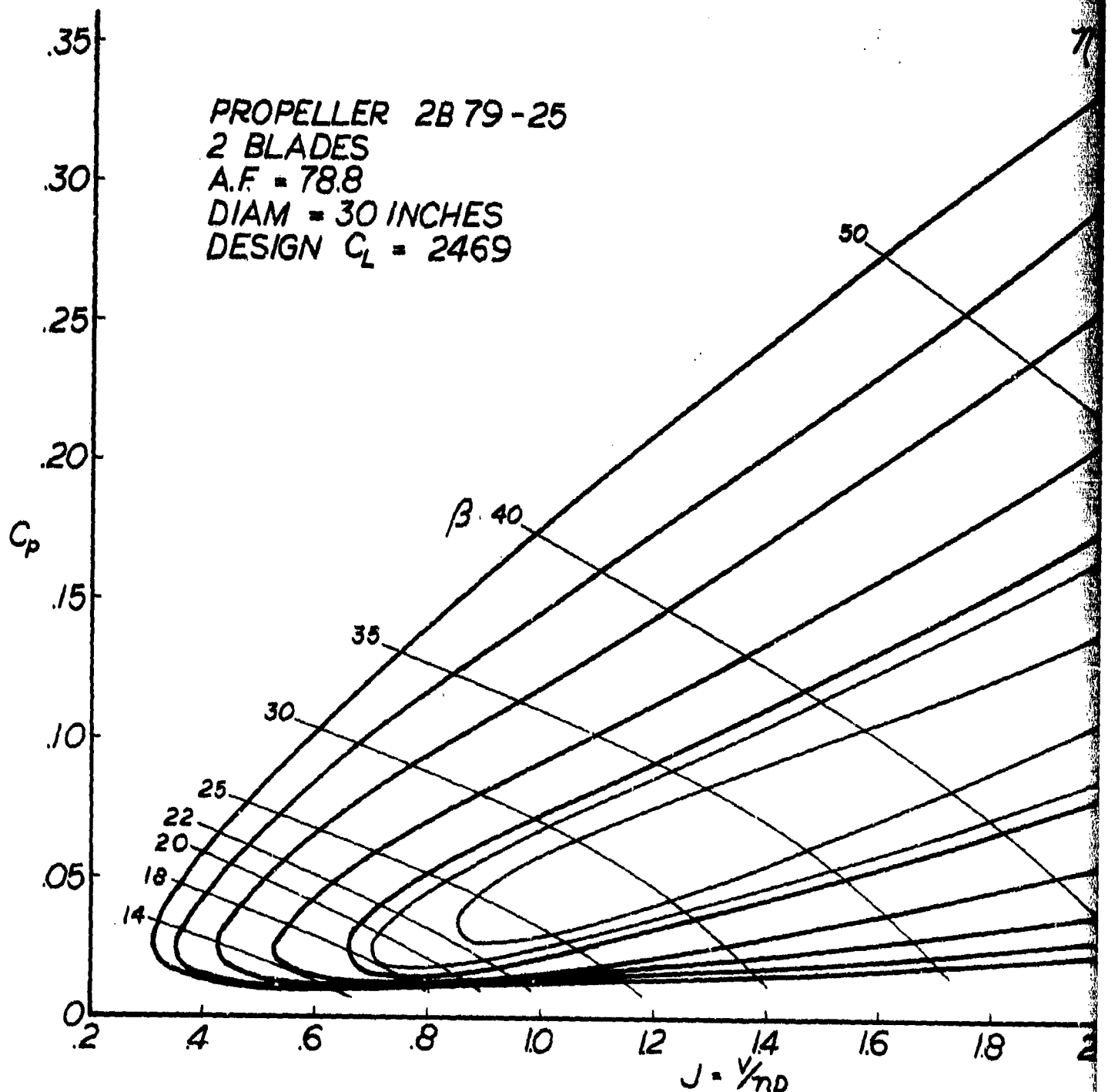

Figure 34. Performance Efficiency Map, Propeller Optimized for Cruise - Advanced RPV Propeller 2B79-2.5.

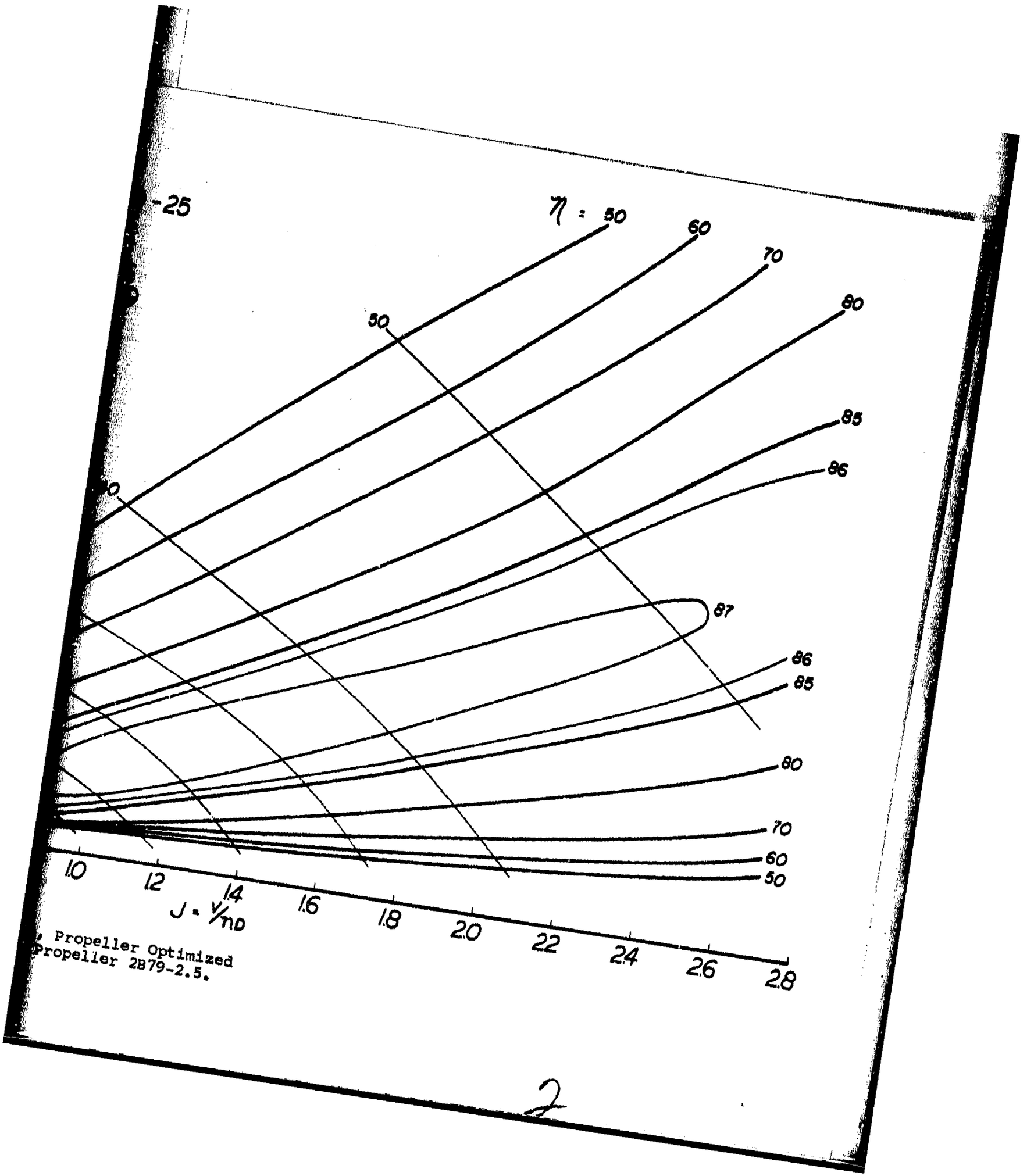

Propeller Optimized
Propeller 2B79-2.5.

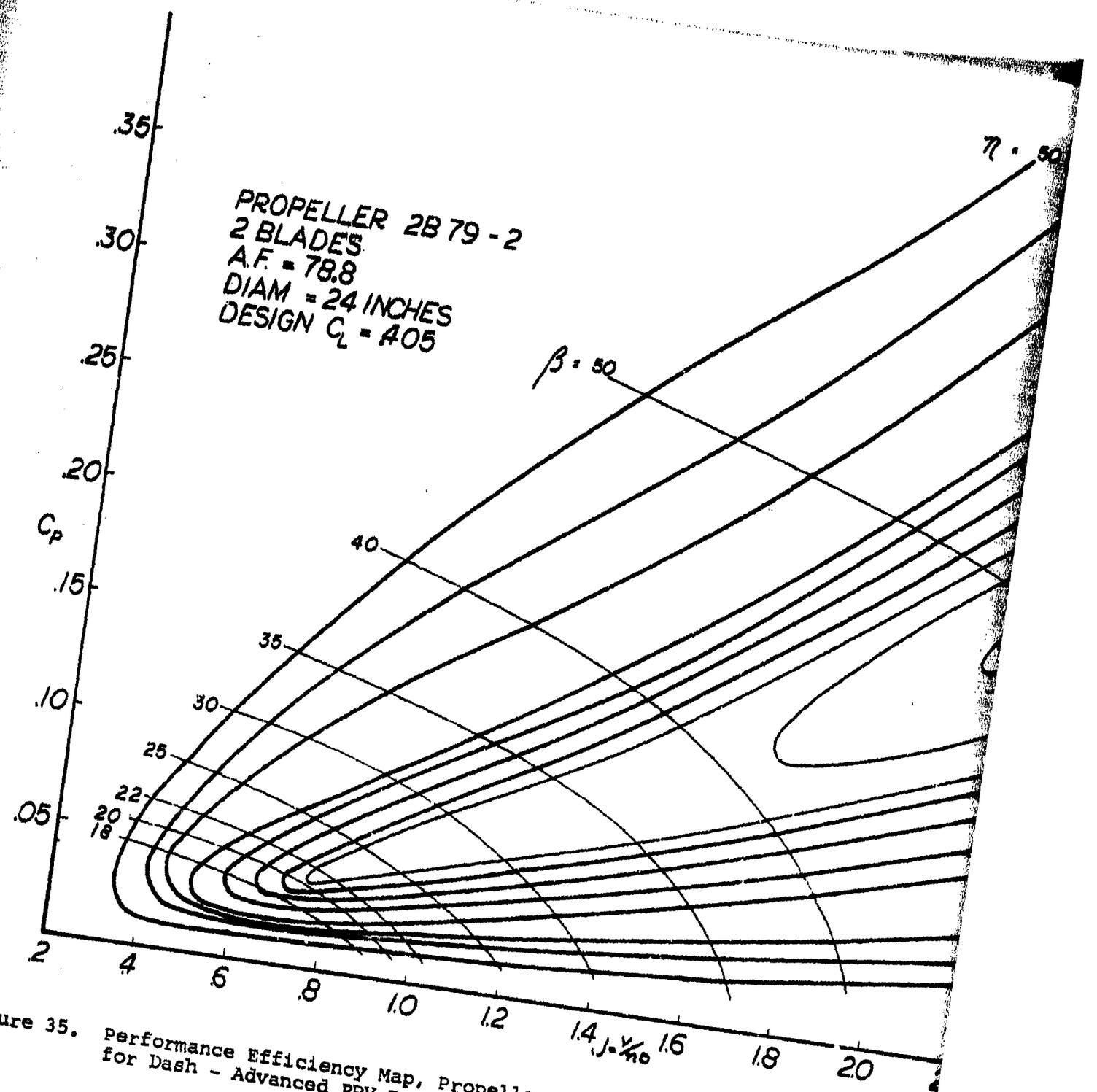

Figure 35. Performance Efficiency Map, Propeller Optimized for Dash - Advanced RPV Propeller 2B79-2.

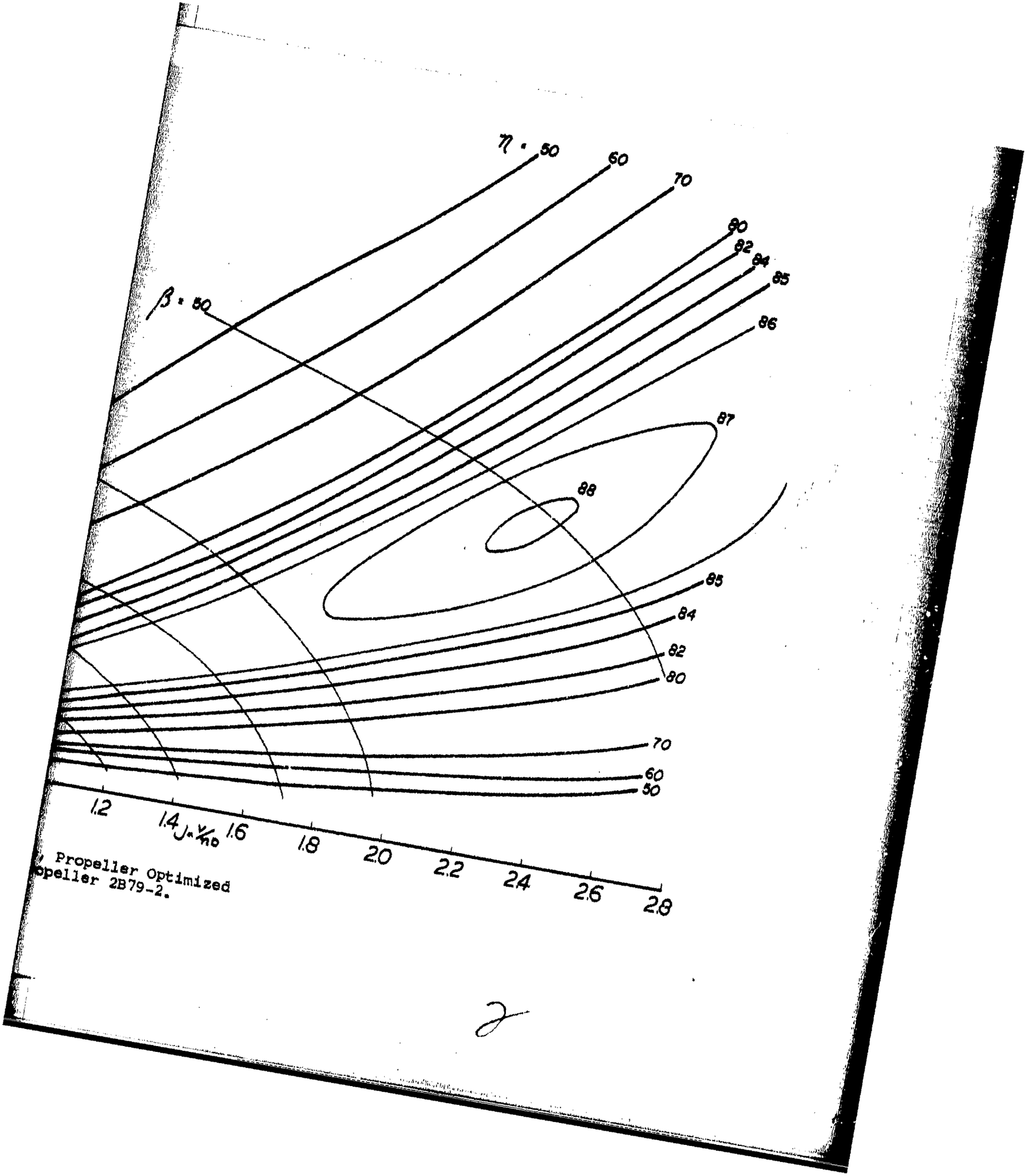

Propeller Optimized
opeller 2B79-2.

TABLE 7. CALCULATED PERFORMANCE OF ADVANCED RPV — PROPELLER OPTIMIZED FOR LAUNCH

Engine	15 HP @ 8000 RPM	No. of Blades	2	Integrated Design Lift Coefficient	.493
Propeller	2B81-2.5	Diameter	2.5 ft	Activity Factor	81
		πnD(Take-off)	760(β=16°)	h/b @ Station x = .75	.105

Condition	Alt/temp	Engine HP *	Engine RPM	Velocity (kts)	β (deg)	η_T	R/C	THP	C_p	J	Remarks
Launch	4000'/95°	14.0	7000	60	12	62	726	8.34	.025	.347	Requirement - 610 fpm Rate of Climb @ 60 kts.
		12.0	5800	60	16	68	643	7.79	.037	.42	
		11.0	5400	60	18	68	541 **	7.10	.042	.45	
		10.05	4950	60	20	69	458 **	6.6	.050	.49	
Cruise	4000'/95°	11.0	7250	116	16	82	-	8.32	.017	.65	Requirement - 75 kt minimum at 11 SHP.
		11.0	6800	117	18	84	-	8.50	.020	.70	
		11.0	6250	116	20	84.3	-	8.56	.026	.75	
		11.0	8200	106	12	73	-	7.4	.0117	.525	
Dash	4000'/95°	14.95	8200	131	16	82	-	11.8	.0166	.65	Requirement - 100 kt minimum at maximum power.
		14.90	7750	135	18	84	-	12.1	.020	.70	
		13.80	6900	128	20	84.3	-	11.1	.026	.75	
Landing	4000'/95°	14.0	7000	60	12	62	516	8.34	.025	.347	Requirement - 200 to 610 fpm Rate of Climb @ 60 kts.
		12.0	5800	60	16	68	433	7.79	.037	.420	
		11.0	5400	60	18	68	331	7.10	.042	.45	
		10.05	4950	60	20	69	255	6.6	.050	.49	
		5.77	4800	60	16	77	-131				Glide Path 1.2°

* Propeller HP reduced by 0.55 HP for Launch, Landing and Dash, and by 0.85 HP for Cruise to allow for electrical load.

** Below Requirement.

TABLE 8. CALCULATED PERFORMANCE OF ADVANCED RPV — PROPELLER OPTIMIZED FOR CRUISE

Engine 15 HP @ 8000 rpm
Propeller 2B79-2.5

No. of Blades 2
Diameter 2.5 ft
πnD(Take-Off) 916(β=12°)

Integrated Design Lift Coefficient .247
Activity Factor 79
h/b @ Station x = .75 .105

Condition	Alt/temp	Engine HP *	Engine RPM	Velocity (kts)	β (deg)	η	R/C	THP	C_p	J	Remarks
Launch	4000'/95°	14.00	7000	60	12	60	686	8.07	.025	.347	Requirement - 610
		13.15	6500	60	14	62	647	7.81	.029	.374	fpm Rate of
		12.20	6000	60	17	65	611	7.57	.034	.405	Climb @ 60 kts.
		9.25	4600	60	22	67	350	5.8	.057	.53	
Cruise	4000'/95°	11.00	7800	111	14	77	-	7.82	.0136	.577	Requirement - 75
		11.00	7200	116	17	83	-	8.42	.017	.653	kt minimum at
		11.00	6000	118	22	86.5	-	8.78	.030	.80	11 SHP.
		11.00	8000	105	12	70	-	7.1	.013	.53	
Dash	4000'/95°	11.05	8000	114	14	77	-	8.1	.013	.58	Requirement - 100
		15.00	8000	134	17	83	-	12.0	.018	.67	kt minimum at
		13.00	6400	128	22	86.6	-	10.8	.030	.81	maximum power.
		11.00	8000	105	12	70	-	7.1	.013	.53	
Landing	4000'/95°	14.00	7000	60	12	60	476	8.07	.025	.347	Requirement - 200
		13.15	6500	60	14	62	437	7.81	.029	.374	to 610 fpm Rate
		12.2	6000	60	17	65	400	7.57	.034	.405	of Climb @ 60 kts.
		9.25	4600	60	22	67	135	5.8	.057	.53	
		3.85	4800	60	14	77	-342				Glide Path 3.2°
		5.6	4800	60	17	77	-151				Glide Path 1.4°

* Propeller HP reduced by 0.55 HP for Launch, Landing and Dash, and by 0.85 HP for Cruise to allow for electrical load.

TABLE 9. CALCULATED PERFORMANCE OF ADVANCED RPV — PROPELLER OPTIMIZED FOR DASH

Engine	15 HP @ 8000 rpm	No. of Blades	2	Integrated Design Lift Coefficient	.405
Propeller	2B79-2	Diameter	2 ft	Activity Factor	79
		πnD(Take-off)	838(β=20°)	h/b @ Station x = .75	.105

Condition	Alt/temp	Engine HP*	Engine RPM	Velocity (kts)	β (deg)	η_T	R/C	THP	C_p	J	Remarks
Launch	4000'/95°	15.0	8000	60	20	50	560**	7.23	.055	.38	Requirement - 610 fpm Rate of Climb @ 60 kts.
		13.8	6800	60	25	59	469**	6.625	.082	.447	
Cruise	4000'/95°	11.0	8100	118	20	85.5	-	8.70	.037	.74	Requirement - 75 kt minimum at 11 SHP.
		11.0	6970	117	25	85	-	8.63	.058	.85	
Dash	4000'/95°	10.0	8000	115	20	85.5	-	8.56	.038	.73	Requirement - 100 kt minimum at maximum power.
		15.0	8000	136	25	85.5	-	12.35	.055	.861	
Landing	4000'/95°	15.0	8000	60	20	50	350	7.23	.055	.38	Requirement - 200 to 610 fpm Rate of Climb @ 60 kts.
		13.8	6800	60	25	50	259	6.625	.082	.447	
		3.06	4800	60	20	83.5	-428				Glide Path L=4.0°

* Propeller HP reduced by 0.55 HP for Launch, Landing and Dash, and by 0.85 HP for Cruise to allow for electrical load.

** Below requirement.

For best performance in dash, the initial analysis indicated that a diameter of 2.5 feet was too large. A 2-foot-diameter propeller was, therefore, optimized for the dash condition. Its performance is given for the range of conditions in Table 9. With this propeller an efficiency gain of only 2 to 3% was obtained for the dash and cruise; however, this optimum propeller design for dash did not meet the required climb rate performance at launch.

From the study of the three fixed pitch propeller designs it appears that the launch rate of climb performance establishes the design configuration. Further, for propellers of equal diameter the performance advantage is small, whether the design is optimized for cruise or launch. By selecting the lowest value of camber consistent with high lift/drag ratios, the performance differences between the launch and cruise are minimized.

The performance of the optimized propellers for launch and cruise is near the peak that could be expected for the stated load condition of diameter and rpm. At the cruise and dash conditions high noise levels can be expected, due to the tip speed exceeding 900 feet per second at these conditions when using the fixed pitch propellers. To reduce the noise level, the propeller tip speeds must be reduced. This can be accomplished using variable pitch propellers of the constant speed type or the two-position blade angle type. Other steps that can be taken to reduce noise are: (1) reduce the forward speed at cruise and dash, (2) reduce the climb requirement at launch and landing, (3) consider the use of gear reductions between the engine and propeller, and (4) select engines developing the required power at lower rotational speeds. In all cases the propeller size required will be increased.

As noted in Tables 7 and 8, two-position or variable pitch propellers will improve performance at the dash and cruise conditions while maintaining the required performance at launch. Consider the propeller designed for launch: at this condition the required climb rate is obtained with a 16° blade angle, while the best cruise and dash performance is obtained with a 20° blade angle at a reduced rotational speed compared to cruise obtained with a 16° blade angle. By dropping down to 5400 rpm, even greater improvements in noise can be achieved with no loss in performance. Therefore, it appears that in the case of the advanced RPV the greatest advantage of either the two-position propeller or the variable pitch controllable type would be the possibility of reduced rpm and, thus, reduced noise at the cruise and dash conditions. Performance in this case would be of secondary importance.

Advanced RPV Propeller - Supercritical Sections

The best fixed pitch propeller for the advanced RPV is considered to be the two-bladed 2.5-foot-diameter configuration. The blades of this propeller, designated 2B81-2.5, have an 81 activity factor with an integrated design C_L of 0.493 when using NACA 65 series airfoils. The design C_L and blade angle distributions of this blade were optimized for the launch condition.

As indicated in the Airfoil Selection Section, the new supercritical airfoils are recommended for RPV propellers because of potential performance improvements and structural advantages. Because of the lack of airfoil data, especially at the lower Reynolds numbers, it is not possible to determine the optimized characteristics of a blade using these new airfoils. A blade with the new NASA supercritical airfoil can, however, be derived from the optimum 2B81-2.5 blade by maintaining the same load distribution and operating C_L to design C_L relationship. The characteristics of such a blade are presented in Figure 36 in comparison with the 2B81-2.5 blade.

Ducted Propellers for Advanced RPV

The optimized propellers for the advanced RPV discussed above were designed as free propellers, as the ducts used were considered to have a large tip clearance for protection of the propeller and crew. To determine the possible advantages of true ducted propellers, studies were made for the advanced RPV design conditions. A ducted fan with five blades and stator vanes designed for low-speed operation was used. The ducted fan was considered to be fixed pitch and operated at the same rotational speed as that of the engine. To reduce tip speed, the ducted fan was sized for the lowest possible diameter consistent with meeting the rate of climb requirement at launch. The results of this analysis are given in Table 10.

The 20-inch-diameter ducted fan develops the thrust necessary at an rpm of 5400 to achieve the required 610 fpm rate of climb at launch. This results in a tip speed of 470 ft/sec vs 785 ft/sec for the open propeller. At the cruise and dash conditions, even larger reductions of tip speed are obtained with the ducted fan in comparison with the open propeller. For instance at cruise, a tip speed of 400 ft/sec in comparison with 942 ft/sec for the open propeller should result in an important reduction of noise. Based on this analysis it appears that a true ducted fan or propeller should be further considered for the advanced RPV. To achieve the desired performance, the tip clearance must be reduced to the lowest practical level and the entrance to the duct must be clean.

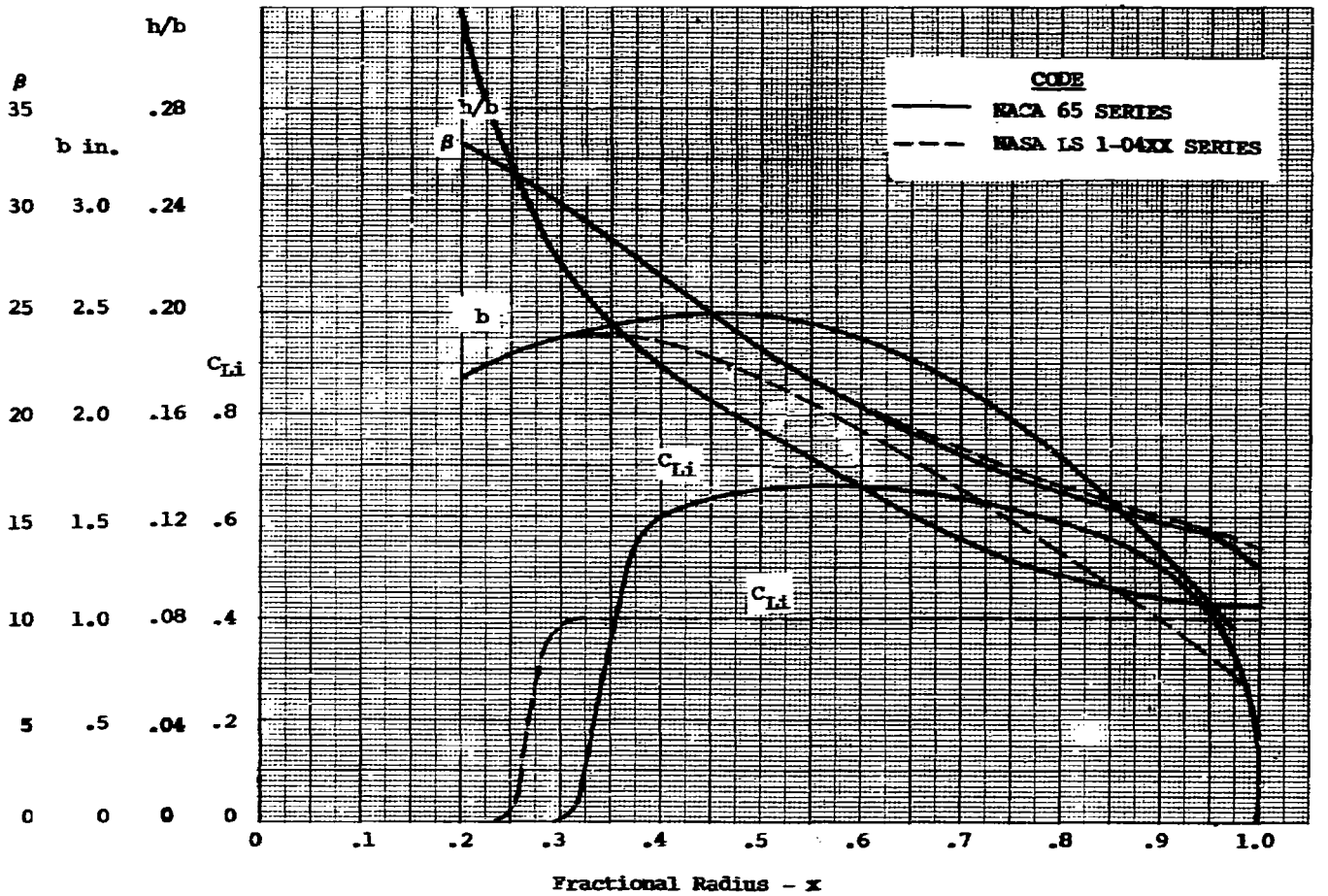

Figure 36. Blade Characteristics for Configuration With NACA 65 Series Sections and NASA LS(1) — Thickness Airfoils.

TABLE 10. CALCULATED PERFORMANCE OF ADVANCED RPV — DUCTED PROPELLER OPTIMIZED FOR CRUISE

Engine 15 HP @ 8000 RPM
Propeller Ducted Fan

No. of Blades 5
Diameter 20 in
πD(Take-off) 471(=35°)

Integrated Design Lift Coefficient .4
Activity Factor 160
Duct Diameter to Length Ratio 1.2

Condition	Alt/temp	Engine HP	Engine RPM	Velocity (kts)	β (deg)	T_2	R/C	THP	C_p	J	Remarks
Launch	4000'/95°	15	8000	60	21	70	992	10.12	.136	.456	
		14	7000	60	26	73	948	9.82	.189	.521	
		12.2	6000	60	32	76	807	8.88	.26	.608	
		10.15	5000	60	37	75	555	7.20	.37	.73	(Does not meet R/C Spec.)
		11.0	5400	60	35	75	650	7.83	.32	.675	Select β = 35°
Cruise	4000'/95°	11.0	6000	114	35	83	–	8.42	.227	1.15	Tip Speed 523 fps
			4500	77	35	86	–	4.14	.255	1.04	Desired 392 fps
Dash	4000'/95°	11.25	6000	114	35	83	–	8.37	.225	1.16	520 fps
Landing	4000'/95°		5400	60	35	75	440	7.83	.32	6.75	471 fps

OPTIMUM PROPELLER STUDY -- AQUILA

From the preliminary design study of the Aquila, three different configurations were selected to be optimized. Two 19.5-inch-diameter, two-bladed propellers with different solidities were analyzed for the launch and landing condition at the maximum power, rpm, of the engine. The procedure used for the optimization study is the same as that used for the advanced RPV. To determine the effects of changing diameter, a two-bladed 21-inch-diameter propeller was also optimized at the launch condition. The blade characteristics for these optimized propellers are given in Tables 11 through 13.

With the B-87 computer program, the performance of the three optimized propellers was determined for a wide range of operating conditions. From the results of these calculations, efficiency maps were prepared and are presented in Figures 37 through 39. The performance of fixed pitch, constant speed, two-position propellers can be determined using these maps for a wide range of operating conditions.

PROPELLER PERFORMANCE RESULTS -- AQUILA

The calculated performance for the above three optimized RPV propellers operating at the given design conditions of the Aquila RPV are given in Tables 14 through 16. Due to the large clearance between the blade tip and the duct wall for the Aquila, it was assumed that the propeller performance would be the same as that obtained with a free propeller. Since the duct in this case will not be effective, its drag should be charged to the airframe.

As shown in Tables 14 and 16, propeller performance is improved at the launch and landing conditions using the blades with higher design lift coefficients. This improvement would be expected, due to the improved lift/drag ratio and maximum lift coefficients obtained with the high cambered airfoil sections. At the cruise and dash conditions the lower design C_L blades are better, as the loading is reduced, which gives a better match between the operating and design lift coefficients. A comparison of the performance of the two-bladed 1.625-foot-diameter propellers with that of the two-bladed 1.75-foot-diameter propeller given in Table 15 shows that the higher diameter propeller has improved performance at all flight conditions. This improved performance would be expected due to the reduction of the induced losses as a result of the increased diameter.

TABLE 11. BLADE DESIGN CHARACTERISTICS

Aquila Propeller 2B130-1.625 No. of Blades 2

Integrated Design Lift Coefficient .621
Activity Factor 129.7

Airfoil Section NACA 65-XXX

x	C_{Li}	h/b	b/D	β
.200	0.0	.300	.115	40.0
.300	.30	.210	.126	39.1
.400	.65	.180	.132	37.0
.500	.70	.154	.133	31.5
.600	.70	.130	.126	25.0
.700	.70	.110	.113	21.2
.800	.70	.098	.095	19.0
.900	.70	.089	.072	16.5
.950	.70	.085	.058	15.2
.975	.50	.084	.051	14.5

Note: h = Thickness
x = r/R
C_{Li} = Section Design C_L
b = Chord
D = Diameter
β = Blade Angle

TABLE 12. BLADE DESIGN CHARACTERISTICS

Aquila Propeller 2B127-1.75 No. of Blades 2

Integrated Design Lift Coefficient .444
Activity Factor 127.3

Airfoil Section NACA 65-XXX

x	C_{Li}	h/b	b/D	β
.200	.700	.230	.100	55.0
.300	.700	.165	.100	42.0
.400	.700	.134	.100	32.0
.500	.700	.105	.100	26.0
.600	.680	.080	.099	21.5
.700	.610	.061	.098	18.5
.800	.525	.049	.095	16.0
.900	.400	.042	.086	14.0
.950	.280	.036	.074	12.6
.975	.200	.030	.062	12.0

Note: h = Thickness
x = r/R
C_{Li} = Section Design C_L
b = Chord
D = Diameter
β = Blade Angle

TABLE 13. BLADE DESIGN CHARACTERISTICS

Aquila Propeller 2B137-1.625 No. of Blades 2

Integrated Design Lift Coefficient .488
Activity Factor 137.1

Airfoil Section NACA 65-XXX

x	C_{Li}	h/b	b/D	β
.200	.70	.215	.139	54.0
.300	.70	.175	.134	45.0
.400	.70	.140	.128	36.5
.500	.70	.105	.121	30.0
.600	.70	.080	.113	26.0
.700	.67	.060	.105	22.5
.800	.60	.049	.096	19.5
.900	.46	.037	.0850	16.5
.950	.32	.032	.0820	15.0
.975	.20	.030	.0810	14.5

Note: h = Thickness
x = r/R
C_{Li} = Section Design C_L
b = Chord
D = Diameter
β = Blade Angle

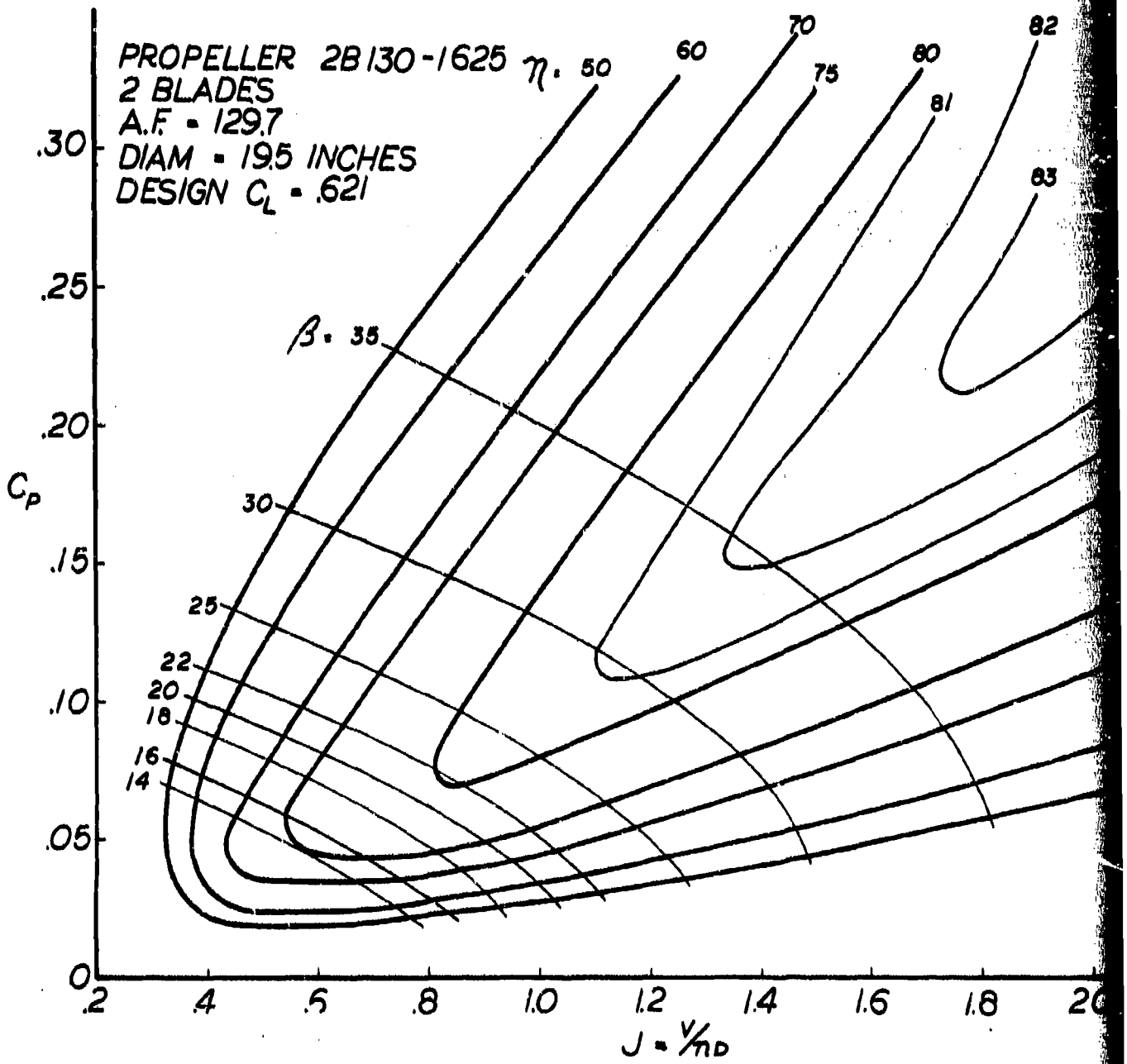

Figure 37. Performance Efficiency Map, Propeller Optimized for Launch - Advanced Aquila Propeller 2B130-1.625.

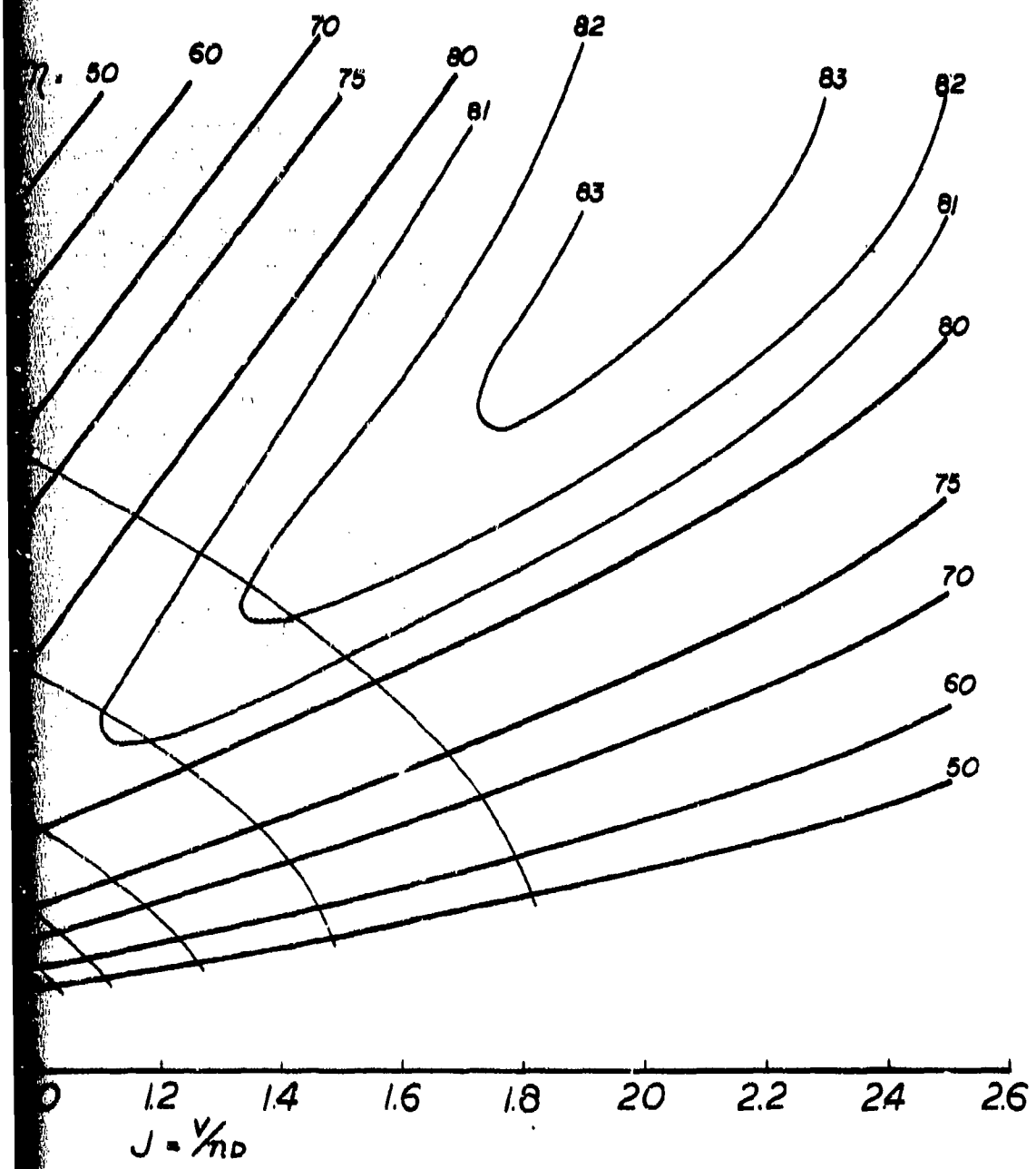

p, Propeller Optimized
lla Propeller 2B130-L625.

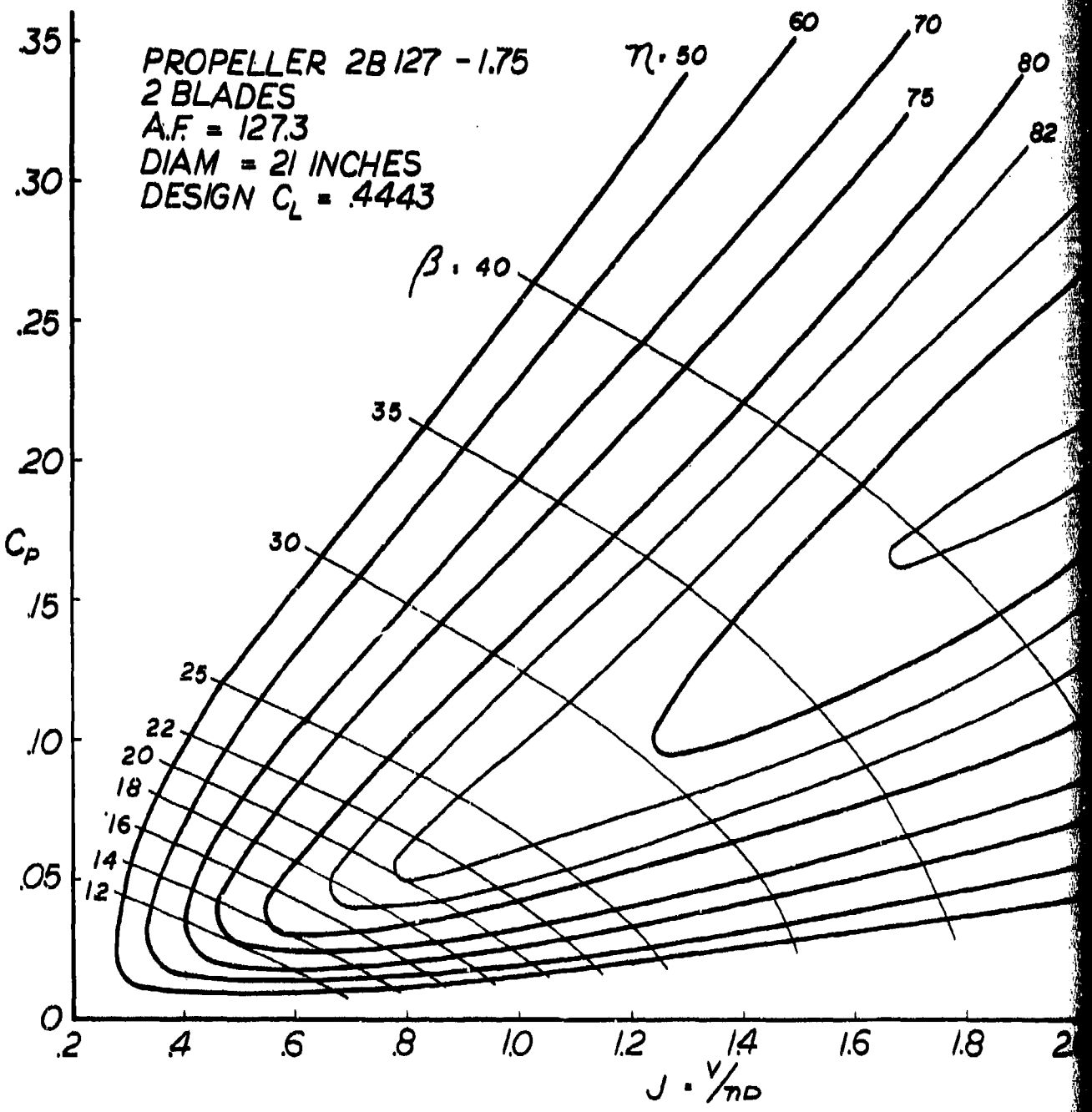

Figure 38. Performance Efficiency Map, Propeller Optimized for Launch - Advanced Aquila Propeller 2B127-1.75.

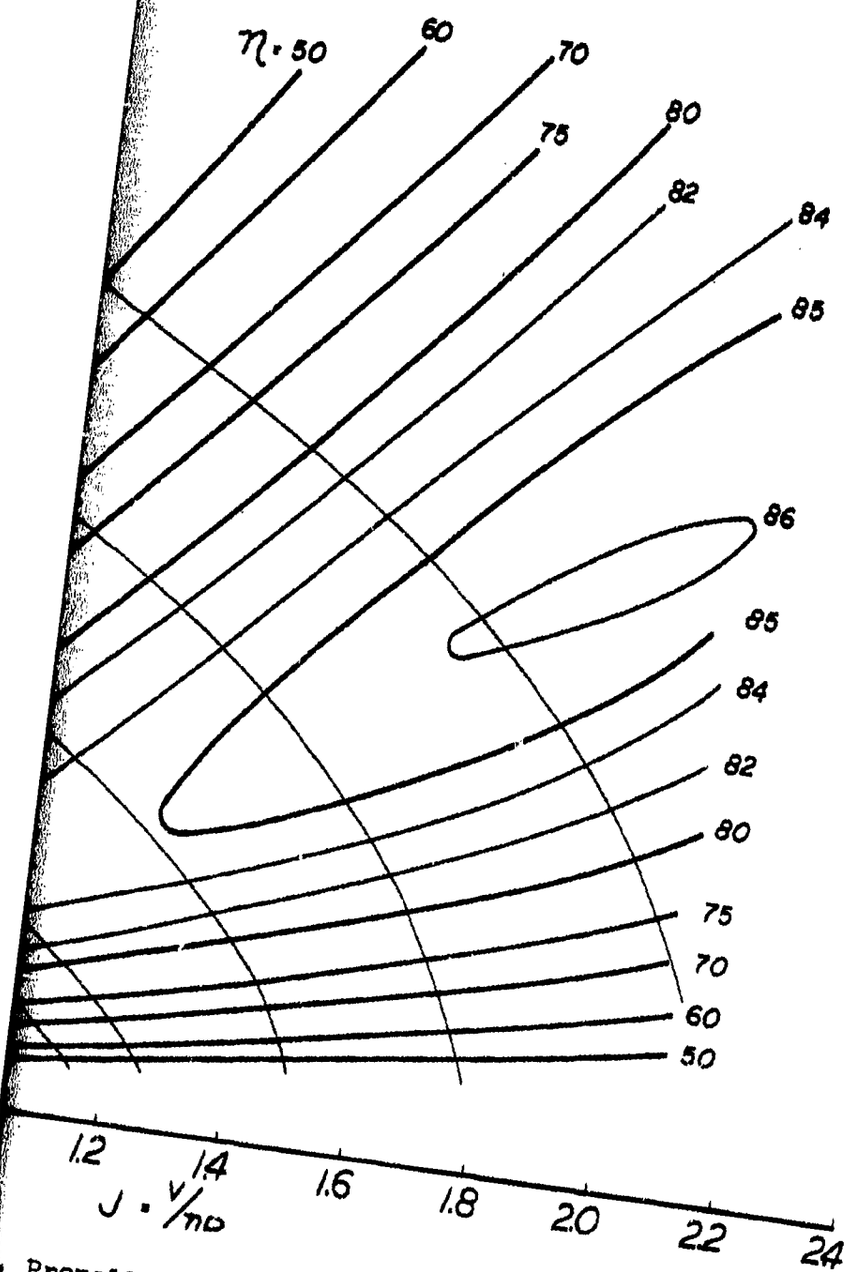

Propeller Optimized
ia Propeller 2B127-1.75.

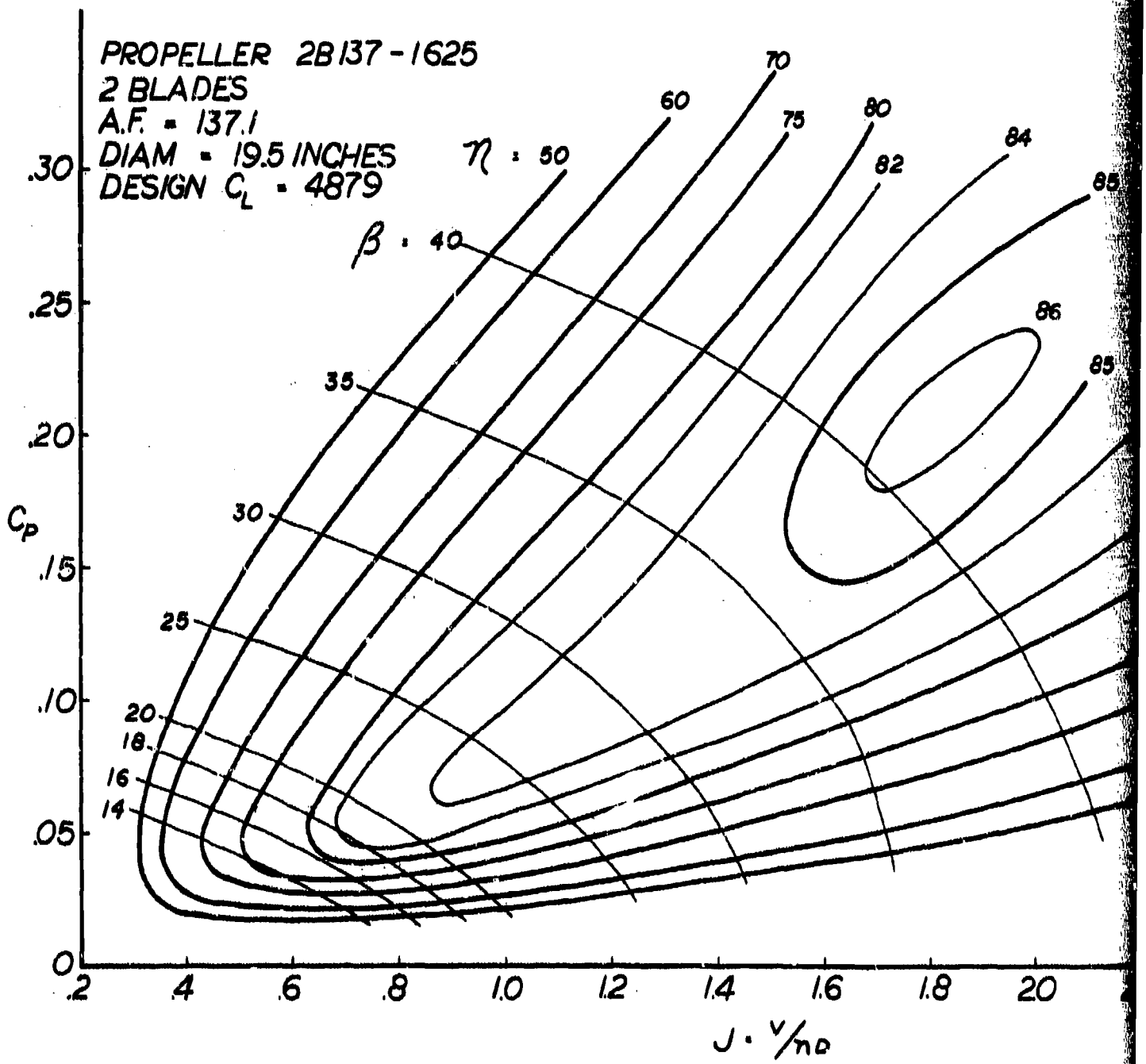

Figure 39. Performance Efficiency Map, Propeller Optimized for Launch - Advanced Aquila Propeller 2B137-1.625.

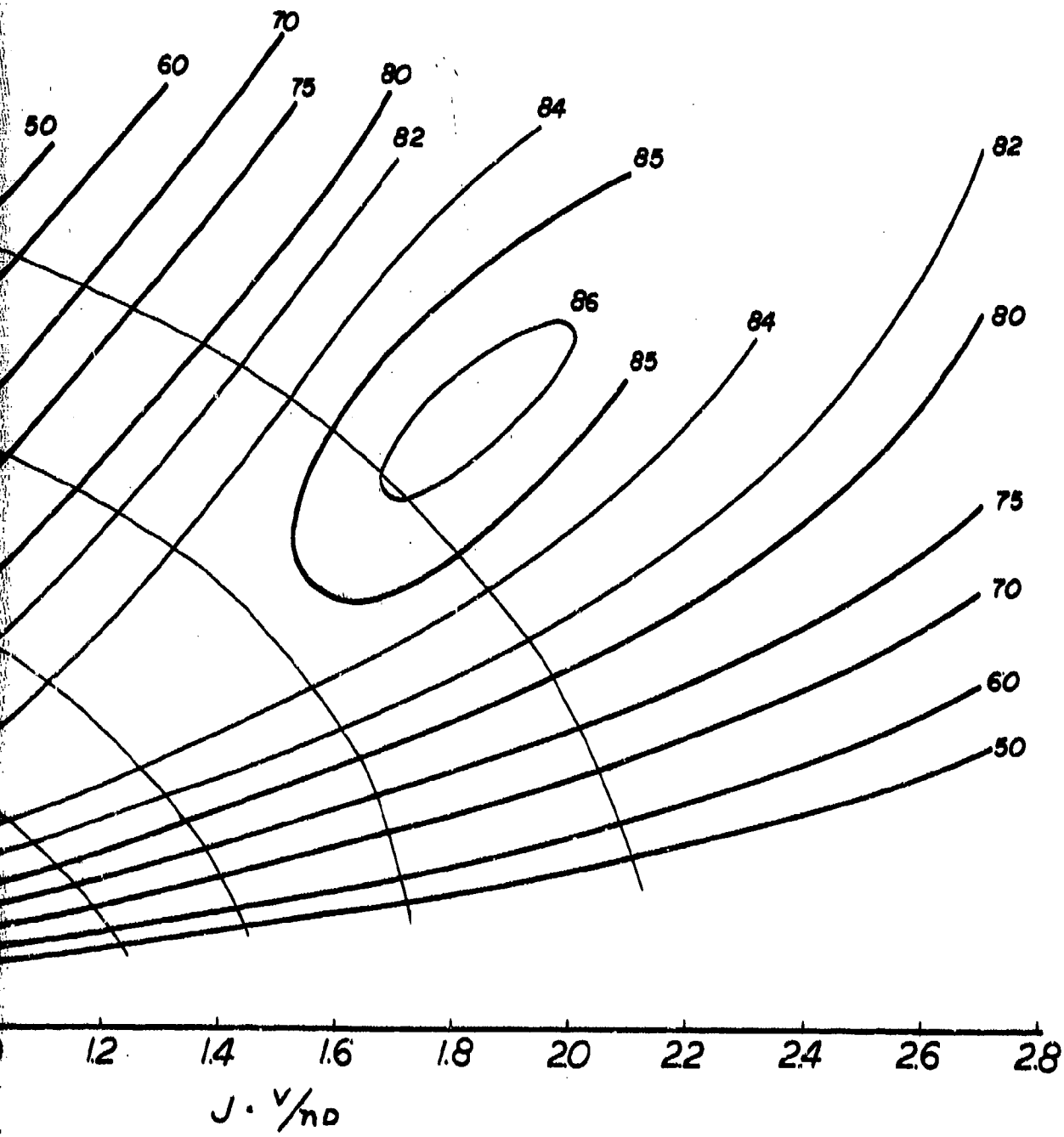

, Propeller Optimized
la Propeller 2B137-1.625.

TABLE 14. CALCULATED PERFORMANCE OF AQUILA - PROPELLER OPTIMIZED FOR LAUNCH

Engine McCulloch 101 MC
Propeller 2B130-1.625

No. of Blades 2
Diameter 1.625 ft
πnD(Take-off) 681(=18.5°)

Integrated Design Lift Coefficient .62
Activity Factor 130
h/b @ Station x = .75 .105

Condition	Alt/temp	Engine HP*	Engine RPM	Velocity (kts)	β (deg)	η	R/C	THP	C_p	J	Remarks
Launch	4000'/95°	8.80	8000	60	18.5	65	797	5.36	.085	.462	Requirement - 667
		8.30	7100	60	24	63	679	4.88	.118	.53	fpm average
		7.05	5900	60	31	55	362 **	3.58	.173	.63	0 - 10,000 ft alt.
		8.75	7800	60	20.5	64	770	5.25	.095	.48	
Cruise	4000'/95°	6.15	8050	94	18.5	78	-	4.37	.059	.73	Requirement - 75
		6.15	7000	95	24	80	-	4.48	.089	.846	-120 kt cruise
		6.15	6000	94	31	79	-	4.42	.142	.977	speed.
		6.45	7600	92	20.5	78	-	4.37	.070	.75	
Dash	4000'/95°	6.15	8050	94	18.5	78	-	4.37	.059	.73	
		8.75	8000	110	24	80.1	-	6.57	.088	.86	
		7.8	6550	105	31	80	-	5.80	.141	1.00	
		7.05	8000	100	20.5	78	-	5.07	.069	.74	
Landing	4000'/95°	8.80	8000	60	18.5	65	523	5.36	.085	.462	
		8.30	7100	60	24	63	406	4.88	.118	.53	
		7.05	5900	60	31	55	88	3.58	.173	.63	
		8.75	7800	60	20.5	64	496	5.25	.095	.48	
		2.55	4850	60	24	77.5	+134				Glide Slope 1.3°

* Propeller HP reduced by 0.55 HP for Launch, Landing and Dash, and by 0.85 HP for Cruise to allow for electrical load.

** Below Requirement.

TABLE 15. CALCULATED PERFORMANCE OF AQUILA - PROPELLER OPTIMIZED FOR LAUNCH

Engine	McCulloch 101 MC	No. of Blades	2	Integrated Design Lift Coefficient	.444
Propeller	2B127-1.75	Diameter	1.75 ft	Activity Factor	127
		πnD(Take-off)	733(=16°)	h/b @ Station x = .75	.056

Condition	Alt/temp	Engine HP *	Engine RPM	Velocity (kts)	β (deg)	η	R/C	THP	C_p	J	Remarks
Launch	4000'/95°	8.8	8000	60	16	70	898	5.78	.060	.434	Requirement - 667 fpm average 0-10,000 ft alt.
		8.6	7500	60	18	69	844	5.55	.072	.463	
		6.8	5700	60	27	61	418 **	3.81	.127	.610	
		8.65	7200	60	20	65	774	5.27	.081	.48	
		7.90	6700	60	22	66	672	4.85	.092	.52	
Cruise	4000'/95°	5.55	8000	91	16	81	-	4.05	.037	.660	Requirement - 75 to 120 kt cruise speed.
		6.15	7800	96	18	82.7	-	4.63	.045	.715	
		6.15	6000	96	27	82.8	-	4.64	.098	.927	
		6.45	7400	98	20	84	-	4.7	.052	.77	
		6.45	6900	98	22	84	-	4.7	.064	.82	
Dash	4000'/95°	5.55	8000	91	16	81	-	4.05	.037	.660	
		6.65	8000	100	18	82.6	-	5.03	.045	.72	
		7.85	6600	107	27	83	-	6.06	.096	.94	
		7.00	8000	105	20	84	-	5.8	.065	.78	
		8.75	7900	112	22	84	-	6.9	.063	.82	
Landing	4000'/95°	8.8	8000	60	16	70	626				
		8.6	7500	60	18	69	569				
		6.8	5700	60	27	61	144				
		8.65	7200	60	20	65	501				
		7.90	6700	60	22	66	398				
		1.91	4850	60	18	82.5	-239				Glide Path 2.3°

* Propeller HP reduced by 0.55 HP for Launch, Landing and Dash, and by 0.85 HP for Cruise to allow for electrical load.

** Below requirement.

TABLE 16. CALCULATED PERFORMANCE OF AQUILA
– PROPELLER OPTIMIZED FOR LAUNCH

Engine Accullocn 101 hp
Propeller [illegible]

No. of Blades 2
Diameter 1.625 ft
rpD'Take-off) 681(=20.5°)

Integrated Design Lift Coefficient .488
Activity Factor 137
h/b ● Station x = .75 .056

Condition	Alt/temp	Engine HP *	RPM	Velocity (kts)	β (deg)	η	R/C	THP	C_p	J	Remarks
Launch	4000'/95°	8.8	8000	60	20.5	65	797	5.36	.088	.468	Requirement – 667
		7.05	5900	60	31	54	345 **	3.51	.173	.63	fpm average
		8.6	7600	60	22.5	63	726	5.07	.100	.49	0–10,000 ft alt.
		8.4	7300	60	24.5	60	675	4.86	.110	.51	
Cruise	4000'/95°	6.15	8000	98	20.5	84.5	–	4.73	.060	.760	Requirement – 75
		6.15	6000	95	31	80.5	–	4.51	.142	.988	to 120 kt cruise
		6.45	7600	97	22.5	83	–	4.65	.700	.796	speed.
		6.45	7000	97	24.5	83	–	4.65	.089	.86	
Dash	4000'/95°	6.15	8000	98	20.5	84.5	–	4.73	.060	.760	
		7.8	6550	105	31	80.7	–	5.85	.141	1.00	
		7.05	7950	103	22.5	83	–	5.4	.071	.81	
		8.05	7700	107	24.5	82.5	–	6.2	.090	.87	
Landing	4000'/95°	8.8	8000	60	20.5	65	523	5.36	.088	.468	
		7.05	5900	60	31	54	71	3.51	.173	.63	
		8.6	7600	60	22.5	63	452	5.07	.100	.49	
		8.4	7300	60	24.5	60	401	4.86	.110	.51	
		1.80	4850	60	20.5	83	-259				Glide Path 2.4°

* Propeller HP reduced by 0.55 for Launch, Landing and Dash, and by 0.85 HP for Cruise to allow for electrical load.

** Below requirement.

PROPELLER WING BODY INTERFERENCE

The interference losses between propellers and bodies including wings have been studied by many investigators.[27-32] Much of the work done was in the early days of aircraft development. Although considerable testing was done, the data is not suitable for predicting the interference corrections by empirical procedures. Examples of typical test results from Reference 29 are given in Figure 40. These results are misleading as they include all the changes due to the propeller body interaction, including the increase of drag due to a velocity increase. The best approach for considering the change in performance of propellers is that of Glauert [28] and Theodorsen.[2]

INTERFERENCE OF WING AND BODY ON PROPELLER

The interference of a body and wing on the performance and design of a propeller depends on whether the propeller is a tractor or pusher and the relative sizes of each. For instance, if a large propeller is operating in the tractor position on a small body, the interference effects will be very small or zero. However, if a pusher propeller is installed behind a large body, such as a lighter-than-air vehicle, the interference effects can be very large with apparent levels of efficiency exceeding 100% being achieved.[32] The level of

---

2 Theodorsen.

27 Weick, F.E., AIRCRAFT PROPELLER DESIGN, McGraw-Hill, 1930.

28 Glauert, H., AIRPLANE PROPELLERS VOL. 4 DIV. L OF AERODYNAMIC THEORY, Durand Editor, Dover, New York.

29 Von, Dr. G. Cordes, Dessau, DIE LUFTSCHRAUBE BEI GESTORTEM ZUSTROM, Abgeschlossen am 10 January 1938.

30 Wood, D. H., TESTS OF NACELLE-PROPELLER COMBINATIONS IN VARIOUS POSITIONS WITH REFERENCE TO WINGS II — THICK WING - VARIOUS RADIAL-ENGINE COWLINGS - TRACTOR PROPELLER, NACA TR 436, 1932.

31 Stickle, G.W., Crigler, J.L., & Naiman, EFFECT OF BODY NOSE SHAPE ON THE PROPULSIVE EFFICIENCY OF A PROPELLER, NACA TR 725.

32 McLemore, H. Clyde, WIND-TUNNEL TESTS OF A 1/20-SCALE AIRSHIP MODEL WITH STERN PROPELLERS, NASA TN D-1026.

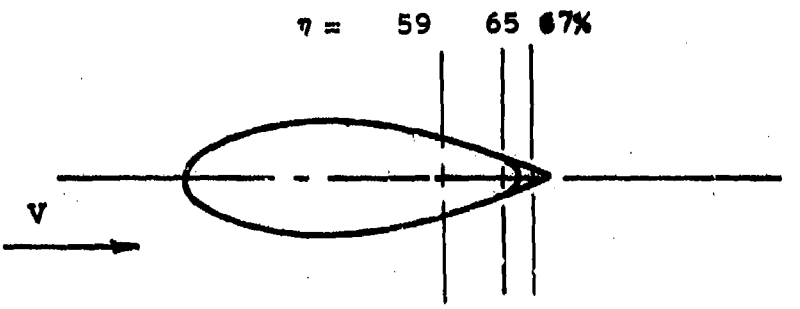

Propellers in Pusher Position

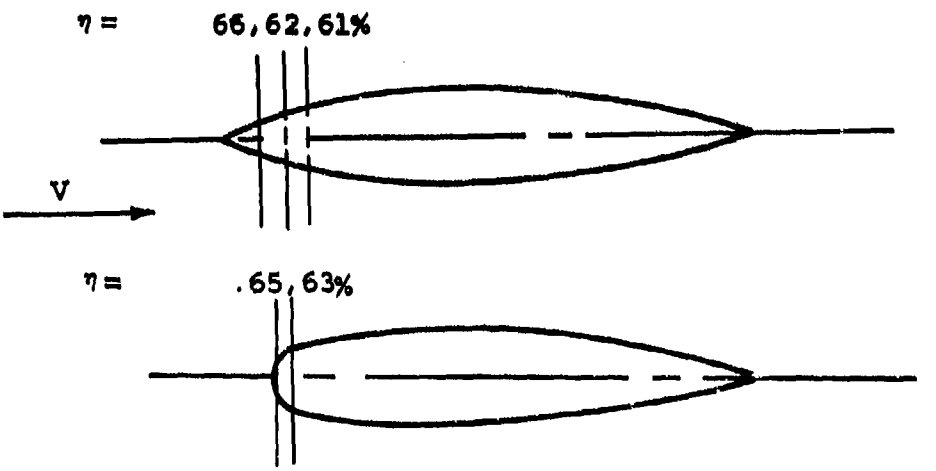

Propellers in Tractor Position

Figure 40. Effect of Propeller Location on Efficiency.

interference of a wing and body on the performance also depends on whether the losses are charged to the airplane drag or to the propeller thrust. Thus, if the increase of velocity due to the propeller wake results in a drag increase on the body this could be charged to the propeller thrust or the aircraft drag. The following definitions of terms are used and have been found to avoid confusion in considering the installed propeller performance:

T_S = Propeller shaft thrust, tractor or pusher

$T_N = T_S - \Delta D$ (Net Thrust)

ΔD = Change in aircraft drag due to propeller

$$\text{Propeller shaft efficiency} = \eta_s = \frac{T_S V_o}{550\ HP} \tag{18}$$

V_o = The free-stream velocity, ft/sec

HP = The net shaft horsepower to the propeller

$$\text{True propeller efficiency} = \eta_T = \frac{T_S V_L}{550\ HP} \tag{19}$$

V_L = The integrated average velocity in the plane of the propeller

$$\text{Propulsion Efficiency} = \eta_p = \frac{T_N V_L}{550\ HP} \tag{20}$$

The propeller shaft thrust is often the value measured and is actually the force on the shaft due to the development of the propeller thrust operating in this local environment. It is the actual thrust produced by the propeller and is calculated by strip analysis using the actual local velocity at each blade section as influenced by the body and wing. If there is a large gradient of velocity between the leading and trailing edges of the propeller, a pressure change will exist causing a buoyancy force to be developed. This must be added to thrust calculated by strip analysis to find the shaft thrust.

The shaft efficiency, Equation 18, is the value usually quoted for propeller performance. This definition is used as the shaft thrust is easily determined from η_s knowing the power input and the free stream velocity. The shaft thrust is the quantity used to find the performance of the airplane.

If the interference of the body causes a large reduction in the axial velocity in the plane of the propeller, the shaft efficiency will be higher than the true efficiency. It is not

uncommon to have shaft efficiencies over 100% for both tractor and pusher propellers operating in conjunction with large bodies. These high apparent values of shaft efficiency are obtained due to the velocity decrease which results in an increase of propeller thrust. The true propeller efficiency equation is never over 100%, as it is found based on the integrated average velocity. This efficiency is equal to the shaft efficiency when the blockage is zero.

The change in efficiency due to the blockage of a body can best be illustrated by an example. Consider a propeller operating at a J of .6 based on the free-stream velocity. The power coefficient of this propeller is equal to .1 and the body blocks the flow so that the average velocity in the plane of the propeller is 0.5. From an efficiency map the performance of the propeller would be

J	C_P	η_T	C_T	η_S
.5	.1	.66	.132	79.2
.6	.1	.74	.1233	74.0

In the above case η_S is based on the free stream J of 0.6. Thus, a 5-point increase in shaft efficiency is obtained due to the body blockage even though the true efficiency actually goes down by 8 percentage points.

The propulsion efficiency and net propeller thrust are determined from the increase in drag due to the propeller interference on the airplane. The drag of the airplane is increased by the propeller due to the increase in slipstream velocity and thus skin friction, due to changes in pressure drag and due to separation from the rotation of the wake. A wing operating in the propeller wake can actually remove some of the losses due to slipstream rotation and result in an efficiency increase.

INTERFERENCE VELOCITY -- TRACTOR POSITION

Body

The interference velocity ratio due only to the presence of the body relative to the propeller is defined as the ratio of the actual velocity V_L to the free-stream velocity V_o. The axial velocity induced by the propeller u adds to V_L, but is not considered to be part of the interference velocity. The ratio of V_L/V_o is needed to calculate the forces at each blade station by strip analysis. If the body is large and complex, measurements of V_L should be made for best results. With normal types of streamline bodies, V_L can be estimated by potential flow theory with good accuracy.

Using the potential flow theory,[33] a computer program was set up and V_L/V_O was determined as a function of radial distance at two axial propeller locations for a series of prolate spheroids. The length-to-diameter ratio of the bodies covered was 3, 5, 6 and 10. The results of the calculations are presented in Figures 41 and 42 in terms of V_L/V_O as a function of r/R_b. This ratio can be converted to the r/R_p value, needed for strip analysis calculations, with the equation

$$r/R_p = r/R_b \cdot R_b/R_p \qquad (21)$$

From the data given in Figures 41 and 42 the velocity ratio due to the body can be estimated by determining the prolate spheroid that is the nearest in shape to the body or fuselage being considered.

Wing

The wing interference velocity on a propeller operating in the tractor position is generally small, especially for a single-engine airplane. If the propeller is mounted on the wing, the upwash velocity can change the angle of flow into the propeller and this can be important in determining the alternating stress on the blade. As the blockage of the wing is small, due to the low relative thickness to propeller diameter ratio, the change of efficiency is small and is neglected.

Efficiency Change Due to Propeller Wake

The wake of a propeller operating in the tractor position causes an increase in drag on the fuselage due to the axial velocity increase compared with free stream. This increase in drag is the result of the increase in dynamic pressure; the drag coefficient change is usually not significant. The rotational component of velocity in the wake of a propeller can also change the fuselage drag by causing separation at the wing juncture or a similar component. This drag increase can easily be reduced by a change of the blade load distribution. The drag due to the wake on a fuselage is generally neglected as it is small.

A wing operating in the wake of a propeller will often improve the overall efficiency due to the recovery of the rotational losses in the propeller slipstream. Increases in efficiency as high as 1 to 2% have been measured in a wind tunnel. Since this gain tends to offset the losses due to the increased q in the wake, it is usually neglected in calculating propeller performance.

---

[33] Durand, AERODYNAMIC THEORY, Vol 1, Dover, N.Y., pp 277-285.

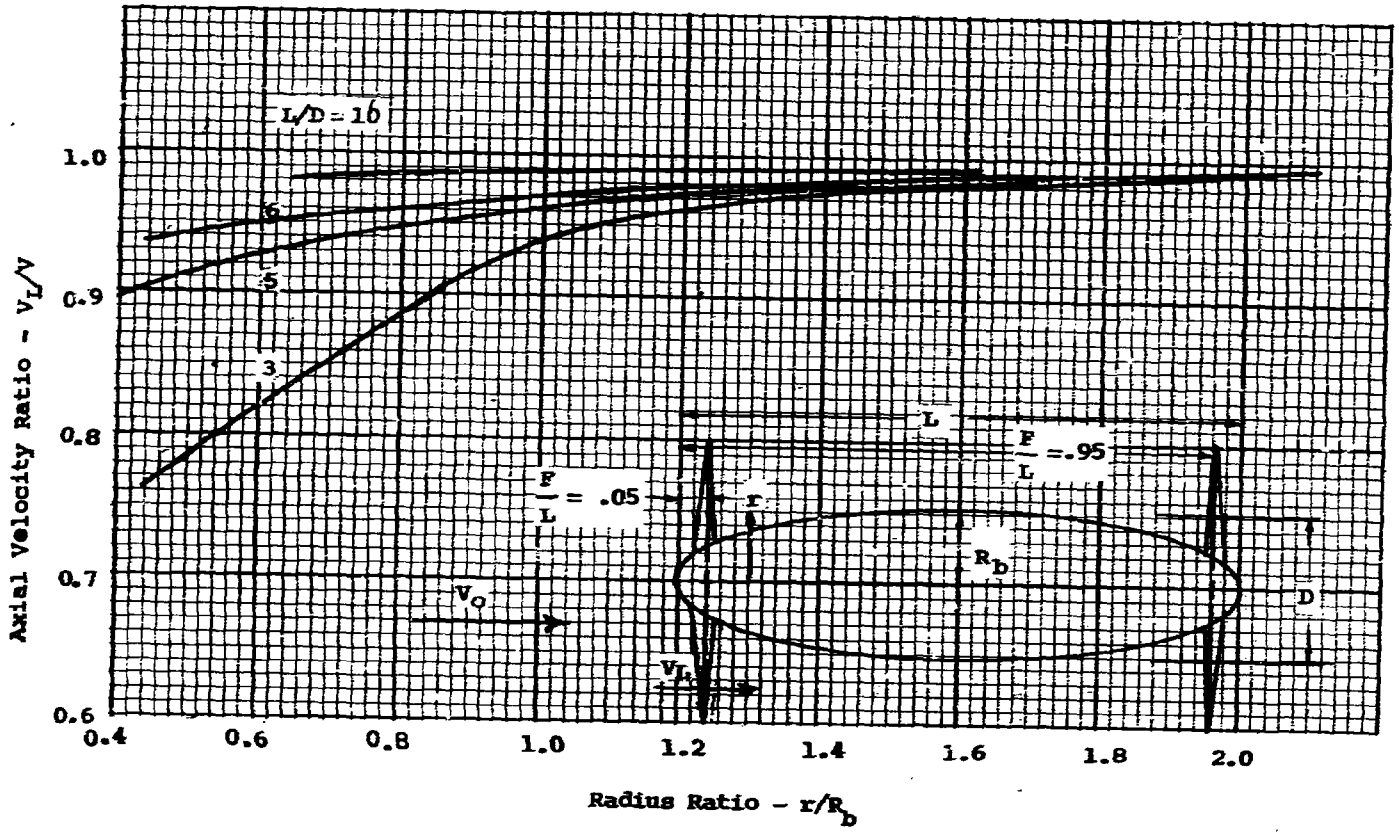

Figure 41. Axial Velocity Change at Propeller Plane Due to Body Size for Tractor and Pusher Locations, F/L = .05 or .95.

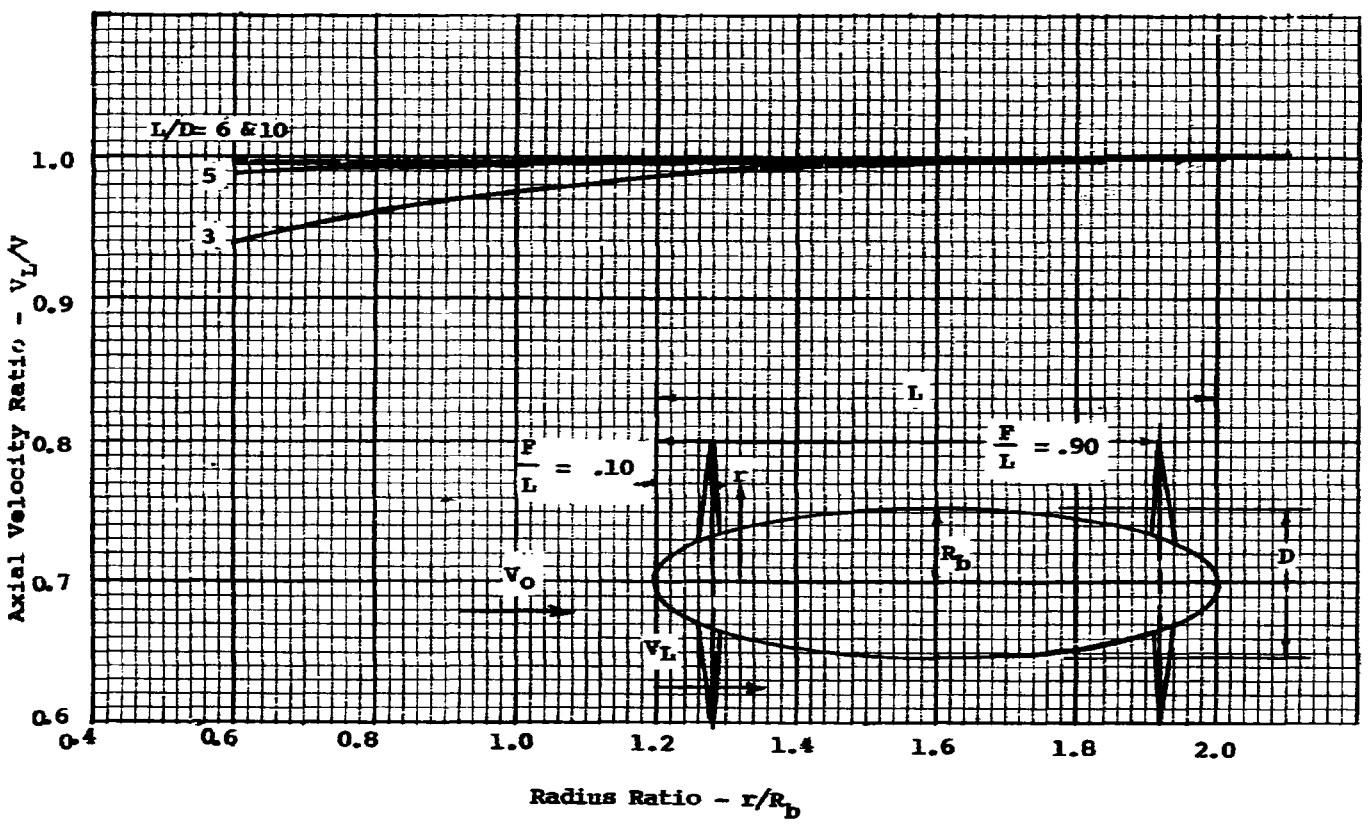

Figure 42. Axial Velocity Change at Propeller Plane Due to Body Size for Tractor and Pusher Locations, F/L = 0.1 or .90.

INTERFERENCE VELOCITY -- PUSHER POSITION

Body

When a propeller is mounted behind a large body such as an airship hull, large changes in efficiency are obtained. For instance, in Reference 32 the shaft efficiency measured was 123%. This high value of efficiency is caused by the propeller operating in the reduced velocity field of the large body. At the lower local velocity the thrust-to-power ratio of the propeller increases, so when this is multiplied by the higher free-stream velocity the efficiency can exceed 100%. The true efficiency is of course less than 100% when the actual velocity in the plane of the propeller is used.

When finding the local axial velocity in the propeller plane (V_L) for the pusher case, the effect of separation on the body and the relieving action of the propeller should be considered. For instance, with the body alone the flow will tend to separate sooner than in the case where the propeller is acting as a sink and is reducing the adverse pressure gradient on the body. This trend has been observed in the wind tunnel tests of pusher propellers mounted on large bodies and in the flight test of a general aviation aircraft with tractor and pusher propellers. From this it appears that the potential flow solution discussed for the tractor case can also be used for the pusher propeller case, Figures 41 and 42.

If there is a large protuberance in front of the propeller, such as an engine cylinder, the velocity in the propeller plane must be modified. The ratio of loss of head (ΔH) to the free-stream q due to such a body is of the order of magnitude as the drag coefficient for the projected area. Averaging this loss over the disk and adding V_L, determined from Figures 41 and 42, will give net local velocity at the propeller plane.

---

[32] McLemore.

In addition to the velocity change encountered due to operation in a potential flow, the skin friction developed on the body will further reduce the velocity in the plane of the pusher propeller. This reduction of velocity aft of the body will reduce the total head. The average local velocity over the wake area can be determined knowing the drag coefficient of the body from the equation

$$V_{La} = \sqrt{V_o^2 - C_D V_o^2 D_b^2 / D_w^2} \qquad (22)$$

where V_{La} = the average velocity in the wake of the body

D_w = the diameter of the wake

D_b = the body diameter

C_D = the drag coefficient of the body based on frontal area.

The wake diameter, D_w, for a streamline body can be estimated from the equation given by Hoerner

$$D_w = \sqrt{.462\,(L)\,D_b\,RN^{1/7}} \qquad (23)$$

where L = the body length

RN = the Reynolds number

Wing

The drag of a wing results in a decrement in velocity in its wake, which will influence the velocity in the propeller plane. In the tests of two-dimensional wings, the drag is measured from wake survey measurements. Typical measurements of the wake behind the wings are given in Figures 43 through 45.

Since the distribution of ΔH across the wake of the wing can be read from Figures 43 through 45, the variation of the local velocity can easily be found. Thus

$$V_L^1 = V_o\sqrt{1 - \Delta H/q} \qquad (24)$$

The propeller will tend to average the local wake velocity so that if V_L is the average in the wing wake having a width W_w

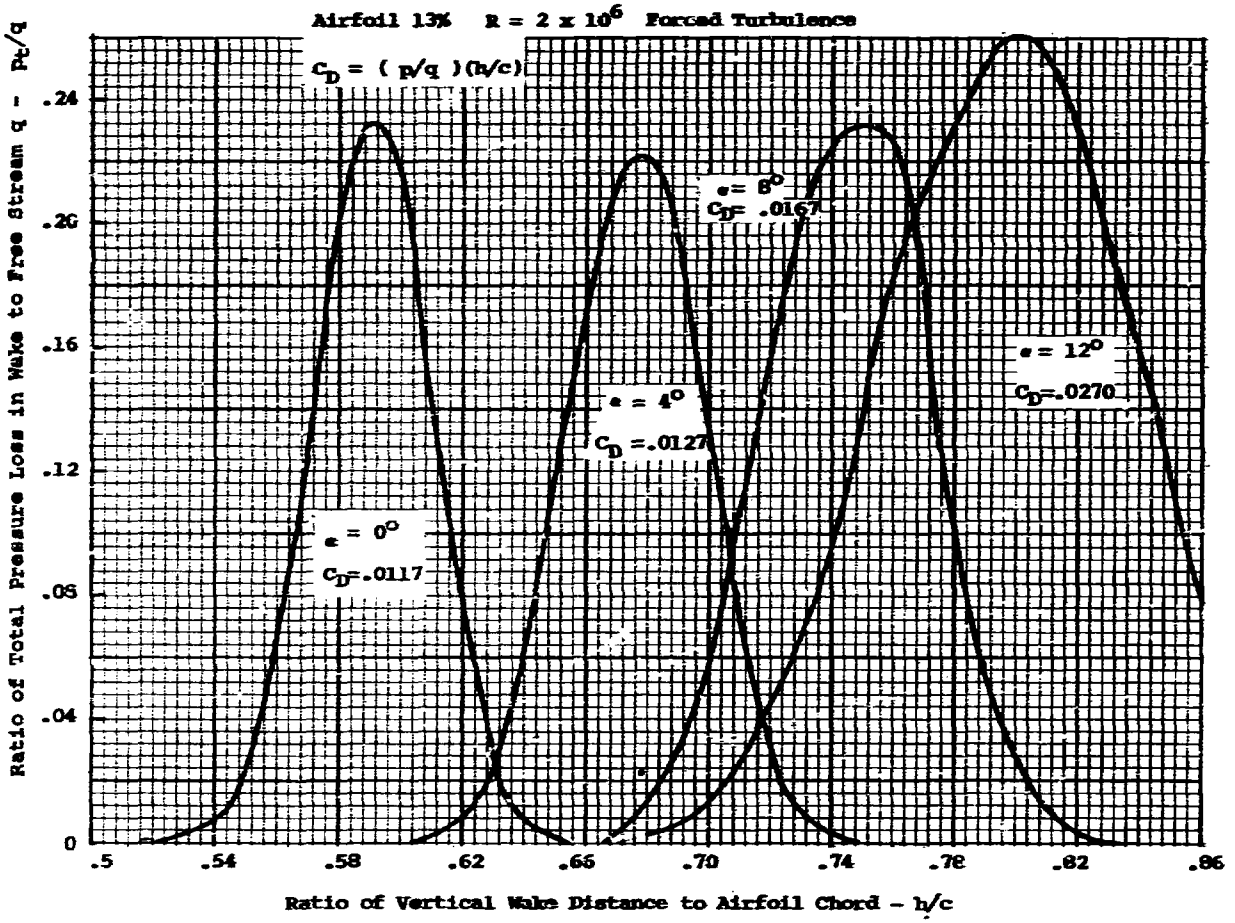

Figure 43. Pressure Loss in the Wake of an Airfoil - Thickness Ratio = 13%.

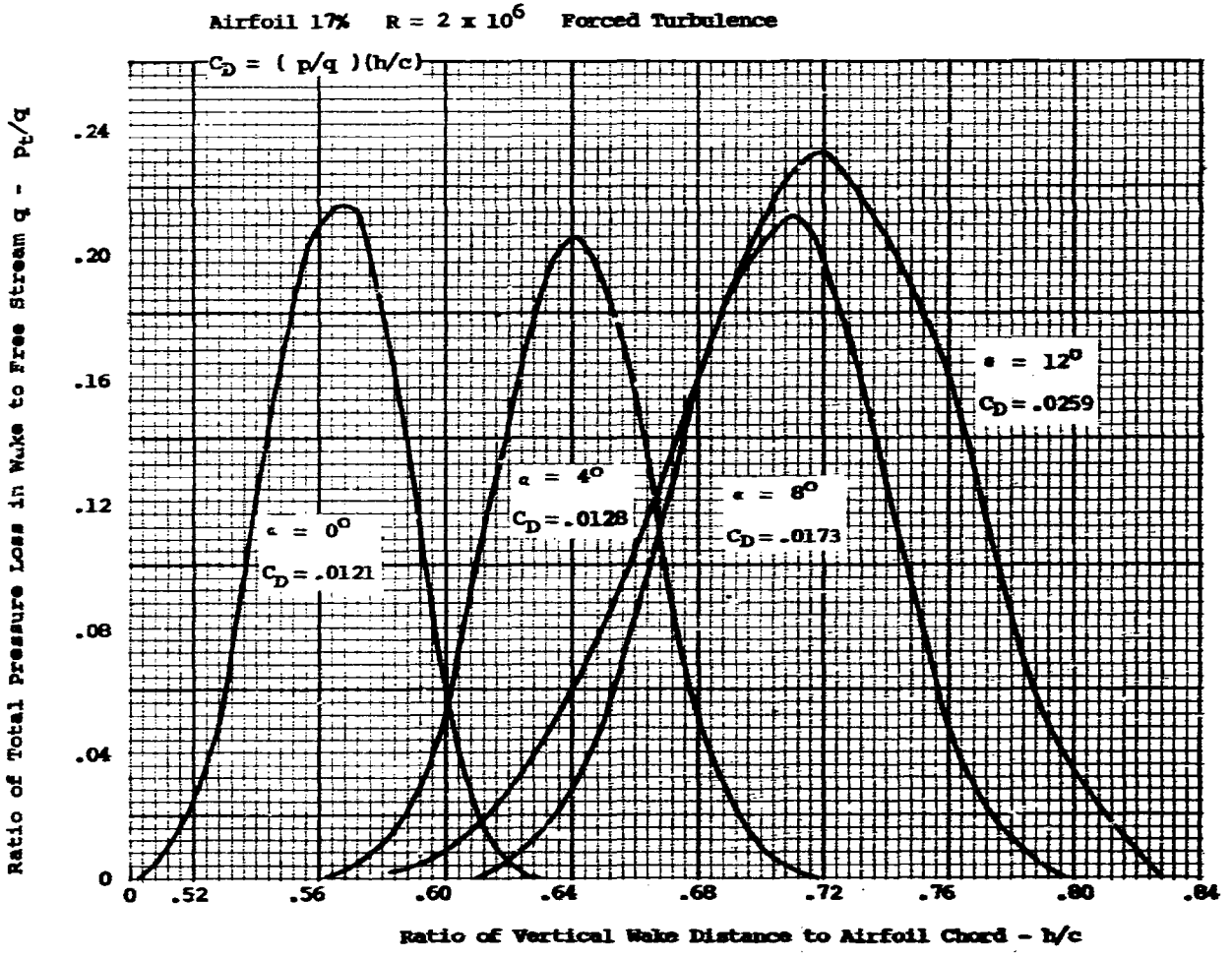

Figure 44. Pressure Loss in the Wake of an Airfoil - Thickness Ratio = 17%.

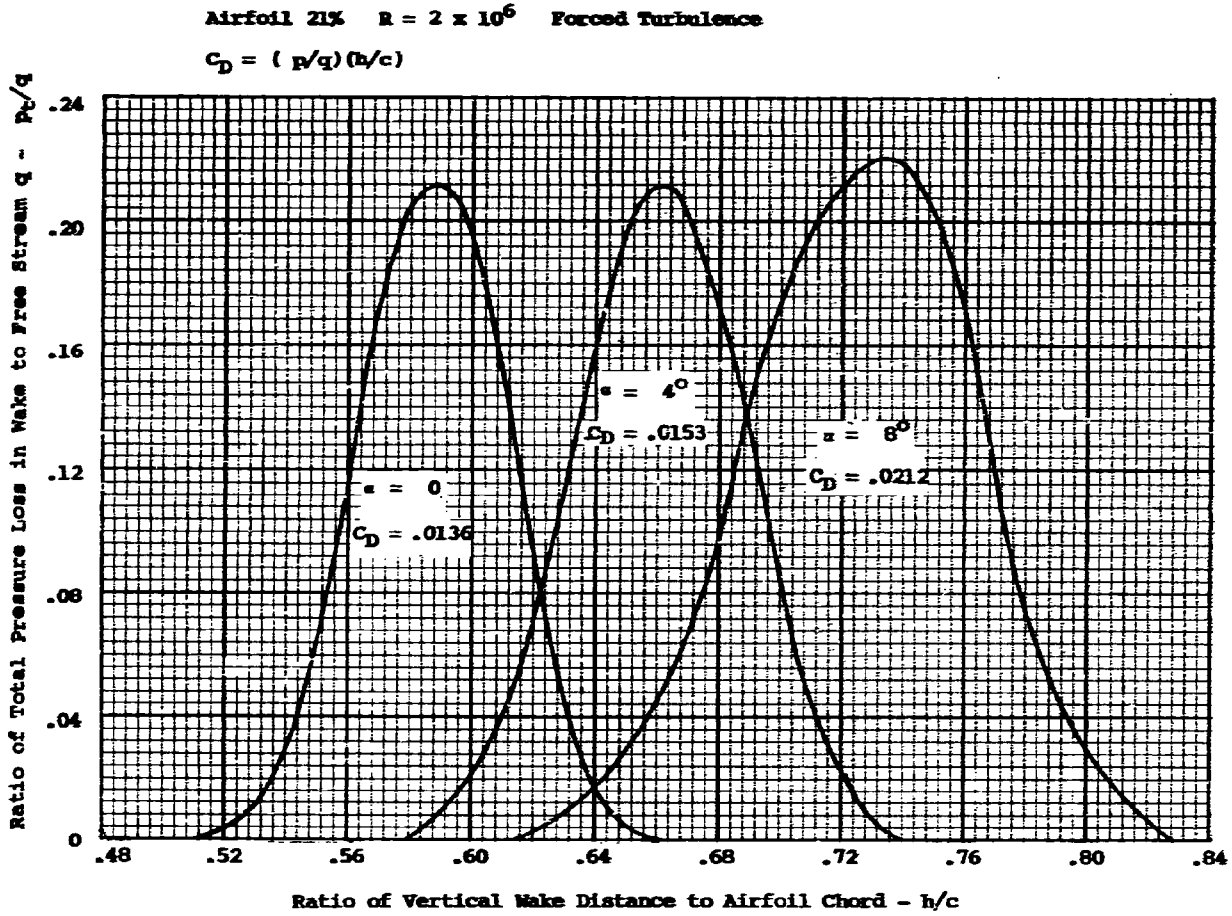

Figure 45. Pressure Loss in the Wake of an Airfoil - Thickness Ratio = 21%.

at a blade station x then the effective local velocity is

$$V_{Le} = \frac{V_L \cdot (\pi x D - 2W_w) + V_L^1 \, 2W_w}{\pi x D} \qquad (25)$$

where V_L = the local velocity at the propeller influenced by the central body

V_L^1 = local velocity influenced by the wing

V_{Le} = effective local velocity at propeller

PERFORMANCE SENSITIVITY OF RPV PROPELLERS

With conventional propellers in the 8- to 19-foot-diameter range changes in performance due to manufacturing tolerances were difficult to measure, apparently due to the small differences of efficiency encountered. Many attempts were made to find changes in performance due to changes of the blade aerodynamic shape from that specified. The differences in efficiency were apparently within the ± 1% accuracy of measurement. In the case of conventional propellers, the induced losses are predominant with losses due to profile drag being only 2 to 10% of the total. Thus, the effect of manufacturing tolerances influencing profile losses due to changes in the blade chord and profile shape will have a small influence on the overall results. A change of 20% in the profile losses due to the effects of manufacturing tolerances would change the efficiency by a maximum of only 2%.

MANUFACTURING TOLERANCES

The change in performance due to shape deviations on the blades of RPV propellers are potentially more important than for conventional propellers, as the profile losses are a much larger percentage of the total. For instance, the profile losses at the launch condition are of the order of 20 to 25 percentage points in efficiency and the corresponding losses in cruise are 15 percentage points. Thus, a 20% loss in drag could mean an efficiency difference of 3 to 5%.

Blade Section Shape and Chord

In the low Reynolds number range a specification can be formulated for the surface finish and profile shape from Hoerner[34] that should prevent drag loss over and above those predicted. For a blade section in the 2- to 3-inch chord size, the surface finish should be the same as an aircraft sheet metal surface. That is, the equivalent grain size would be of the order of .1 mil. Such a surface should easily be obtainable even on a wooden surface, if reasonable care is exercised.

The camber surface shape of the airfoil section should be maintained so that when a straight edge is worked over the surface no discontinuities will be noted from the 0.4 to the tip. The

---

[34] Hoerner, S.F., FLUID-DYNAMIC DRAG, published by the Author, 1965.

surface waviness should be within .001. The overall tolerance on thickness and chord can be ± .02 without influencing the efficiency within measurable accuracy. This is the result of drag being relatively insensitive to changes in small changes of thickness and operating C_L. The leading-edge radius should blend smoothly into the upper and lower blade surface. The radius should not be less than the drawing, but can be up to .02 inch greater as long as no local bumps are encountered.

Blade Angle Distribution

Studies of changes in blade angle distribution indicate that the efficiency does not change as long as it is held within ± .2 degree from the .5 station to the tip, and ± .5 degree from the .5 station inboard. In considering the accuracy needed on the blade angle, a change of .5 degree over the entire radius will result in a power change of .8%. This will cause an efficiency change of .5% in cruise and 1% in launch.

CONCLUSIONS

1. Using the procedures and data developed, propellers with improved performance can be designed for mini remote piloted vehicles.

2. The operating Reynolds number is an important design parameter in the design and performance analysis of mini-RPV propellers.

3. Corrections to drag as a function of Reynolds number must be applied to conventional high Reynolds number airfoil data to find the profile losses at the operating conditions of mini-RPV propellers.

4. The induced losses and corrections predicted by theory are not affected by propeller size and can be found with satisfactory accuracy.

5. The performance of propellers operating at low Reynolds numbers can now be predicted with satisfactory accuracy for the range of operating parameters expected with mini-RPV's.

6. Due to the low speed operation of RPV's, the skin friction and profile drag of the shroud of a ducted propeller is low relative to the gain of induced efficiency of the rotor. As a result, the efficiency of an optimized ducted propeller installed on RPV's will be higher than that of an open propeller.

7. The rotor diameter of a ducted propeller will be lower than that of an open propeller when installed on identical engines, resulting in reduced tip speeds with a corresponding reduction in noise level.

8. The new computer-designed airfoils appear to offer blade structural advantages along with possible improved performance. Further basic data are needed before propellers can be designed to use these airfoil sections.

9. Propellers with variable blade angles, either of the two-position or constant speed type, will have performance advantages.

RECOMMENDATIONS

Based on the results of this effort, it is recommended that:

1. New computer-designed airfoils be developed with thickness ratios in the 6% to 21% range for a range of cambers along with wind tunnel test data covering Mach numbers to the critical and Reynolds numbers down to at least 200,000.

2. A series of optimum ducted fans be designed and evaluated in comparison with open propellers for mini-RPV.

LITERATURE CITED

1. Borst, H.V., et al, SUMMARY OF PROPELLER DESIGN PROCEDURES AND DATA, Vols. I, II and III, USAAMRDL Technical Report 73-34A,B, and C, H.V. Borst & Associates, Eustis Directorate, U.S. Army Air Mobility Research & Development Laboratory, Fort Eustis, Virginia, Nov. 1973, AD 774831, AD 774836, and AD 776998, November 1973.

2. Theodorsen, T., THEORY OF PROPELLERS, McGraw Hill, 1948.

3. Delano, James B., and Carmel, Melvin M., TESTS OF TWO-BLADE PROPELLERS IN THE LANGLEY 8-FOOT HIGH-SPEED TUNNEL TO DETERMINE THE EFFECT ON PROPELLER PERFORMANCE OF A MODIFICATION OF INBOARD PITCH DISTRIBUTION, NACA TN 2268, Langley Aeronautical Laboratory, Langley Field, Virginia, February 1951, Washington.

4. Pendley, Robert E., EFFECT OF PROPELLER-AXIS ANGLE OF ATTACK ON THRUST DISTRIBUTION OVER THE PROPELLER DISK IN RELATION TO WAKE-SURVEY MEASUREMENT OF THRUST, ARR No. L5J02b, NACA, Washington, Wartime Report.

5. Maynard, J.D., and Steinberg, S., EFFECT OF BLADE SECTION THICKNESS RATIOS ON AERO. CHARACTERISTICS OF RELATED FULL-SCALE PROPELLERS AT MACH NOS. UP TO 0.65, NACA Rpt. 1126, 1953.

6. Jacobs, E.N., and Sherman, A., AIRFOIL SECTION CHARACTERISTICS AS AFFECTED BY VARIATIONS OF THE REYNOLDS NUMBER, NACA TR 586, 1937.

7. Relf, E.F., Jones, R., and Bell, A.H., TESTS OF SIX AIRFOIL SECTIONS AT VARIOUS REYNOLDS NUMBERS IN THE COMPRESSED AIR TUNNEL, Rpts. & Memoranda No. 1706, April 1936.

8. Jones, R., and Williams, D.H., THE EFFECT OF SURFACE ROUGHNESS ON THE CHARACTERISTICS OF THE AIRFOILS NACA 0012 AND RAF 34, Rpts. & Memoranda 1708.

9. Lnenicka, Jaroslav, UNPUBLISHED TEST OF A NACA 4412 AIRFOIL AT REYNOLDS NUMBER 20,000 to 250,000, Letter to L.K. Loftin of NASA, 19 March 1974.

10. Althaus, D., EXPERIMENTAL RESULTS FROM THE LAMINAR WIND TUNNEL OF THE INSTITUT FÜR AERO AND GASDYNAMIK DER UNIVERSITAT STUTTGART, Stuttgarter Profilkatalog I, 1972.

LITERATURE CITED (Continued)

11. Schmitz, F.W., AERODYNAMICS OF THE MODEL AIRPLANE, PART 1, Translated by Translation Branch Redstone Scientific Information Center Research & Development, Directorate, U.S. Army Missile Command, Redstone Arsenal, Ala., N70-39001.

12. Deslauriers, E.J., BLADE PERFORMANCE AT LOW REYNOLDS NUMBERS, General Electric, Rpt. No. R54AGT605, dated 1-14-55.

13. Lippisch, A., UNSTETIGKECTEN IM VERLSUF DES PROFILWIDERSTANDES, Messerschmitt, A.G. Augsburg, March 1941.

14. Lippisch, A.M., WING SECTIONS FOR MODEL PLANES, Air Trails Pictorial, April 1950.

15. Hoerner, S.F., and Borst, H.V., FLUID DYNAMIC LIFT, published by Hoerner Fluid Dynamics, Brick Town, New Jersey 08723, 1975.

16. Reid, E.G., THE INFLUENCE OF BLADE-WIDTH DISTRIBUTION ON PROPELLER CHARACTERISTICS, NACA TN No. 1834, March 1949.

17. Reid, E.G., WAKE STUDIES OF EIGHT MODEL PROPELLERS, NACA TN No. 1040, July 1946.

18. Reid, E.G., STUDIES OF BLADE SHANK FORM AND PITCH DISTRIBUTION FOR CONSTANT-SPEED PROPELLERS, NACA TN No. 947, January 1945.

19. Grose, R.M., and Taylor, H.D., WIND TUNNEL STUDIES OF THE EFFECTS OF BLADE THICKNESS RATIO, CAMBER AND PITCH DISTRIBUTION ON THE PERFORMANCE OF MODEL HIGH-SPEED PROPELLERS, Hamilton Standard Rpt. No. HS-1352, June 1955.

20. Grose, R.M., and Brindley, D.L., A WIND TUNNEL INVESTIGATION OF THE EFFECT OF BLADE ACTIVITY FACTOR ON THE AERODYNAMIC PERFORMANCE OF MODEL PROPELLERS AT FLIGHT MACH NUMBERS FROM 0.3 TO 0.9, Hamilton Standard Rpt. No. HS-1125, March 1954.

21. Abbott, Ira H., and Von Doenhoff, A.E., THEORY OF WING SECTIONS, Dover Publications, Inc.

22. Lindsey, W.F., Stevenson, D.B., and Daley, Bernard N., AERODYNAMIC CHARACTERISTICS OF 24 NACA SERIES AIRFOILS AT MACH NUMBER BETWEEN 0.3 AND 0.8, NACA TN 1546.

23. Whitcomb, Richard T., and Clark, Larry R., AN AIRFOIL SHAPE FOR EFFICIENT FLIGHT AT SUPERCRITICAL MACH NUMBERS, NASA TM X-1109, 1965.

LITERATURE CITED (Continued)

24. Whitcomb, Richard T., REVIEW OF NASA SUPERCRITICAL AIRFOILS, ICAS Paper No. 74-10, Presented at the Ninth Congress of the International Council of the Aeronautical Sciences, Haifa, Israel, August 1974.

25. Wortmann, F.X., A CRITICAL REVIEW OF THE PHYSICAL ASPECTS OF AIRFOIL DESIGN AT LOW MACH NUMBERS, Institut für Aerodynamik u. Gasdynamik, der Universitat Stuttgart, Published at the MIT Symposium "Technology & Science of Motorless Flight", Boston 1972.

26. Bocci, A.J., A NEW SERIES OF AIRFOIL SECTIONS SUITABLE FOR AIRCRAFT PROPELLERS, Aeronautical Quarterly, Feb.1977.

27. Weick, F.E., AIRCRAFT PROPELLER DESIGN, McGraw-Hill, 1930.

28. Glauert, H., AIRPLANE PROPELLERS VOL. 4 DIV. L of AERODYNAMIC THEORY, Durand Editor, Dover, New York.

29. Von Dr. G. Cordes, Dessau, DIE LUFTSCHRAUBE BEI GESTORTEM ZUSTROM, Abgeschlossen am 10 January 1938.

30. Wood, D.H., TESTS OF NACELLE-PROPELLER COMBINATIONS IN VARIOUS POSITIONS WITH REFERENCE TO WINGS II - THICK WING - VARIOUS RADIAL-ENGINE COWLINGS - TRACTOR PROPELLER, NACA TR 436, 1932.

31. Stickle, G.W., Crigler, J.L. & Naiman, EFFECT OF BODY NOSE SHAPE ON THE PROPULSIVE EFFICIENCY OF A PROPELLER, NACA TR 725.

32. McLemore, H. Clyde, WIND-TUNNEL TESTS OF A 1/20-SCALE AIRSHIP MODEL WITH STERN PROPELLERS, NASA TN D-1026.

33. Durand, AERODYNAMIC THEORY, Vol. 1, Dover, New York, pp. 277-285.

34. Hoerner, S.F., FLUID-DYNAMIC DRAG, published by the Author, 1965.

35. Durand, W.F., TESTS ON THIRTEEN NAVY TYPE MODEL PROPELLERS, NACA TR 237.

36. McLemore, AERODYNAMIC INVESTIGATION OF A FOUR-BLADE PROPELLER OPERATING THROUGH AN ANGLE OF ATTACK RANGE FROM 0^{o} to 180^{o}, NACA TN 3228.

LIST OF SYMBOLS

AF	blade activity factor
B	blade number
b	blade chord, in. or ft
C_D	drag coefficient
C_{DP}	profile drag coefficient
C_L	lift coefficient
C_{Li}	section design lift coefficient
C_{Lo}	operating lift coefficient
C_{Lx}	maximum lift coefficient
C_P	power coefficient
C_p	pressure coefficient
C_Q	torque coefficient
C_T	thrust coefficient
D	drag, lbs
D	propeller diameter, ft
D_b	body diameter, ft
D_W	wake diameter, ft
d	distance, ft
F	propeller axial location, ft
f_d	Reynolds number correction for drag = $C_{D_{Low\ R.N.}}/C_{D_{High\ R.N.}}$
FM	figure of merit
GW	gross weight, lbs
H	total pressure head, lb/sq ft

LIST OF SYMBOLS (Continued)

h	maximum blade thickness, ft
HP	horsepower
J	advance ratio = V/nD
K(x)	circulation function — single rotation propellers
L	lift, lb
L	body length, ft
LO_1	unit loading parameter = C_p 400/B(AF)
LO_2	integrated loading parameter = $4000\ C_p\ \sin\phi_{0.75}/J^2B(AF)$
M	Mach number
M_{CR}	critical Mach number
mph	miles per hour
N	propeller rotational speed, rpm
N_R	Reynolds number
n	propeller rotational speed, rps
P	power, ft-lbs/sec
p	pressure, psf
Q	torque, ft-lbs
q	dynamic pressure, psf
R	propeller radius, ft
R_b	body radius, ft
R_p	propeller radius, ft
R/C	rate of climb, fpm
R.N.	Reynolds number

LIST OF SYMBOLS (Continued)

r	propeller radius at any station, ft
Shp	shaft horsepower
T	thrust, lb
Thp	thrust horsepower
T_N	propeller net thrust, lb
T_S	propeller shaft thrust, lb
U	free-stream velocity, fps
u	induced axial inflow velocity, fps
V	airplane velocity, fps
V_L	integrated average velocity in plane of propeller, fps
V_o	free-stream velocity, fps
V_w	velocity in final wake, fps
v	induced radial inflow velocity, fps
W	true wind velocity, fps
w	displacement velocity, fps
$\bar{w}$	displacement velocity ratio = w/V
x	fractional radius at any station = r/R
α	angle of attack, deg
α_i	induced angle of attack, deg
β	blade angle, deg
γ	drag lift angle = $\tan^{-1} C_D/C_L$, deg
η	propeller efficiency

LIST OF SYMBOLS (Continued)

λ	advance ratio = J/π
ρ	mass density of air, slugs/cu ft
σ	propeller solidity
ϕ	helical pitch angle, deg
ϕ_o	apparent wind angle, deg
ω	rotational velocity, rad/sec

SUBSCRIPTS

ref	reference
.75	conditions at x = .75
i	incompressible; induced
p	profile
c	calculated
T	true
t	test